Autonomous Patient Monitoring with a Pressure Sensor Array

Submitted by

Megan Howell Jones, B.Eng.

A thesis submitted to
the Faculty of Graduate Studies and Research
in partial fulfilment of
the requirements for the degree of
Master of Applied Science

Ottawa-Carleton Institute for Electrical and Computer Engineering

Department of Systems and Computer Engineering
Carleton University
Ottawa, Ontario, K1S 5B6
Canada

September 2006

Your file Votre référence
ISBN: 978-0-494-18315-1
Our file Notre référence
ISBN: 978-0-494-18315-1

Abstract

Unobtrusively monitoring older adults in their homes could reduce the physical and cognitive impacts of aging. The problem of autonomous extraction of nocturnal movement times and respiratory rates using a pressure sensor array in bed was investigated.

Four segmentation methods were assessed for movement localization. A new movement detection segmentation algorithm accurately identified over 85% of movements. Six methods were evaluated for the extraction of breathing signals, including a recommended cascade that increased signal to noise ratio by 4.45 decibels. A proposed weighted voting algorithm was compared to two existing methods of data fusion. Finally, a reliability metric for validity evaluation was also presented.

Through use of the proposed methods, respiratory rates and movement times were reliably estimated from participants who slept with a pressure sensor array below their mattress. With these parameters available, decision algorithms could be developed to alert a caregiver when intervention is necessary.

Acknowledgments

Firstly, I would like to thank my co-supervisors, Dr. Rafik Goubran and Dr. Frank Knoefel for their insight, wisdom, and guidance.

Financial support for this research has been provided by Natural Sciences and Engineering Research Council of Canada (NSERC), Carleton University, and the Ontario Research Network for Electronic Commerce (ORNEC), with the participation of Nortel Networks and Tactex Controls Inc. Research equipment has been supplied by Tactex Controls Inc., including the pressure sensor array.

To all my friends, family, and dragonboat teammates who have supported and participated in my research, thank you very much. Invaluable time was spent by Amaya Arcelus to identify the breathing signals from which to build the breathing signal database. I would also like to mention Andrew Preston for providing discussion and distraction at the office. Particular acknowledgment goes to Aaron Holtzman for graphics editing and a wealth of general support.

Table of Contents

Abstract ii

Acknowledgments iii

Table of Contents iv

List of Tables ix

List of Figures x

Nomenclature xiv

1 Introduction 1

1.1 Motivation 1

1.2 Problem Statement 2

1.3 Overview 3

1.4 Objectives and Scope 4

1.5 Thesis Contributions 5

1.6 Thesis Outline 6

2 Background Review 8

2.1 Smart Homes 8

2.2 Sleep Assessment 10
2.2.1 Sleep Logs and Questionnaires 11
2.2.2 Sleep Laboratories 11
2.2.3 Sleep Assessment at Home 12
2.3 Pressure Sensors and Pressure Sensor Arrays 13
2.3.1 Types of Pressure Sensors 13
2.3.2 Pressure Sensor Images and Video 18
2.4 Pressure Sensor Array Monitoring 22
2.4.1 Properties of Bed-Based Pressure Signals 22
2.4.2 Monitoring by a Single Pressure Sensor - Literature 24
2.4.3 Monitoring by Pressure Sensor Array - Literature 25

3 Related Signal Processing Techniques **27**

3.1 Segmentation 27
3.1.1 Testing: The Control Limit Test 30
3.1.2 Testing: CUSUM Test 32
3.1.3 Distance Measure: Filtered Derivative 33
3.1.4 Distance Measure: Generalized Likelihood Ratio 33
3.1.5 Single Model Detector 35
3.1.6 Two Model Detector 36
3.1.7 Higher Dimensions 39
3.1.8 Use in Literature of Pressure Array Monitoring 41
3.2 Source Signal Extraction 42
3.2.1 Digital Filtering 43
3.2.2 Adaptive Filtering 45
3.2.3 Use in Literature of Pressure Array Monitoring 48

3.3 Frequency Estimation Algorithms 49
3.3.1 Zero Crossing / Peak Detection 49
3.3.2 Autocorrelation 49
3.3.3 Fourier Transform 51
3.3.4 Use in Literature of Pressure Array Monitoring 52
3.4 Sensor Array Data Fusion 52
3.4.1 Use in Literature of Pressure Array Monitoring 53
3.5 Validity Evaluation 54
3.5.1 Use in Literature of Pressure Array Monitoring 54

4 Experimental Setup **55**
4.1 Computer Simulation 56
4.2 Data Acquisition Setup 59
4.3 Observed Data Acquisition Experiment 59
4.3.1 Experiment Descriptions 60
4.3.2 Experiment 1 - Bed Entry / Bed Exit 61
4.4 Nocturnal Data Acquisition Experiment 64
4.5 Data Merging and Annotation 65
4.6 Breathing Signal Identification 66
4.7 Respiration Signal Database 67

5 Segmentation **69**
5.1 Methods 70
5.1.1 Control Limit Movement Detector 70
5.1.2 Two Model Control Limits 71
5.1.3 One Model CUSUM 72
5.1.4 Two Model Generalized Likelihood Ratio (GLR) Test 73

5.2 Evaluation 74
5.3 Results 74
5.3.1 Computer Simulation Results 75
5.3.2 Overnight Results 89
5.4 Discussion 96

6 Source Extraction **100**
6.1 Method 101
6.2 Evaluation 102
6.3 Results 103
6.3.1 Comparison of Extraction Algorithm Performance 103
6.3.2 Movement Suppression 108
6.3.3 Digital Filtering 109
6.3.4 Discrete Wavelet Transform Filtering 112
6.3.5 Adaptive Smoothing 114
6.3.6 Cascaded Enhancement 119
6.4 Discussion 120

7 Data Fusion **122**
7.1 Method 123
7.2 Pre-Summation Method 123
7.3 Reference Sensor Method 124
7.4 Proposed Method 124
7.5 Evaluation 127
7.6 Results 127
7.7 Discussion 129

8 Validity Evaluation **130**

8.1 Methods 130

8.1.1 Data Fusion 131

8.2 Evaluation 133

8.3 Results 134

8.4 Discussion 138

9 Conclusions **140**

9.1 Summary of Results 140

9.2 Recommendations for Further Research 141

9.2.1 Experimental Data Acquisition 141

9.2.2 Data Processing Method Investigation 142

9.2.3 Decision-Making 142

10 Contributions **144**

List of References **146**

Appendix A Experimental Procedure for Observed Experiments **155**

A.1 Protocol for Experiment 1 - Bed Entry / Bed Exit 155

A.2 Protocol for Experiment 2 - Position and Movement 157

A.3 Protocol for Experiment 3 - Breathing 159

A.4 Protocol for Experiment 4 - Ballistocardiogram / Heart Rate 160

Appendix B Experiment Questionnaires **162**

B.1 General Questionnaire 162

B.2 Sleep Diary Questionnaire 162

List of Tables

4.1 Types of respiration signals 68

5.1 Segmentation results near a 0.003 false alarm rate 77

5.2 Results for true positive rate > 0.90 78

5.3 Overnight segmentation 91

6.1 Decomposition coefficients used for reconstruction 113

7.1 A comparison of MSE and processing time by data fusion method . . 127

7.2 Comparison of overnight results by data fusion method 129

8.1 Movement corruption estimates 136

List of Figures

1.1 Bed-based monitoring by pressure sensor array 2

1.2 Block diagram of a autonomous monitoring system 3

2.1 Lexicle Limited's smart fridge 9

2.2 TAFETA's smart apartment bedroom 10

2.3 Switch sensor 14

2.4 Capacitive sensor 15

2.5 Kinotex pressure sensor 16

2.6 Creation of a pressure image 18

2.7 A pressure image from a toilet seat, photo credit: Karen Betz, PT . . 19

2.8 Pressure images courtesy of Tekscan Inc., with permission 20

2.9 Torso pressure pictures of a subject lying on back, front and side . . . 20

2.10 Pressure video of a supine subject 21

2.11 Typical temporal sensor outputs 22

2.12 Breathing signal examples: concurrent signals from one individual . . 23

2.13 Example ballistocardiograms 24

3.1 Sample segmentation points 28

3.2 Hard limits and control limits 30

3.3 Example Shewhart control chart 31

3.4 The filtered derivatives detector 33

3.5 Reference and test window schemes 37
3.6 Example voting scheme for video segmentation 40
3.7 Example segment boundaries of a pressure sensor signal 41
3.8 Extraction of source signals 43
3.9 Extraction of source signals with a digital filter 44
3.10 Extraction of source signals with an adaptive filter 45
3.11 The autocorrelation sequence of a 0.5 Hz sinusoid 50
3.12 Data fusion by pre-summation 52
3.13 Data fusion by reference sensor selection 53
4.1 Forty minutes of simulated data 56
4.2 Simulated movement and breathing 57
4.3 The sawtooth model of a breathing signal 58
4.4 Data acquisition setup 59
4.5 Screenshot of the MATLAB annotation GUI 66
4.6 Correlation of breaths to breathing signals 67
5.1 Control limits movement detection scheme 70
5.2 Two model control limits detection scheme 72
5.3 One model with CUSUM detection 73
5.4 Two model GLR detection 73
5.5 True positives in relation to false alarms 75
5.6 Logarithmic plot of detection time vs false alarms 76
5.7 Expected segmentation points 79
5.8 Control limits movement detector: varying L 80
5.9 Proposed movement detector boundaries 81
5.10 Control limits (p=2): varying L 82
5.11 Control limits (L=300): varying p 83

5.12 Control limits boundaries 84
5.13 CUSUM: varying threshold h 85
5.14 CUSUM boundaries 86
5.15 GLR: varying threshold h (L=50) 87
5.16 GLR: varying window size L (h=50) 88
5.17 GLR boundaries 89
5.18 Overnight data from a single sensor 90
5.19 Overnight data segmented with movement detector (L=300) 92
5.20 Overnight data segmented with control limits (L=300, p=2) 93
5.21 Overnight data segmented by control limits (L=75, p=2) 93
5.22 Overnight data segmented with the one model CUSUM test (h=100) 94
5.23 Overnight data segmented with GLR (h=50, L=50) 95
5.24 Overnight data segmented with GLR (h=200, L=50) 96
6.1 Mean enhancement by algorithm 104
6.2 Mean SNR enhancement by algorithm and type 105
6.3 Mean SFDR enhancement by algorithm 107
6.4 Respiration signal enhancement by movement suppression 108
6.5 Enhancement as a function of FIR filter order 110
6.6 Respiration signal enhancement by FIR filtering at order = 32 110
6.7 Enhancement as a function of IIR filter order 111
6.8 Respiration signal enhancement by IIR filtering 112
6.9 Enhancement as a function of DWT filter order 113
6.10 Respiration signal enhancement by DWT filtering 114
6.11 Adaptive smoothing enhancement as a function of delay 115
6.12 Adaptive smoothing enhancement as a function of β 116
6.13 Delay to convergence as a function of β 116

6.14 Adaptive smoothing enhancement by differing AR filter orders 117
6.15 Signal enhancement by MA filters, by filter order 118
6.16 Adaptive smoothing enhancement by signal type 118
6.17 Cascaded enhancement by signal type 119
7.1 Pre-summation data fusion 123
7.2 Reference sensor data fusion 124
7.3 Flow chart of proposed method 125
7.4 Proposed method of data fusion 125
7.5 Example of nocturnal breathing rates results with compared data fusion methods 128
8.1 Block diagram of rate estimation and reliability metric 132
8.2 Example respiratory rate estimation prior to validity evaluation . . . 135
8.3 Example reliability metrics 135
8.4 ROC curve for reliability metrics 137
8.5 Thresholding: true validity and false validity 137
8.6 'Valid' estimates: the example thresholded night 138

Nomenclature

List of Abbreviations

A/D	Analog to Digital
ACM	Autocorrelation Weighting
AR	Autoregressive
ARMA	Autoregressive Moving Average
BOS	Bed Occupancy Sensor
BCG	Ballistocardiogram
BPM	Breaths Per Minute
CUSUM	Cumulative Sum
DCT	Discrete Cosine Transform
DWT	Discrete Wavelet Transform

continued on next page

List of Abbreviations (con't)

ECG	Electrocardiogram
EEG	Electroencephalogram
EMG	Electromyogram
EMI	Electromagnetic Interference
FIR	Finite Impulse Response
FNE	First Night Effect
FFT	Fast Fourier Transform
FSR	Force Sensitive Resistor
GLR	Generalized Likelihood Ratio
IIR	Infinite Impulse Response
LCL	Lower Control Limit
LMS	Least Mean Squares
MA	Moving Average
MCM	Movement Corruption Metric
MRI	Magnetic Resonance Imaging

continued on next page

List of Abbreviations (con't)

MSE	Mean Square Error
NLMS	Normalized Least Mean Squares
NWRSCIS	Northwest Regional Spinal Cord Injury System
PSG	Polysomnography
RLS	Restless Leg Syndrome
RLS	Recursive Least Squares
ROC	Receiver Operating Characteristic
SCSB	Static Charge Sensitive Bed
SFDR	Spurious Free Dynamic Range
SNR	Signal to Noise Ratio
TAFETA	Technology Assisted Friendly Environment for the Third Age
UCL	Upper Control Limit

Symbology

Symbol	Description	Units
a_n	segment boundary if true	logical 0 or 1
A	Area	m^2
C	Capacitance	Farads
ϵ	dielectric constant	$\frac{C^2}{N \cdot m^2}$
d_n	distance measure	
$e_n, e[n]$	residual error at sample time n	
f_s	sampling frequency	Hz
g_n	test statistic	
$G_{(k,i)}$	reliability of estimate k for sensor i	
h	threshold	
L	window length	samples
$m[n]$	movement detected at time n	logical 0 or 1
μ	mean	
$\hat{\mu}$	estimated mean	

continued on next page

Symbology (con't)

Symbol	Description	Units
$M_{(k,i)}$	Percentage uncorrupted by movement during estimate k, sensor i	
ν	minimum drift	
ν	amount of statistical change	
p	samples per group	
$P_{(k,i)}$	Probability of sensor i, estimate k	
$P_n(l,m)$	video pixel at time n, location (l,m)	
ψ	mother wavelet function	
q	charge	Coulombs
r^2	coefficient of determination	
$R_{xx}[m]$	autocorrelation sequence at delay m	
s	scale factor	
σ	standard deviation	
σ^2	variance	
$\hat{\sigma^2}$	estimated variance	

continued on next page

Symbology (con't)

Symbol	Description	Units
τ	delay or translation	samples
$x[n]$	sensor output at sample time n	counts
$x_i[n]$	ith sensor output at sample time n	counts
$\boldsymbol{\phi}$	regression vector	
$\boldsymbol{w}$	adaptation weight vector	
$W[j]$	discrete wavelet transform coefficients at decomposition level j	
W_{c_k}	weighting score of cluster c, estimate k	

Chapter 1

Introduction

1.1 Motivation

As sensors are miniaturized and become ubiquitous in our lives, there exists a great potential for health monitoring. Ultimately, the use of hospitals may be reserved for critical care, while monitoring procedures can be done in an environment that is comfortable for the patient and inexpensive to the health care system: the home. Not only can patients with identified health problems be monitored, but people at risk of developing health problems, such as elderly people, can be monitored for changes in their habits. This allows a faster response time to a crisis and allows preventative steps to be taken before a critical event occurs.

A smart pressure sensor can be used as an unobtrusive device that derives useful information about the human who puts pressure onto it. Such a pressure sensor could be embedded in many areas of the home, including the bed, the floor, the bath, and the furniture. Its data could be used on its own or in conjunction with other sensors in a home monitoring system. For instance, a sensor located in a bed could assess long-term sleep quality, sleep habits, and weight trends as well as nightly respiration, heart rate and bed occupancy parameters. These indices could form

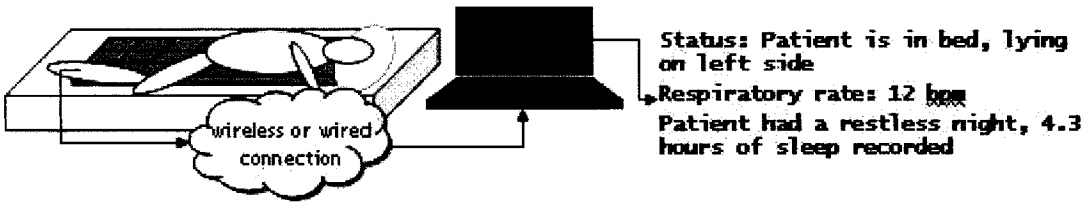

Figure 1.1: Bed-based monitoring by pressure sensor array

part of an autonomous monitoring system capable of sending warning and alarms to caregivers should an abnormal event occur. During check-ups, physicians could use the information to review the sleep patterns of the individual, as well as obtain reliable information on parameters such as weight changes.

By employing not just one, but an array of multiple sensors, spatial information can be noted and movements can be localized. Not only does spatial information localize movement, but it also introduces redundancy and allows for a more intelligent estimate of status. For instance, where an arm twitch on a bed pressure sensor may overcome the breathing signal of the upper torso, sensors located under the lower torso may still exhibit the breathing signal.

1.2 Problem Statement

Currently, the use of pressure sensors for patient monitoring is being pursued by a number of researchers, but many signal processing techniques have not yet been evaluated in this context. Moreover, intelligent and reliable autonomous processing of the data has yet to be sufficiently addressed.

This thesis examines the question of what signal processing algorithms are most appropriate for such data, based on its specific characteristics.

Furthermore, algorithms are analyzed for their effectiveness when applied to respiratory rate estimation. While a number of researchers have proven the ability of

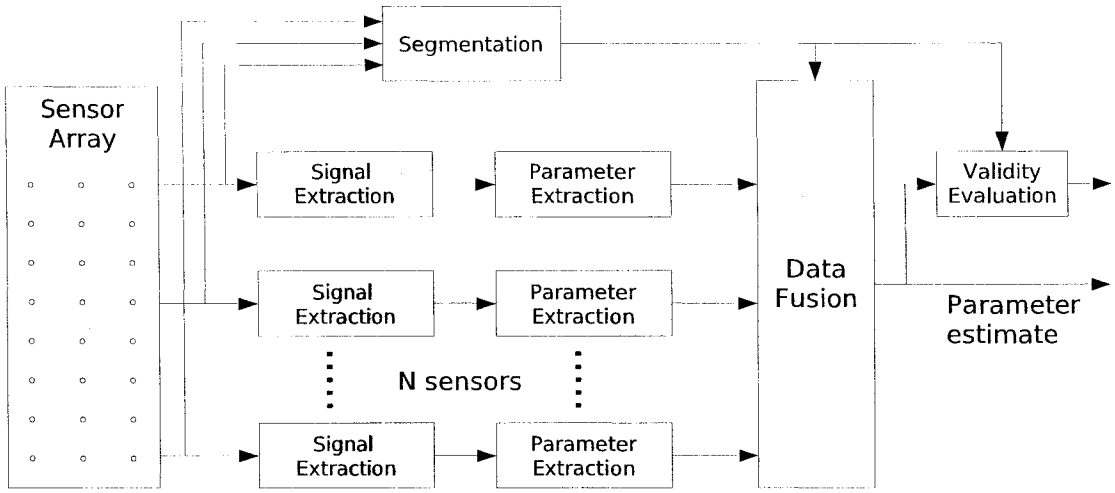

Figure 1.2: Block diagram of a autonomous monitoring system

pressure sensors to evaluate respiratory rate, few, if any, have compared algorithms or investigated improving the reliability of the results.

1.3 Overview

An intelligent pressure-based monitoring system would be able to discern between a person at rest or in motion. If the person is at rest, parameters such as respiratory rate should be available. Signals of interest would then be extracted from the pressure sensor data and the parameters estimated. Where multiple sensors report different values, a decision regarding the best choice would be taken. Finally, an estimate of the validity of this parameter would prevent inaccurate estimations.

The preceding description uses the data processing techniques of segmentation, signal extraction, data fusion, and validity evaluation. Each of these techniques are examined herein in order to create a system with the block diagram shown in Fig. 1.2.

1.4 Objectives and Scope

The following objectives have been identified:

- evaluate segmentation and movement classification algorithms
- compare methods of source signal extraction
- examine, propose, and compare data fusion methods
- propose a validity evaluation method

The thesis will focus on the digital signal processing required for autonomous monitoring of a human loading a pressure sensor array. Since the bed is a convenient place to do such monitoring, experimental results presented herein will use bed-based pressure sensor data. However, many of the identified techniques are useful for monitoring from pressure sensors placed in other locations such as chairs, the floor, hardware in the home, or inside clothing or shoes.

The analysis of results will not attempt any patient diagnosis, nor will designs of the pressure sensors or pressure sensor arrays themselves be proposed. All processing is considered in the context of the digital domain. Although some researchers have used analog filtering schemes prior to analog to digital conversion, this thesis assumes that processing is only available on digital signals from pressure sensors. Additionally, all processing is approached with the aim of real-time analysis. As such, only current and past samples may be used for analysis. This is sometimes referred to as causal, on-line, or sequential processing [1].

Many types of pressure sensors are available and are outlined in 2.3.1. The techniques presented herein for analysis of pressure sensor data are technology independent. Experimental data are obtained from a Kinotex pressure sensors mat, generously donated by Tactex Controls Inc.

1.5 Thesis Contributions

The following is a preview of contributions that were made during research for this thesis. This list can also be found in Chapter 10

- Application of segmentation techniques to overnight monitoring was investigated and results presented here. As part of this analysis, a modified control limits algorithm for movement detection was proposed and published at the IEEE International Workshop on Medical Instrumentation and Applications International 2006 (MeMea 2006) in Benevento, Italy, April 2006 [2]. The detection algorithm provides movement onset and offset detection with a low number of false alarms.

- Existing extraction methods were evaluated and a breathing signal extraction method was proposed based on these evaluations. The proposed method cascades a movement suppression algorithm with discrete wavelet transforms to create a mean 4.45 dB improvement in signal to noise ratio and 2.65 dB improvement in spurious free dynamic range.

- A method for data fusion of parameters estimated from an array of pressure sensors was proposed and compared to two fusion methods that have been in use in the field. This new method showed a marked improvement in mean square error, with up to 33% reduction in this error. A poster presentation regarding this method was accepted and presented at the 2005 Conference of the Canadian Association on Gerontology in Halifax, Nova Scotia, October 2005 [3].

- Validity evaluation was investigated and a method for validity evaluation by a reliability metric was proposed and published at the EMBS 2006 Conference in New York, USA , September 2006 [4]. This metric improved the true positive

rate by over 6%, compared to a standard reliability metric. The metric was also proposed for use as a restlessness index.

- Experimental evaluation required data collection. Data was acquired from experiments with ten participants. Four separate experiments were undertaken with participants under observation. Additionally, a nocturnal experiment acquired overnight data. A database of respiratory signals from multiple participants was created from the annotated observed experiments. These sources of data are useful not only for this thesis, but also for future work in this field.

- A MATLAB graphical user interface for sensor array data annotation was created. This interface enables fast and simple data annotation addition and correction.

1.6 Thesis Outline

Each Chapter presented in the thesis builds on the previous chapter's results in order to create the system shown in Fig. 1.2.

Chapter 2 provides an overview of previous work in the field, including an introduction to smart homes, sleep monitoring, and pressure sensor arrays. Chapter 3 continues the background review with a review of the included signal processing techniques and their use in pressure sensor monitoring literature.

Chapter 4 describes the experimental setup and the experiments that were undertaken for data collection. It includes data acquisition setup, computer simulation description, four observed experimental procedures, nocturnal experimental procedure, and the introduction of a breathing signal database.

In Chapter 5, segmentation algorithms are investigated by application to both

computer simulated data and to data from participants sleeping during the night. Three algorithms are investigated: control limits, one-model CUSUM and two-model GLR.

Chapter 6 evaluates methods of signal extraction in order to improve signal to noise ratio of a source signal. Digital filtering, wavelet filtering, adaptive filtering and a proposed movement suppression and filtering method are evaluated by application to breathing signal extraction.

In Chapter 7, data fusion methods are compared and a proposed system is introduced. The proposed method finds sensors of interest and applies a weighted voting technique to the parameters estimated from their output. This method is compared to pre-summation and a reference sensor technique.

Chapter 8 investigates validity evaluation by suggesting a reliability metric based on both a weighting of the estimation and corruption information. This reliability metric is applied to respiratory rate measurements taken from overnight data.

Concluding remarks are made in Chapter 9. A brief synopsis of the results presented in the thesis and suggestions for further research are presented here as well.

References are listed at the end and appendices that detail the experiment protocols, questionnaires, and derivations are also appended.

Chapter 2

Background Review

This chapter presents background information regarding smart homes, sleep assessments, pressure sensors, and pertinent literature in the processing of pressure sensor signals.

2.1 Smart Homes

Home appliances are including a greater amount of sensor technology that can respond to an occupant's specific habits and use. Where a fridge used to simply keep items cool, some fridges can suggest recipes or a shopping list based on the fridge contents (Fig. 2.1, sourced from [5]). The expansion of such intelligence into domestic life leads to the idea of the 'smart' home.

From learning your preferred lighting and temperature settings, to suggesting wardrobe choices based on the current weather [6], the smart home allows unobtrusive technology to support occupants' lifestyles. Challenges to be addressed in the implementation of smart homes include installation of devices in current homes, interoperability between devices, the lack of a system administrator, human oriented design, social implications, reliability, and careful study of the required intelligence

Figure 2.1: Lexicle Limited's smart fridge

and decision-making of the home [7].

The "Technology Assisted Friendly Environment for the Third Age" (TAFETA) project is aiming to harness the smart home ideal to aid physical and mental health in older adults. In particular, the project is researching and applying technology to address declining cognition, declining mobility, and increasing medical complexity in older adults. This research ultimately facilitates aging in place, defined as "not having to move from one's present residence in order to secure necessary support services in response to changing need [8]".

The TAFETA project has set up a smart apartment in the Elisabeth Bruyère Health Centre of the SCO Health Service in Ottawa, Canada. This apartment contains sensors embedded in everyday items. For instance, a sensor on the fridge door will alert the occupant if the door is open for too long. The apartment looks similar

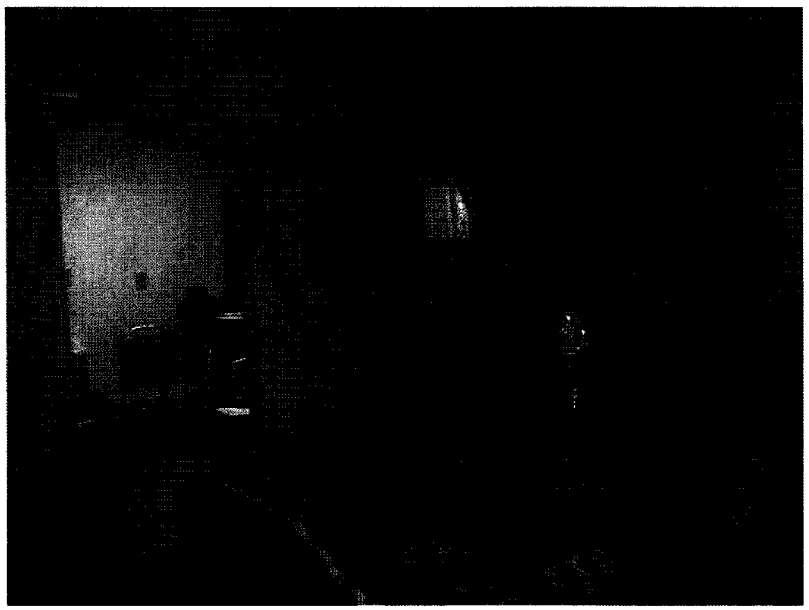

Figure 2.2: TAFETA's smart apartment bedroom

to other older adults' apartments since the sensors are quite unobtrusive. Figure 2.2 shows the bedroom in this apartment where a Tactex Controls Inc. Bed Occupancy Sensor (BOS) is located below the mattress of the bed to determine bed occupancy. The BOS also activates low-intensity lighting around the bathroom door when a bed occupant leaves the bed.

2.2 Sleep Assessment

Since the thesis proposes the use of the pressure sensor array for nocturnal monitoring, a brief review of sleep assessment is given here. Sleep assessment tools encompass the use of sleep diaries or logs, sophisticated equipment in sleep laboratories, or home-based devices.

2.2.1 Sleep Logs and Questionnaires

Sleep logs and questionnaires are subjective measurements of sleep, but are routinely used in sleep research due to their low cost and ease of implementation [9]. These questionnaires ask subjects about the quality of their sleep, the time they fell asleep, the times they woke up, and factors that may have affected their sleep during the night. Commonly used questionnaires include the the Pittsburgh Sleep Diary, the Pittsburgh Sleep Quality Index, the Insomnia Severity Index, and the Medical Outcomes Study Sleep Scale [9].

The Pittsburgh Sleep Diary is useful in the overnight research presented here as the questions it includes are specific to each night and are useful in the annotation and comparison of a nighttime data recording.

2.2.2 Sleep Laboratories

Sleep laboratories offer objective measurements of sleep using polysomnography (PSG), a test that records multiple parameters while the subject sleeps. PSG is considered the 'gold standard' of sleep assessment [10]. Electroencephalography (EEG) is used as part of PSG to determine sleeping and waking states as well as sleep phases.

The first night effect (FNE) is a common problem in sleep laboratories. Due to the strangeness of the environment, and perhaps just the knowledge that someone is watching you, a subject sleeps poorly or differently than normal at first. Although it is generally only considered a problem during the first night, it is possible that this effect lasts longer [11].

2.2.3 Sleep Assessment at Home

Nocturnal monitoring in the home must be simple to use and unobtrusive. Although a subject is in his or her accustomed sleep environment, FNE is still a factor [12]. It has been argued that sleep laboratories are preferred over home monitoring, even with their higher expense, since the expense incurred due to missed diagnosis may be high [10]. It is therefore imperative that monitoring in the home is not only inexpensive, but is also accurate. One of the current practices for objectively evaluating sleep at home is actigraphy.

Actigraphy

Actigraphy is the science of studying a person's activity levels using actigraphs, and has been demonstrated to be a reliable and valid means for sleep detection, circadian rhythm assessment, and restless leg syndrome detections [13]. Actigraphs are devices that are most often worn on the wrist, mimicking the look of a wristwatch. Instead of showing the current time, the actigraph collects movement data from an internal accelerometer. This data can then be uploaded to a computer for analysis with specialized software.

Since the memory available on the actigraph is limited, sampled activity is averaged over an epoch. An epoch can range from two seconds to greater than one minute. One minute epochs have been determined to be acceptable for clinical sleep assessment uses [13]. Some actigraphs allow a choice of epoch length. Shorter epoch lengths result in more data storage requirements and thus a shorter available recording span, while longer epochs may not provide adequate resolution.

The use of actigraphy in sleep evaluation is based on the presumption that there is a reduction in movement when a person is asleep [13]. Determining sleep periods

may be done manually, by a person trained to identify these periods from actigraph data; or automatically, by one of a number of available algorithms [14].

Although actigraphy is a valid measure of sleep times, sleep logs are still recommended in order to confirm an assessment. Also, clinicians are recommended to look at the raw data to remove any odd data [13]. Since people can lay still in bed without being asleep, actigraphy can overestimate the amount of sleep. In fact, this has been shown to occur to a small degree in the general population, and to a larger degree specifically in insomniac or depressive patients [14].

No first night effect has been related to actigraphy [14], [15], but most sleep/wake algorithms require more than one night's data.

2.3 Pressure Sensors and Pressure Sensor Arrays

While actigraphs are now well-known and are widely used for sleep assessment, pressure sensors are still in their infancy for use in home-based sleep assessment. Pressure sensor arrays measure the force applied at a number of sensing points. The use of multiple sensing points allows more localized data to be reviewed and allows for the creation of pressure images and videos. These arrays have been developed for applications such as tactile sensing in robots [16], plantar foot distribution assessment, and bed-based monitoring.

2.3.1 Types of Pressure Sensors

A number of different types of pressure sensors exist to transduce exerted pressure into a voltage signal. Most pressure sensors do not actually provide measurements in pressure units such as Pascals, but instead provide a non-unit based count value of relative detected pressure from a baseline. In fact, the measurand is often force

instead of pressure and the use of arrays of sensors allow an estimation of pressure (force per unit of area) [17].

Switch Sensors

Switch sensors give a binary output that denotes whether there is pressure on the sensor or not. A switch sensor may use two substrates that are normally not in contact with each other until the pressure pushes them together. Switch sensors have been used for pressure sensor arrays in floors [18].

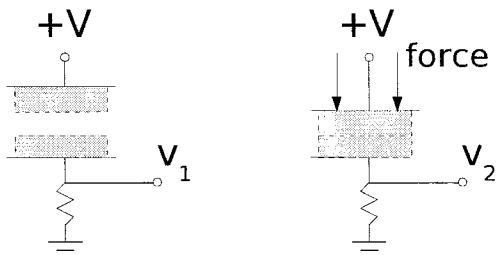

Figure 2.3: Switch sensor

Force sensitive resistor (FSR) sensors are types of switch sensors where the substrates are separated by a conductive material that allows current to flow. The resistance decreases when the substrates get closer together as contact pressure is increased. This allows a measure of force to be made [17].

FSRs have been used in a number of bed-based monitoring projects [19]. They have even been used in the soles of dancing shoes [20]. A disadvantage of FSRs is that their sensitivity may change after prolonged use [17] and. Non-linear behaviour and hysteresis of up to 21% has also been reported [21].

Capacitive Sensors

Capacitive sensors rely on the effect of small changes in distance between charged parallel plates to affect the voltage across them. Capacitance is defined as

$$C = \frac{\epsilon A}{d} \tag{2.1}$$

where C is the capacitance, A is the area of the plates, d is the distance between plates and ϵ is the dielectric constant. If the dielectric between the plates allows deformation, the distance d varies when a force is applied. As d is decreased, capacitance increases. For a static charge on the plates, the measured voltage is given by:

$$V(t) = \frac{q}{C(t)}, \tag{2.2}$$

where q is the static charge in Coulombs, $C(t)$ is the changing capacitance due to a distance change between the plates, and V(t) is the measured voltage across the capacitor [22].

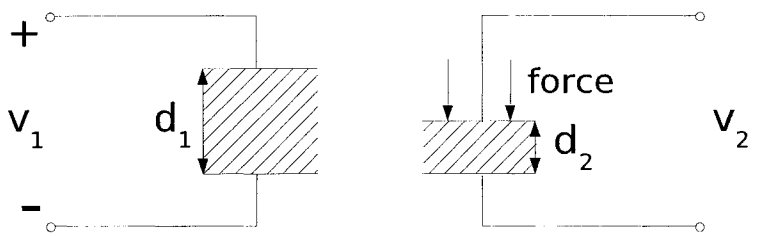

Figure 2.4: Capacitive sensor

The static charge sensitive bed (SCSB) uses such a capacitive sensor [23]. A high-resolution array of capacitive sensors was also created for robotic tactile sensing applications [24].

Hysteresis and non-linearity is a problem with capacitive sensors as the dielectric used between plates may not rebound very quickly [17]. Additionally, sensors such as the SCSB must be shielded [25] to avoid electromagnetic interference (EMI).

Piezoelectric Sensors

Compression of the material from an applied pressure changes its resistance value [26] and an output can be resolved from a voltage across this resistor. This is similar to FSRs, but piezoelectric sensors are made of ceramic materials, while FSRs use carbon or ink as the conductive layer [17].

Some researchers report that the disadvantages of piezoelectric sensors include hysteresis, contact noise, fatigue, low sensitivity, and nonlinear response [26]. However, it is also reported that piezoelectric materials have little hysteresis and instead their disadvantage lies in their temperature instability [17].

Kinotex Sensors

Kinotex uses optical fibres embedded in a foam medium, such as polyurethane, to sense pressure. Light is shone through optical fibres to a sensing point where it illuminates the end of a second optical fibre. The light is then conducted to a photosensitive receiver.

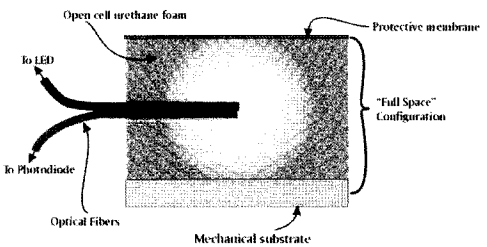

Figure 2.5: Kinotex pressure sensor

Kinotex takes advantage of the change of the amount of light that is conducted to the receiver when the foam is deformed. As a force is exerted on the material, it will compress, increasing the material's density and the light intensity that is scattered to

the receiving fibre. Fig. 2.5, included with permission from Canpolar East Inc. [27], shows the Kinotex pressure sensor.

Eq. 2.3 gives the light intensity E_s as a function of the material thickness. C_{sl} is a constant set according to the properties of the foam and x is the thickness [27].

$$E_s = E_0 - E_0 e^{-x/C_{sl}} \tag{2.3}$$

Some advantages of this type of sensor are an insensitivity to 60Hz interference, little or no damage from heavy loads, and a good price point [27]. Additionally, electronics may be located away from the subject, reducing the risk of electric shock.

However, polyurethane foam is affected by temperature [28], [29], and humidity [29]. As temperature increases, the foam can 'relax', becoming softer and more pliable. This effect can be seen even from small changes in room temperature or from body heat [30], although Canpolar East Inc., the creator of Kinotex, shows only small changes over a $-39°$C to 23°C temperature range [27]. Another property of the foam is hysteresis. Foam may not retain all of its firmness after compression [31].

Other types of Sensors

Pneumatic sensors have been used by a number of researchers in the area of pressure sensor monitoring [32], [33], [34], [35], principally for applications using only a single pressure sensor. Pneumatic sensors use applied pressure to mechanically move a transducer such as a potentiometer. Such pressure sensors reduce the risk of shock or damage to electronics since the electronics can be located away from the body [32].

Strain gauges that convert an applied pressure into a resistance are load cells [36]. These have been used with the aim to detect and classify movement in bed [36].

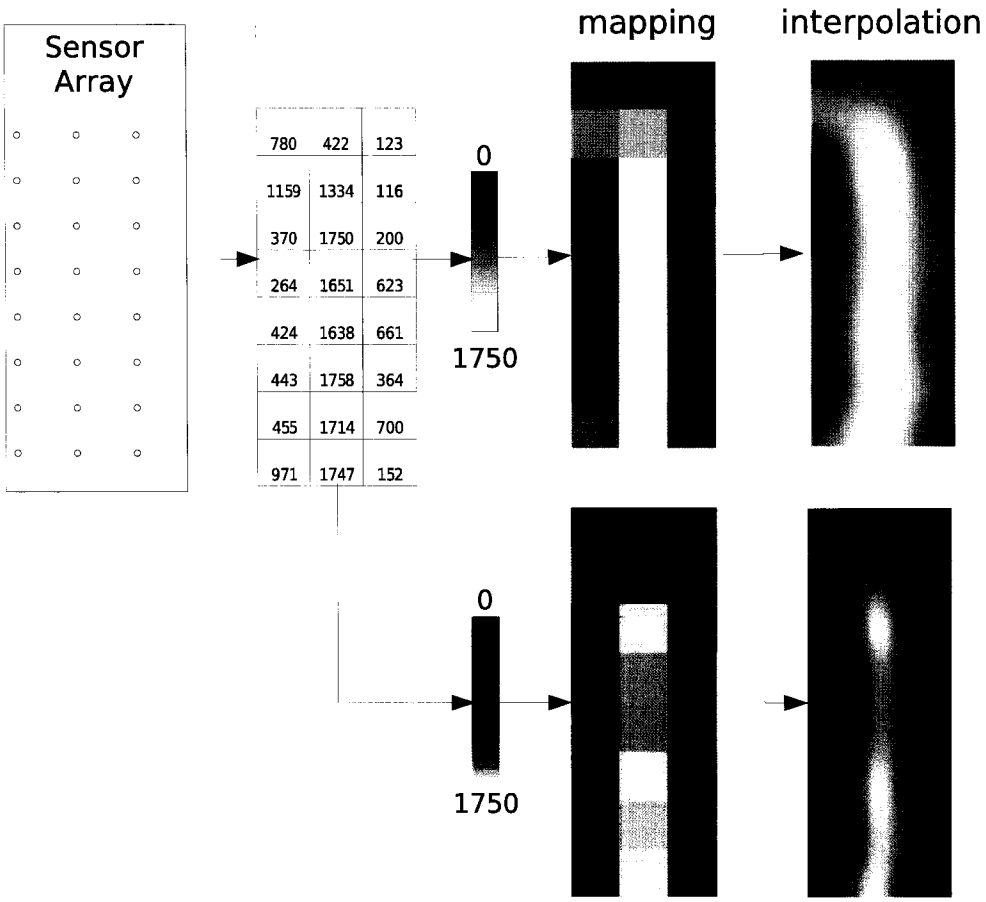

Figure 2.6: Creation of a pressure image

2.3.2 Pressure Sensor Images and Video

Pressure images can be made from the pressure distribution at an instance in time, or can be created from the average pressure outputs during a time period. Pressure sensor images have been used for analysis of objects on a floor [18], plantar foot pressure [17], and fingerprinting [37].

Fig. 2.6 is an outline of the steps required to create a grayscale or colour pressure image. To create the image, the data from each sensor is presented according to the column and row it occupies in the pressure sensor array. Intensity is assigned as the pressure output of the sensor normalized to the maximum possible output to give a

value between 0 and 1. This value can then be mapped to a pixel intensity, either to a grayscale image where the lightness of the gray is proportional to the intensity, or to a colour image where intensity is mapped to a colour scale, which often varies according to the software package used to create the images.

The final step in the process is optional. This step is image upsampling, or interpolation. Interpolated images can be easier for our eyes to interpret than boxy squares.

A number of example pressure images are presented here from pressure sensors in various locations, with pressure applied from various parts of the human body. The Northwest Regional Spinal Cord Injury System (NWRSCIS) website

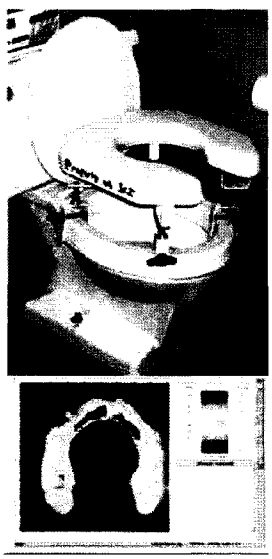

Figure 2.7: A pressure image from a toilet seat, photo credit: Karen Betz, PT

(http://depts.washington.edu/rehab/sci/) includes pressure images as part of an article on pressure mapping assessment. Fig. 2.7 is shown with permission, depicting a pressure distribution on a toilet seat [38].

Fig. 2.8 shows a pressure image of a foot, which may be used to assess plantar

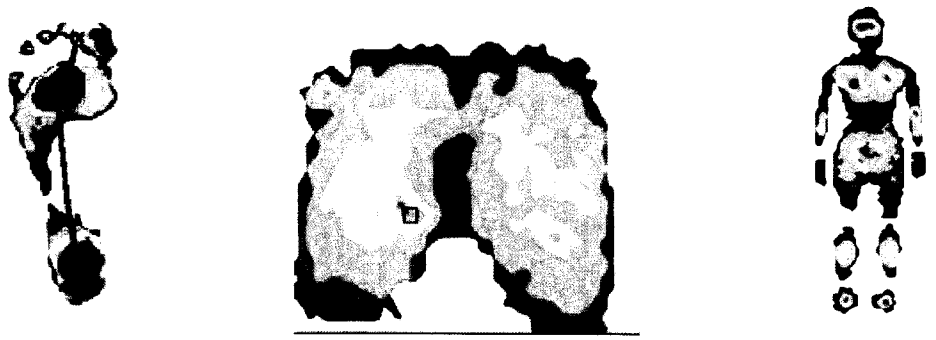

(a) Foot (b) Wheelchair (c) Person

Figure 2.8: Pressure images courtesy of Tekscan Inc., with permission

pressure distribution, the pressure image from the seat of a wheelchair, and the pressure image of a subject lying supine [39]. Fig. 2.9 presents grayscale pressure images

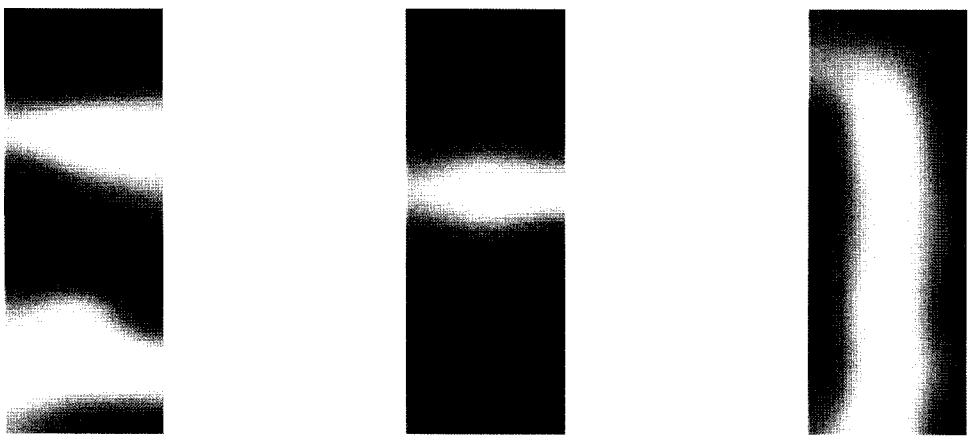

(a) Supine (b) Prone (c) Right

Figure 2.9: Torso pressure pictures of a subject lying on back, front and side

from a Tactex Controls Inc. BOS pressure sensor array. This array is not full-body sized and instead provides images of the torso only. The person's head is resting on a pillow, above the array and the pressure on the top area of the array is due to the shoulder. Lighter areas are more heavily loaded than darker areas.

Pressure sensor video can be made by sequencing pressure sensor images in time. Figure 2.10 presents three sequential frames, each spaced 2 seconds apart, of the same subject lying on his or her right side. The change is pressure from breathing is just visible as the shoulder (near the top) moves up and then down.

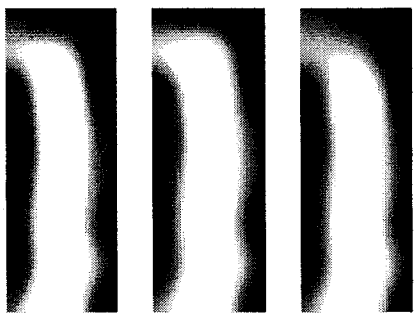

Figure 2.10: Pressure video of a supine subject

2.4 Pressure Sensor Array Monitoring

This section provides information regarding the properties of pressure signals acquired from a pressure sensor array located under a person lying down.

2.4.1 Properties of Bed-Based Pressure Signals

Bed-based pressure signals are not necessarily stationary or linear. Fig. 2.11 presents a temporal view of typical pressure signals.

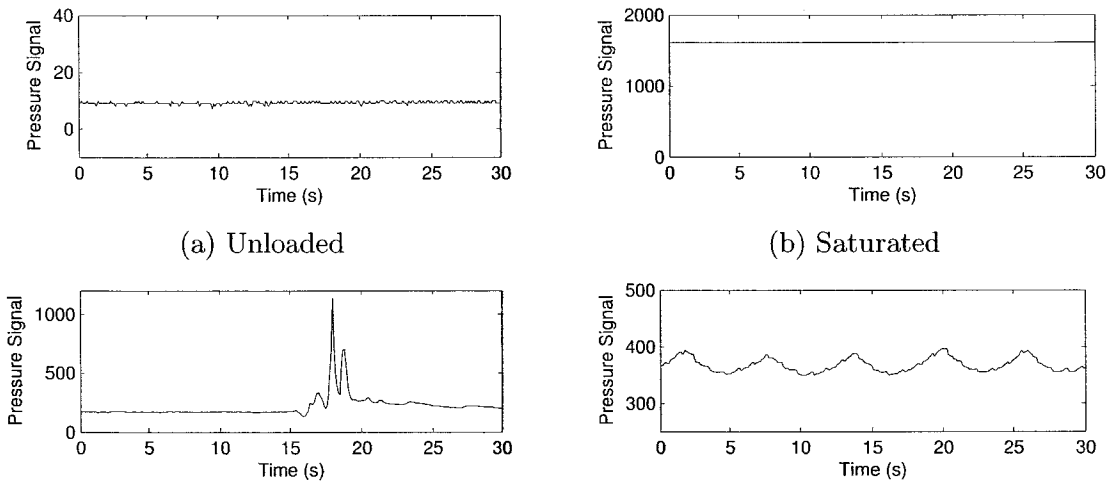

Figure 2.11: Typical temporal sensor outputs

Breathing Signals

Breathing signals from pressure sensors are different from person to person and even from a single person their shape may be different between sensor locations. Fig. 2.12 demonstrates some breathing pressure signals from one subject during the same period.

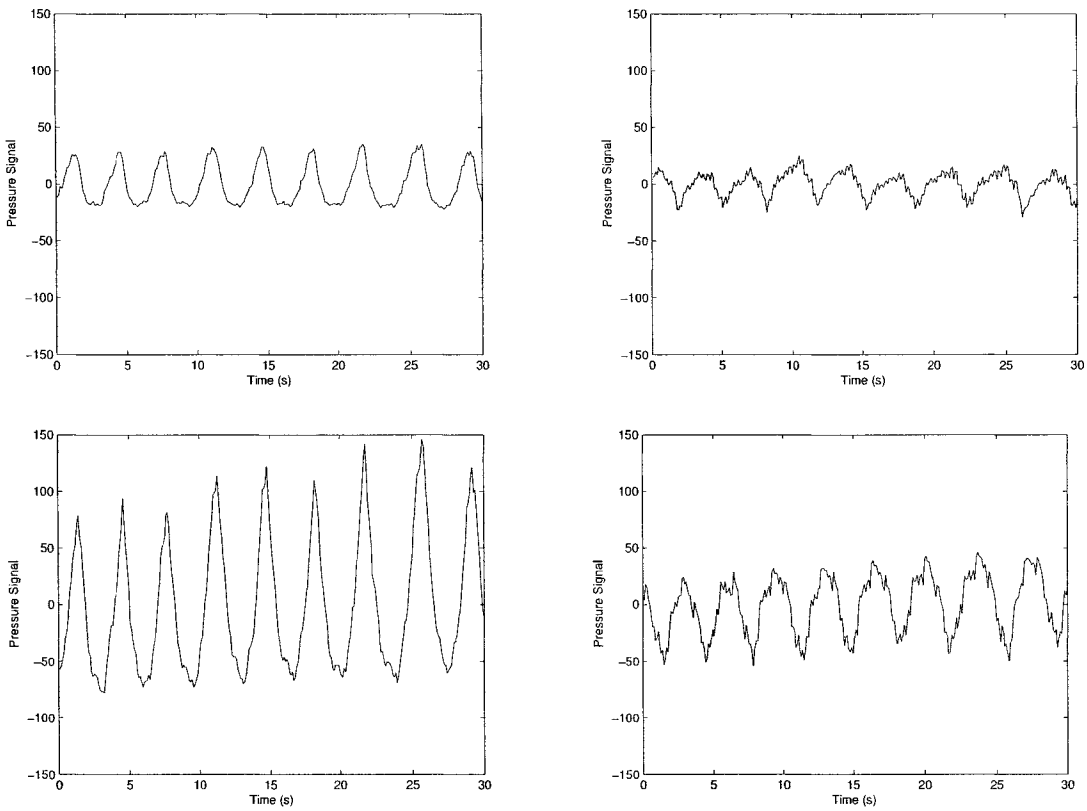

Figure 2.12: Breathing signal examples: concurrent signals from one individual

Clinical instrumentation for respiratory rate extraction should be able to detect rates between 2-50 breaths per minute (bpm), which is equivalent to 0.03Hz to 0.8Hz [40].

Ballistocardiogram

Ballistocardiogram (BCGs) are the pressure sensor signals that arise due to the pulse flowing through the body. Fig. 2.13 shows several ballistocardiograms (BCGs). The top two occur during a period when a subject is holding his or her breath. The bottom two are the BCGs seen while a subject is breathing. The BCG on the bottom left has a relatively high SNR but the BCG is more frequently seen as in the bottom

right with a lower SNR.

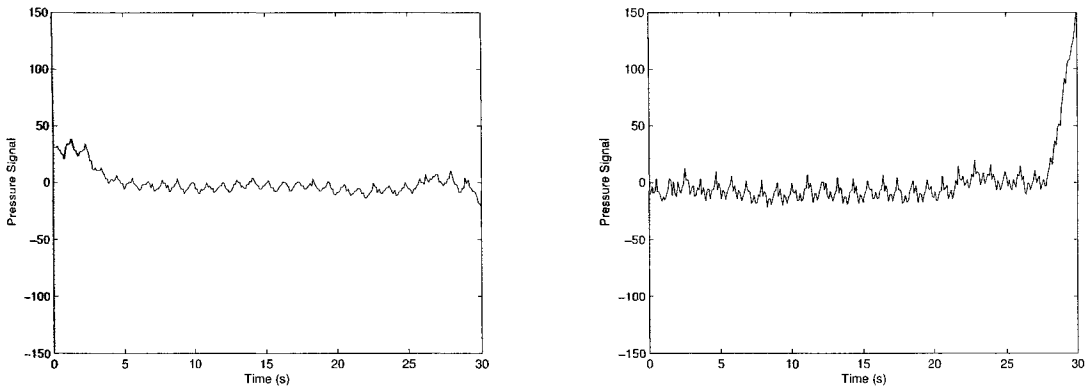

(a) BCGs during no respiration

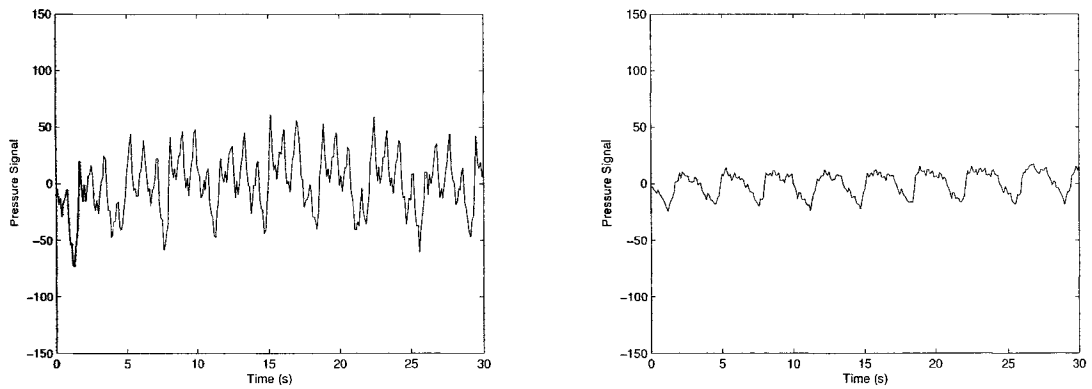

(b) BCGs with breathing

Figure 2.13: Example ballistocardiograms

2.4.2 Monitoring by a Single Pressure Sensor - Literature

The static charge sensitive bed (SCSB) was introduced in the early 1980's by Alihanka et al., [23] as a unobtrusive device to monitor (manually) respiratory rates and the BCG. Processing from data from the SCSB has continued and automated methods of respiratory and BCG analysis have been proposed [25]. The SCSB has also been part of a home health system, named TERVA, that incorporates a range of sensor

devices, including blood pressure monitors and activity monitors [41].

Other single sensors systems have been proposed: [42], [35]. A notable recent use of a single-sensor monitoring system was presented by Watanabe in 2005 [35]. This system was developed to calculate heart rate and breathing rate from an air cushion below a bed. These parameters were used to accurately estimate sleep stage [43].

2.4.3 Monitoring by Pressure Sensor Array - Literature

The use in literature of pressure sensor arrays for patient monitoring has grown since the late 1990's. The following section presents a resume of the work that has been done previously in the field of pressure sensor array monitoring.

Nishida et al. used 221 pressure sensors in a bed to determine bed occupancy as well as posture in bed. Initially, this system detected respiratory rate from these sensors [44], but more recent publications have proposed the use of microphones [32] and video cameras [45] to find the occupant's respiratory rate and detect sleep apnea.

Harada et al. have used pressure sensor mats located under the pillow [46] and under the mattress [47], [48] to determine restlessness, position, respiratory rates, and heart rates. A position tracking system was also developed based on the same sensor array outputs [49], [50].

The SleepSmart project used an array of 54 sensors at a 10 cm spacing under the torso and a 20 cm spacing between elements under the legs [19]. Respiratory rate, heart rate, body center of mass, and a restlessness index were calculated. Additionally, 54 temperature sensors enabled temperature to be recorded. In-lab testing showed that heart rate could be determined successfully when the heart was located less than 5 cm away from a sensor, but in the field, during overnight experiments, heart rate measurements were not reliable [19].

Small arrays have also been employed, using less than five sensors. Adami et al.

used an array of four load cells under each leg of a bed to measure applied weight [51]. With this system, sleep profiles of subjects in a nursing home were created over a one month period. Additionally, a movement detection system and a method for classification into 'big' and 'small' movements was proposed [36]. Movements were detected through mean square pressure differences. Classifications were made by feature extraction of discrete wavelet transform (DWT) coefficients and the duration of movements. Linear classifiers were input with these features and their output was combined by a weighted voting scheme [36]. Chen et al. [33] used two water-based sensors under a pillow for detection of respiration and pulse.

Chapter 3

Related Signal Processing Techniques

This chapter will detail signal processing techniques that could be applied to autonomous pressure sensor array monitoring. A resume of the state of the art in the application of these techniques to such monitoring is given at the end of each section. This includes an overview of segmentation, source signal extraction, frequency estimation, multi-sensor data fusion and reliability techniques.

3.1 Segmentation

Segmentation may be referred to as 'partitioning'. This technique divides a signal which undergoes abrupt changes at one or multiple locations into several quasi-stationary parts [1]. It is an application of change detection [52] or abrupt change detection techniques. Segmentation can also refer to the classification of a segment after partitioning [53], or the 'diagnosis' of why the signal changed [54]. In this thesis, segmentation will only refer to segment boundary detection, without diagnosis of what has changed.

For a single dimension time-based signal, segmentation delineates when changes occur in the signal. Examples of applications of single dimension signal segmentation

include EEG analysis [55], [56], [57] and audio segmentation for speech and sound recognition [53]. Fig. 3.1 shows possible segmentation points on an example one-dimensional signal.

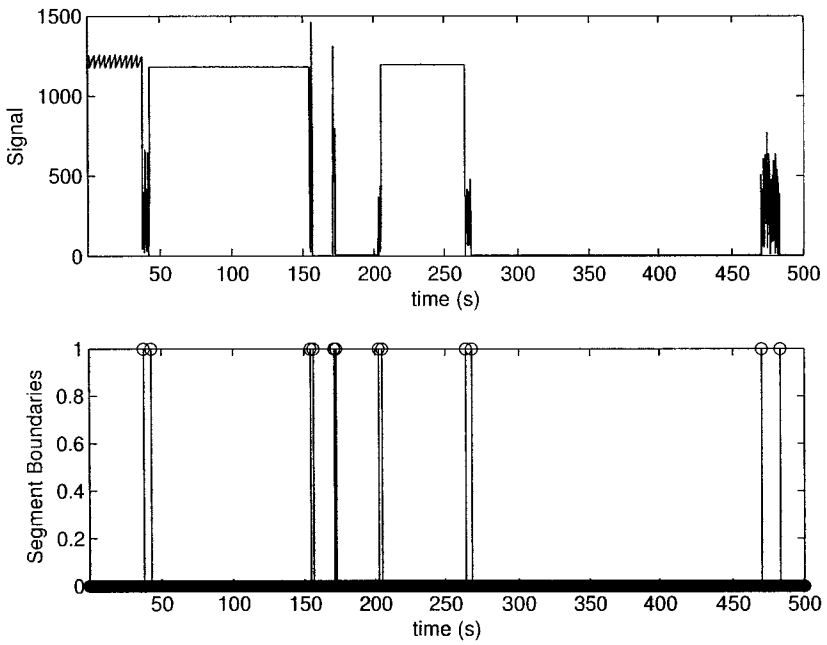

Figure 3.1: Sample segmentation points

Two dimensional segmentation is used extensively in image segmentation [58], including medical imaging [59], [60], and it also finds a place in multi-channel EEG recordings [61].

Three-dimensional segmentation can be used to detect scene changes in video feeds or to create indexing for of a video database [62], [63]. Video can comprise four-dimensions when colour channels are included. Abrupt video changes between one scene and another are more easily detected than gradual scene changes that use techniques such as fades or dissolves [62], [63].

Ideally, a change detection algorithm would yield few false alarms and missed

detections while the delay between the change detection and the actual change occurrence would be minimized [54], [64], [52]. The false alarm rate can be given as the expectation of an alarm when no change occurs [64]. The optimization of an algorithm will often try to minimize the delay to detection at a fixed false alarm rate [52].

Another desirable feature of an algorithm is to display symmetrical detection [52]. This occurs if the segment boundaries are detected similarly whether the data is analyzed forward in time or backward in time. This third feature is especially important for the detection of drops in energy, or segment boundaries where the new variance is less than the previous variance [54].

At the beginning of a data set and after each newly found segment boundary, some algorithms require a 'dead interval' during which the detector is not activated [54]. For instance, threshold values that are calculated from the data itself may need to be reset and cannot be recalculated until enough new data is present. Since new segments are not detected during this time, the dead interval must be less than the minimum required detectable segment length. It has been argued that it must be less than or equal to 70% of this minimum segment length [1].

While there are many applications of segmentation for one or multiple dimensions, the underlying segmentation techniques are quite similar. Two methods of threshold testing are described, the control limit test and the cumulative sum (CUSUM) test in 3.1.1 and 3.1.2 respectively. Two methods of distance measurements, the filtered derivative distance and the Generalized Likelihood Ratio (GLR) are introduced in 3.1.3 and 3.1.4. Single model (Sec. 5.1.3) and two-model (Sec. 3.1.6) approaches are also examined. Finally, the application of segmentation methods to multiple dimensions is considered in Sec. 3.1.7.

3.1.1 Testing: The Control Limit Test

An early method of change detection comes from the field of quality control in the form of the Shewhart control chart. Introduced in 1924 by Walter Shewhart as the 'statistical control chart', the chart is used to detect a change in the state of control of a manufacturing process. Control limits are soft limits within the hard tolerances required of the output manufactured item. When the output falls outside of these limits, a change in the state of process control can be detected and corrected before outputs fall outside of the hard tolerances required [65].

Fig. 3.2 demonstrates these limits. H_U and H_L are the upper and lower hard limits, while UCL and LCL denote the upper and lower control limits. μ denotes the mean, which should fall between UCL and LCL.

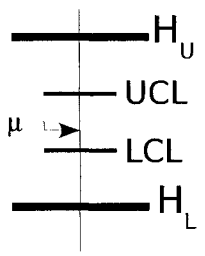

Figure 3.2: Hard limits and control limits

The Shewhart control chart plots the mean of groups of samples, denoted $\bar{m_k}$. The groups of samples used to calculate each $\bar{m_k}$ are comprised of p successive samples.

$$\bar{m_k} = \frac{1}{p} \sum_{n=p*(k-1)+1}^{k*p} x[n] \tag{3.1}$$

Fig. 3.3 shows an example control chart with one group mean outside of control limits. Groups of four samples each ($p = 4$) are advocated by Shewhart [65].

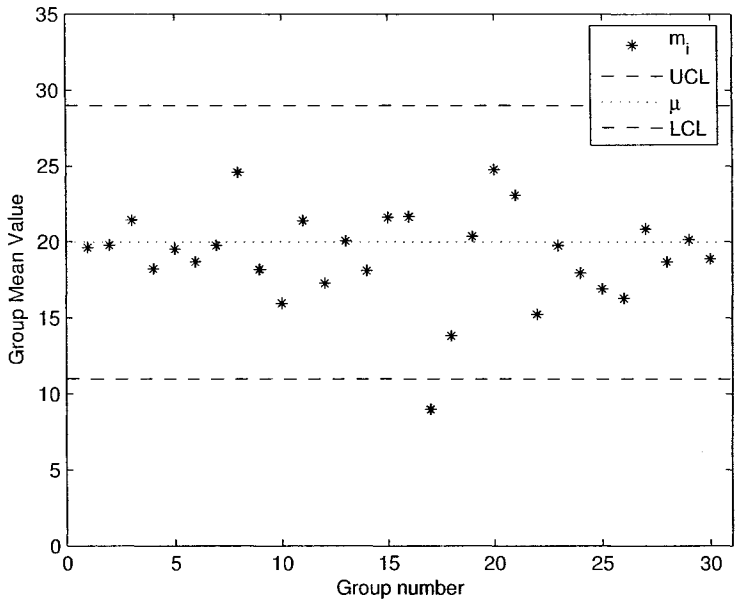

Figure 3.3: Example Shewhart control chart

UCL and LCL can be assigned by:

$$UCL = \mu + \frac{3\sigma}{\sqrt{p}} \tag{3.2}$$

$$LCL = \mu - \frac{3\sigma}{\sqrt{p}} \tag{3.3}$$

where μ is the mean and σ is the standard deviation of the samples. This assignment of control limits ensures that the probability of staying within the control limits is 0.9783 for a normal distribution, but cannot be ensured for an unknown distribution [65].

When the mean and standard deviation are unknown, they may be estimated from the data. Unbiased estimates of μ and σ may be found using the following equations [66]:

$$\hat{\mu} = \frac{\sum_{k=1}^{L} \bar{m}_k}{L} \tag{3.4}$$

$$\hat{\sigma} = \frac{\sum_{k=1}^{L} \bar{s_k}}{L} \frac{\sqrt{p-1}\Gamma(\frac{p-1}{2})}{\sqrt{2}\Gamma(\frac{p}{2})} \tag{3.5}$$

where p is the number of samples per grouping, L is the number of groupings used to estimate the control limits, Γ is the gamma function and $\bar{s_i}$ is the standard deviation of each grouping.

3.1.2 Testing: CUSUM Test

The cumulative sum (CUSUM) test also has a background in quality control [66]. The CUSUM test uses a stopping rule $g_n > h$ that detects both abrupt changes and slow changes. g_n is formed by an accumulation of distances, d_n as is shows in Eq. 3.6 [54] and h is a threshold.

$$g_n = g_{n-1} + d_n - \nu; \tag{3.6}$$

Once g_n rises above the threshold h, an alarm is signaled, the current segment is determined to end and a new one is begun. The test statistic d_n can be any desired distance measure, such as the distance of the current sample from the mean (for mean change detection). The factor ν ensures that system drift does not cause a large number of false alarms. ν can be defined as the minimum d_n since the beginning of the segment.

$$\nu = min(d_k) \quad \forall n_a < k \leq n \tag{3.7}$$

n_a is the beginning of the segment, or the last sample at which an alarm was signaled [54].

Since this test only looks for unidirectional changes, two tests, an upper limit test and a lower limit test must be used in order to detect changes in both direction. These tests, from [64], are summarized in Eq. 3.8 and Eq. 3.9

$$g_{n_u} = max(g_{n-1_u} + d_n - \nu, 0) \tag{3.8}$$

$$g_{n_l} = max(g_{n-1_l} - d_n - \nu, 0) \tag{3.9}$$

An alarm occurs if either g_{n_u} or g_{n_l} is greater than h and they are reset to zero after the alarm. The max function ensures that they does not drift too far away from the threshold.

The CUSUM detector requires a distance input d_n. The next two sections will review two popular distance measures.

3.1.3 Distance Measure: Filtered Derivative

A simple distance measure is the difference from sample to sample, smoothed by a low pass filter. This is called a filtered derivatives detector [54] and its block diagram is shown in Fig. 3.4.

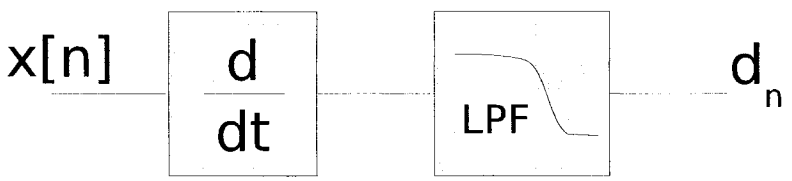

Figure 3.4: The filtered derivatives detector

3.1.4 Distance Measure: Generalized Likelihood Ratio

The Generalized Likelihood Ratio (GLR) is based on the likelihood ratio test. A likelihood ratio test compares the hypothesis of no change in the system statistics to the hypothesis of a change in the system statistics as follows:

H_0: no change has occurred

H_1: change has occurred

To test these hypotheses, the probability that the samples belong to the original distributions is examined against the probability that the samples belong to a new distribution. The log-likelihood ratio is given as

$$d_n = 2 \ln \frac{p(y_n|H_1(k,\nu))}{p(y_n|H_0)} \tag{3.10}$$

which compares the probability that there is a change during the samples y_n, with a change in statistics ν after sample time k, to the the probability that there is no statistical change over all n samples of y.

The probability of a number of samples belonging to a given distribution is the product of the probabilities of each sample belonging to that distribution. For an independent Gaussian signal, this likelihood l_n of n samples belonging to a distribution with mean μ and standard deviation σ is given by [64]:

$$l_n(\mu,\sigma) = \frac{e^{-\sum_{i=1}^{n} \frac{(y_i-\mu)^2}{2\sigma^2}}}{(\sigma\sqrt{2\pi})^n} \tag{3.11}$$

where y_i is the observed noisy signal at sample i.

The likelihood that a change occurred at sample k is the likelihood that samples prior to k belonged to an initial distribution multiplied by the probability that samples from k on belonged to a new distribution. The log-likelihood ratio of this with Gaussian distributions becomes

$$d_n = 2 \ln \frac{l_{1:k-1}(\mu_0,\sigma_0) * l_{k:n}(\mu_1,\sigma_1)}{l_{1:n}(\mu_0,\sigma_0)} = 2 \ln \frac{l_{k:n}(\mu_1,\sigma_1)}{l_{k:n}(\mu_0,\sigma_0)} \tag{3.12}$$

When the distance d_n is maximized over both possible statistical changes ν and change times k, we have the GLR method [54].

Since the actual mean and variance are often not known, estimation of these parameters based on previous samples may be required [64]. These estimates can be made by computing a model for the signal, resulting in the single model detector.

3.1.5 Single Model Detector

When a signal can be represented by a model, such as a moving average (MA) or autoregressive (AR) model, the model outputs may be used to estimate when changes occur. A detector using two models is outlined in the next section, Sec. 3.1.6.

The model is estimated using an adaptive filter and the error of the actual output signal to the estimates is examined. If the error is white noise, the model is following the signal well, but if the error becomes coloured, the estimated model parameters will be changing. By capturing these error or parameter drifts, the detector can sense when the signal changes [54]. This is sometimes termed a 'whitening filter' [54]. The model can be created by using an adaptive filtering technique such as recursive least squares or least mean squares.

A classic distance measure extracted from the residual error signal is as follows [54]:

$$d_n = \frac{1}{\sqrt{2L}} \sum_{n=1}^{L} \left(\frac{e_n}{\sigma_0^2} - 1\right) \tag{3.13}$$

where e_n is the residual error at sample time n, L is the window length, and σ_0 is the variance of the errors.

The CUSUM test may be used with the single model's distance measure to detect segment boundaries [54], [64].

$$g_{n_u} = max(g_{n-1_u} + d_n - \nu, 0) \tag{3.14}$$

$$g_{n_l} = max(g_{n-1_l} - d_n - \nu, 0) \tag{3.15}$$

$$a_n = g_{n_u} > h \quad || \quad g_{n_l} > h \tag{3.16}$$

Segments boundaries are placed where a_n is true.

It has been argued that a one model detector does not deal well with the case of a new $\sigma_1 < \sigma_0$ [67]. This means this test may not be symmetrical as backward detection will yield different results than forward detection. The two model detector may relieve this problem [67].

3.1.6 Two Model Detector

A two-model detector uses one model to act as a reference and a second model to compare the current samples to the reference for segment boundary detection. The reference model may be of fixed length at the beginning of the segment or may grow to include all available samples. Fig. 3.5 shows the possible configurations. The growing window schemes may provide better results since a small reference window size may result in a poor estimation of the model [52]. The growing model takes into account all of the available information in order to create the reference model [68].

Several distance measures between the reference and the test model have been introduced:

- Autocorrelation function procedure: energy difference between autocorrelation functions [69]
- Spectral error measure procedure: MA model prediction error autocorrelation function ratios [61].
- AR model residual error GLR [70], [1]

These three algorithms have been compared, with results showing that the GLR algorithm locates the highest number of correct boundaries, with the lowest false alarm rate and delay to detection [68].

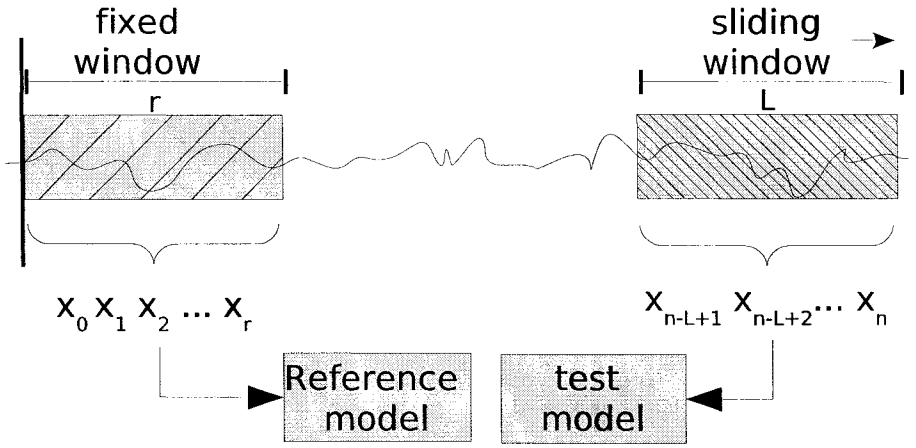

(a) Fixed reference

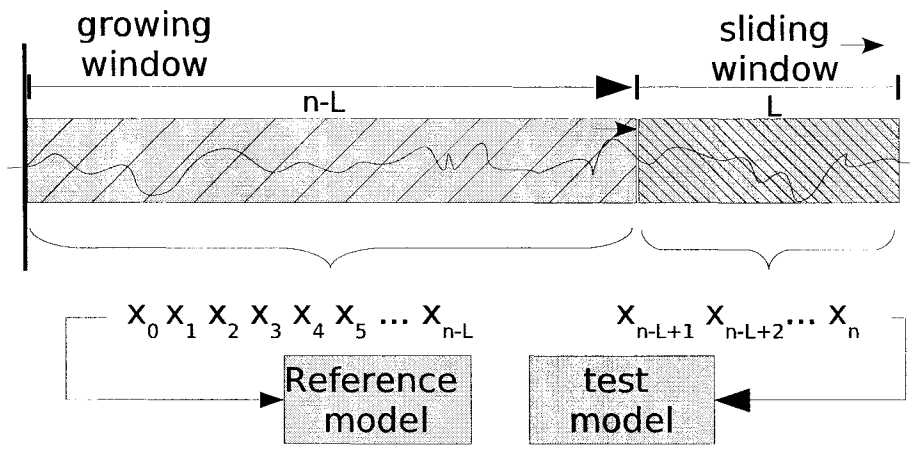

(b) Growing reference

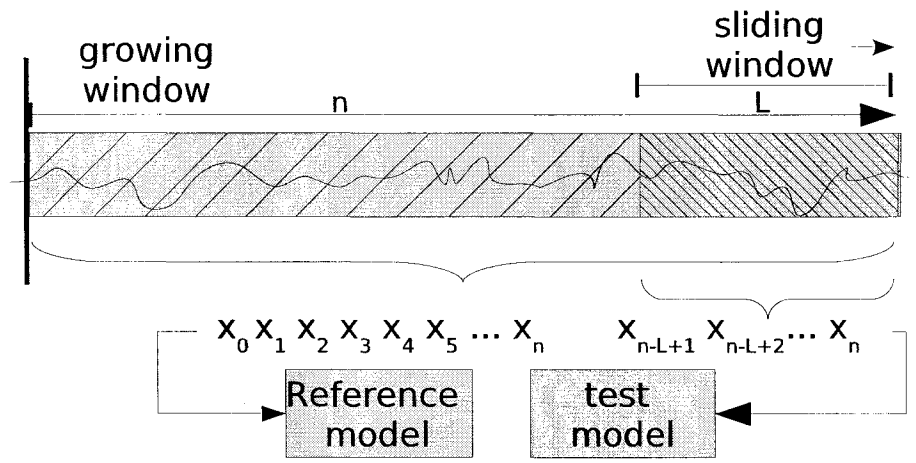

(c) Up-to-date growing reference

Figure 3.5: Reference and test window schemes

The two model detector allows simplification to GLR for a Gaussian signal, since maximization is not needed for the distance measure reduced to Eq. 3.17 [54], [64].

$$d_n = -\frac{(x_n - \mu_2)^2}{\sigma_2} + \frac{(x_n - \mu_1)^2}{\sigma_1} + \ln\frac{\sigma_1}{\sigma_2} \tag{3.17}$$

With this result, a difference measure can be constructed based on the estimated mean and standard deviation from the reference window and from the test window. One simple method of reference and test window comparison uses unbiased estimators of the mean and standard deviation of the reference signal and the test signal [64]. This method, using the 'up-to-date' growing window configuration, is summarized in Eq. 3.18 through 3.21.

$$\hat{\mu}_{ref} = \frac{1}{n - n_0}\sum_{k=n_0}^{n} x[k] \tag{3.18}$$

$$\hat{\mu}_{test} = \frac{1}{n - n_0 - L}\sum_{k=n-L+1}^{n} x[k] \tag{3.19}$$

$$\hat{\sigma}_{ref} = \frac{1}{n - n_0 - 1}\sum_{k=n_0}^{n} (x[k] - \hat{\mu}_{ref})^2 \tag{3.20}$$

$$\hat{\sigma}_{test} = \frac{1}{n - n_0 - L - 1}\sum_{k=n-L+1}^{n} (x[k] - \hat{\mu}_{ref})^2 \tag{3.21}$$

Here, $\hat{\mu}_{ref}$ is the estimated mean of the reference window, $\hat{\mu}_{test}$ is the estimated mean of the test window, $\hat{\sigma}_{ref}$ is the estimated standard deviation of the reference window, and $\hat{\sigma}_{test}$ is the estimated standard deviation of the test window. L is the length of the test window, $x[k]$ is the input at sample time k, n is the most recent sample time and n_0 is the sample time of the first sample of the segment.

3.1.7 Higher Dimensions

The previous techniques have been presented for single dimension signals. For signals of higher dimension, three methods for incorporating the additional information available are as follows:

- dimension reduction by summation of distances
- voting
- dimension reduction by feature extraction

The following examples examine these methods as applied to video analysis.

One example of dimension reduction by summation of distances in video analysis is to calculate the sum of the time-based differences at each $P_n(l,m)$, representing a pixel at sample time n at l in the vertical direction and m in the horizontal direction [62].

$$d_n = \sum_{k=1,l=1}^{L,M} |P_n(l,m) - P_{n-1}(l,m)|; \tag{3.22}$$

The video frame here is LxM pixels. This distance measure may then be used with any of the previously defined segmentation tests.

The second method of a voting scheme applied to video analysis may use a likelihood ratio test over multiple pixels or on a block-wise basis. The block-wise basis is described at the end of this section. Once the number of pixels or blocks reporting a change exceeds the voting threshold requirements, a change is accepted [62]. Eq. 3.23 shows the equation involved where hv is the voting threshold required for the stopping test.

$$a_n = (\sum_{k=1,l=1}^{M,N} g_{n,i} > h_i) > hv \tag{3.23}$$

Fig. 3.6 illustrates such a scheme, where light blocks are 'no change detected' and dark blocks are 'change detected'. Once greater than two blocks ($hv = 2$) out of the

four blocks detect a change, the alarm is raised. Here, the last frame is detected as the start of a new segment.

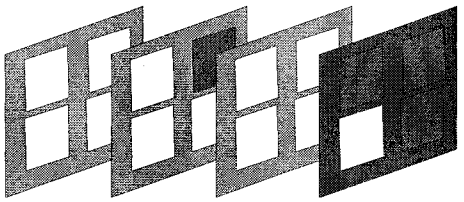

Figure 3.6: Example voting scheme for video segmentation

The third method is to use feature extraction for dimension reduction. An example extracted feature from a video is an intensity level histogram [62] for each frame. The histogram converts the three dimensional signal into a two dimensional signal of time and histograms. Either of the previous two methods, summation or voting, can then be applied. While it is possible that two very different images could have the same histogram, Zhang et al. argues that this probability is low [62]. Another feature extraction method is to examine the Discrete Cosine Transform (DCT) coefficients that are available from compressed MPEG video [63].

Higher dimensions also allow statistical parameters to be estimated in one or two dimensions while distances d_n are compared in the other dimension. In a video feed, for instance, the intensity values in a block or region in a frame can be examined for their mean and variance and then these parameters used in a likelihood ratio test across time [62]. This is the block-wise method mentioned earlier. The advantage for video segmentation using blocks is that small movements in a block will not create false alarms [62].

While segmentation schemes for multiple dimensions are concerned with reducing the number of dimensions, sometimes uni-dimension signals are converted into multi-dimension signals and processing continues as previously detailed. Researchers have used this approach with EEG signals [55], [71]. These signals are decomposed by

wavelet analysis into multiple signals and segments are found by analyzing each of the wavelet decompositions.

3.1.8 Use in Literature of Pressure Array Monitoring

Segmentation would allow a night to be broken up into different phases. Fig. 3.7 shows a pressure signal from a single sensor acquired during a 15 minute experiment with a participant and the possible segment boundaries. Each segment is composed of a stable position and posture in the bed, delineated by regions of movement between positions, segmented manually by observation.

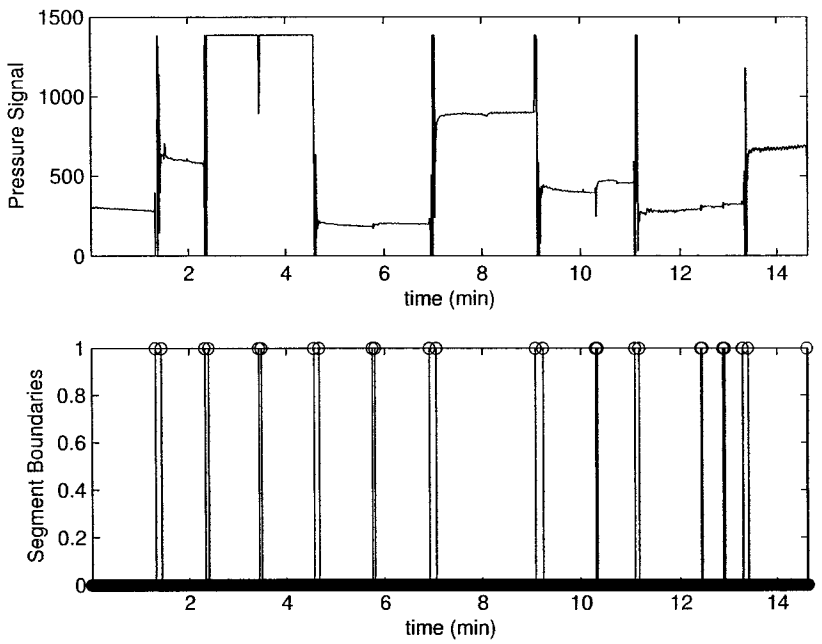

Figure 3.7: Example segment boundaries of a pressure sensor signal

Segmentation is yet to be formally presented in conjunction with bed-based monitoring, however a movement detection algorithm has been presented based on mean square pressure difference between overlapping reference windows [36]. This could

be classified as a filtered derivatives segmentation algorithm. However, segmentation techniques have been used in other biomedical applications.

Control limits have been used for the most part for production process monitoring [66], but have also been used in a biomedical context for electrocardiogram (ECG) segmentation [72]. Additionally, appropriate thresholds for video segmentation have been found using control limits [62].

The CUSUM test has been used in a number of biomedical applications. Examples include uterine electromyogram (EMG) detection [71], real time analysis of EEG signals in intensive care [57], and ultrasound image contour segmentation [60].

The Generalized Likelihood Ratio (GLR) has also been used in a number of biomedical applications, including in EEG segmentation [55] and magnetic resonance imaging (MRI) change detection [73].

3.2 Source Signal Extraction

Pressure signals from a person lying on top of a pressure sensor are a combination of weight, respiration, BCG, noise, and movement [48]. It is often desirable to pull out a single source from this combination to perform an analysis procedure. The aim of signal extraction is to improve the signal to noise ratio of the extracted signal, considering the desired source as the signal and all other sources as noise.

Fig. 3.8 demonstrates this procedure. The signal P shows the addition of a weight on top of the pressure sensor, for instance a person rolling onto the sensor. The signal Q is the breathing signal of the person, while R is the BCG. Noise, which could be systemic noise or environmental noise, such as vibrations from a truck passing in the street, is combined with each of the previous signals. Optimally, the source extraction procedure will extract an estimate of the original signal of interest, excluding all other

sources. Here, the estimated breathing signal, Q, is extracted.

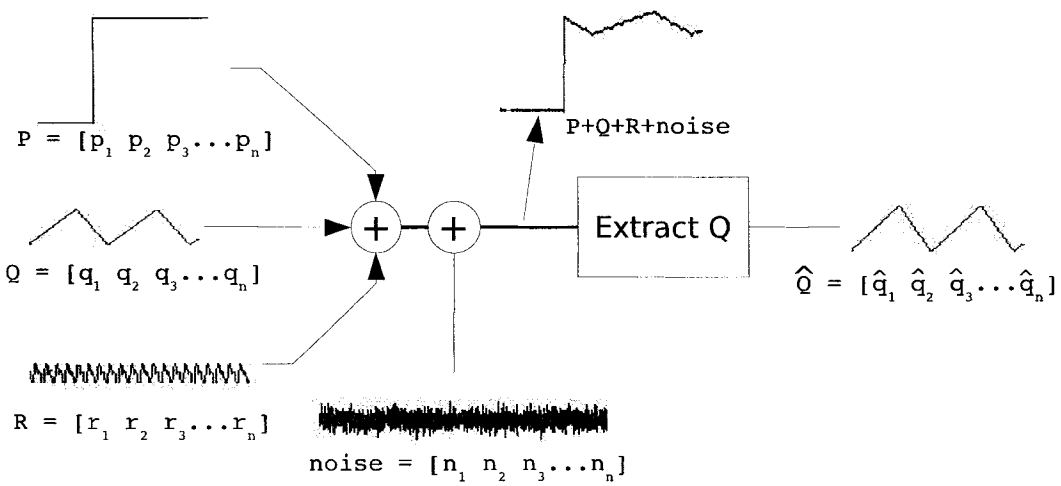

Figure 3.8: Extraction of source signals

A strong source of noise for respiratory signal extraction is movement, which is both transient and random, while the breathing components are a strong source of noise during BCG extraction.

3.2.1 Digital Filtering

If the source signal frequencies do not overlap and the source signal frequency bandwidth is known beforehand, digital filtering can be used to separate the signals based on their frequency content. An excellent reference for digital filters can be found in [74]. Either finite impulse response (FIR) filters or infinite impulse response (IIR) filters may be designed to suppress signals outside of the given bandwidth.

Fig. 3.9 demonstrates the digital filtering for source extraction of both a breathing signal and a BCG.

A review of wavelet theory can be found in [75], while a simplified tutorial can be found in [76]. A wavelet transform is essentially the correlation of a signal to a scaled

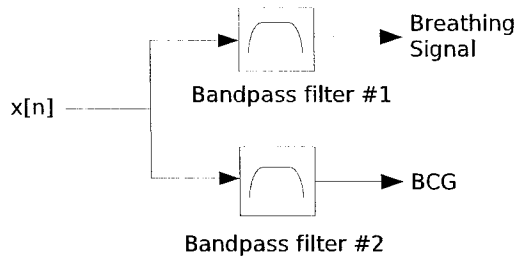

Figure 3.9: Extraction of source signals with a digital filter

and translated mother wavelet. The equation of the continuous wavelet transform is as follows [77], [76]:

$$W(s,\tau) = \frac{1}{\sqrt{|s|}} \int_{-\infty}^{\infty} x(t)\psi^*(\frac{(t-\tau)}{s})dt \tag{3.24}$$

where $\psi(t)$ is called a mother wavelet, a basic function. τ represents the translation of the wavelet along the signal x at time t and s represents the scaling factor that allows for multiple resolutions to be analyzed. The mother wavelet must be chosen prior to analysis [77].

The discrete wavelet decomposition procedure decomposes a signal into details and approximations using two wavelet transforms. This is similar to splitting the original signal into two signals: outputs from a low-pass filter (approximations) and outputs from a high pass filter (details). The signals are down-sampled by two and the approximations are sent through the filters again, iteratively for a given number of decomposition levels.

Discrete wavelet decomposition can be done using digital filtering. A discrete decomposition uses translation and scaling factors that are powers of two to provide an orthonormal basis [78] and the equation for the discrete wavelet transform (DWT) at a given decomposition level is shown here:

$$W[j] = (\frac{1}{2^j k} x[n] * \psi[\frac{(-n - 2^j k\tau_0)}{2^j}]_{k\in Z} \tag{3.25}$$

where W is the coefficients of the decomposition of $x[n]$ at decomposition level j and Z includes all possible translations k, each of length τ_0.

The original signal can be reconstructed fully from the decompositions. A reconstruction based only on a single decomposition level's detail coefficients can be viewed as a bandpass filter. Each decomposition level's detail coefficients occupy a touching frequency range [76]. Setting decomposition level coefficients which are outside of the frequency of interest to zeros before recombining is an effective noise cancellation technique.

3.2.2 Adaptive Filtering

Adaptive filtering attempts to find a model of the system that minimizes the error between the model output and the actual output. Fig. 3.10 shows a smoothing adaptive filter which acts similarly to a low-pass filter [79], to separate a low frequency source from a high frequency source. Input $x[n]$ is fed to a delay line, z^k, and into

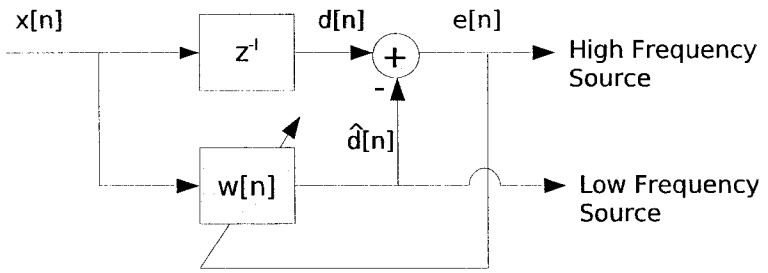

Figure 3.10: Extraction of source signals with an adaptive filter

the filter model, $w[n]$. The model produces an output, $\hat{d}[n]$ which is compared to the signal that has been delayed by k samples. The error between these signals is used to adapt the model. The output of the model is a smoothed, low-frequency, version of the signal, while the error output is the high frequency content of the original signal. Only real valued signals are considered here; complex formulations are not presented.

If the model is a sequence of weights, $\boldsymbol{w}$, multiplied and summed by the transposed regression vector, $\boldsymbol{\phi}^T$, the output of the model at sample time n is

$$\hat{d}[n] = \boldsymbol{\phi}^T[n-1]\boldsymbol{w}[n] \tag{3.26}$$

In matrix format for a model with k parameters, this is:

$$\hat{d}[n] = \begin{bmatrix} \phi_1 \phi_2 \dots \phi_k \end{bmatrix} \begin{bmatrix} w_1 \\ w_2 \\ \vdots \\ w_k \end{bmatrix} \tag{3.27}$$

Often, we are interested in using an autoregressive moving average (ARMA) model, where the generic model is is made up of weights b_i and a_i and the regression vector is formed from both inputs $x[n-i]$ and outputs $\hat{d}[n-i]$. Eq. 3.28 is the equation of an ARMA model.

$$\hat{d}[n] = \sum_{i=0}^{p} b_i x[n-i] + \sum_{i=1}^{m} a_i \hat{d}[n-i] \tag{3.28}$$

For this model, the weights are

$$\boldsymbol{w}^T[n] = [\ b_0 \quad b_1 \quad \dots \quad b_p \quad a_1 \quad a_2 \quad \dots \quad a_m\ ] \tag{3.29}$$

and the regression vector is

$$\boldsymbol{\phi}^T[n] = [\ x[n] \quad x[n-1] \quad \dots \quad x[n-p] \quad d[n-1] \quad d[n-2] \quad \dots \quad d[n-m]\ ] \tag{3.30}$$

This ARMA model can be changed into a MA or AR model by removing the recursive parameters or input parameters respectively.

The adaption changes the values of the weights by examining the input parameters and error of the model compared with the actual output. The fastest convergence of

the model to the actual output occurs when the weights are changed in the direction of the steepest descent [79] towards a minimized error, $e[n]$.

To minimize the mean square error, the weights are updated as follows [79].

$$\boldsymbol{w}_{n+1} = \boldsymbol{w}_n + \mu E\{e[n]\boldsymbol{\phi}[n]\} \tag{3.31}$$

The constant μ multiplies the weight change vector by a value between 0 and 1.

Since we don't necessarily know the expected value of the error multiplied by the parameters, we can estimate it quickly, but not all that accurately, by taking a one sample estimate so that the update equation becomes

$$\boldsymbol{w}_{n+1} = \boldsymbol{w}_n + \mu e[n]\boldsymbol{\phi}[n] \tag{3.32}$$

This type of weight updating is called Least Mean Squares (LMS). Although the individual estimates are not too accurate, on average they will head in the correct direction [79].

A large value of μ may seem attractive as it offers faster convergence, but a high μ means that the system may become unstable and that the error at steady-state will remain higher. For a stationary process, a conservative range that μ can occupy for the model to remain stable is:

$$0 < \mu < \frac{2N}{\sum_{k=0}^{N-1} |x[n-k]|^2} \tag{3.33}$$

and for mean square convergence [79]:

$$0 < \mu < \frac{2}{\sum_{k=0}^{N-1} |x[n-k]|^2} \tag{3.34}$$

The choice of μ becomes a trade off between the speed of convergence and the steady-state error.

Instead of attempting to choose an acceptable value of μ, the Normalized LMS (NLMS) method chooses a new value of μ at each iteration.

$$\mu[n+1] = \frac{\beta}{\epsilon + ||x[n]||^2} \tag{3.35}$$

where $0 < \beta < 2$ and ϵ is a small factor that ensures that small values of $||x[n]||^2$ do not create unduly large swings [79]. NLMS is especially useful for non-stationary systems where a conservative μ cannot be calculated.

3.2.3 Use in Literature of Pressure Array Monitoring

Digital filtering has been used extensively for pressure array monitoring. Low pass, bandpass, and high-pass filters have all been employed. For breathing signal extraction, a low-pass filter with $f_{cut} = 0.5$Hz (30 bpm) has been used [46]. This filtering scheme assumed a healthy adult with a breathing rate between 15 bpm and 20 bpm [46]. A bandpass filter from 0.1 to 0.5 Hz has been employed elsewhere [43]. This allows for rates between 6 bpm and 30 bpm.

For BCG extraction, a bandpass filter with passband between 5 and 10 Hz has been used [35]. The lower cutoff may be somewhat high since regular heart rates of 60 to 100 bpm map to 1 to 1.7 Hz, but may have been purposefully designed to reduce noise from the respiration signal. An analog filter with passband between 0.3-20 Hz has also been employed elsewhere [19].

DWTs have been used for both breathing signal and BCG extraction [19]. Chen et al. extracted breathing from a signal reconstructed from just the approximation coefficients of a 6-level decomposition. Pulse rate was extracted from the reconstruction of just the level 4 and 5 detail coefficients of the same decomposition [33].

No use of LMS smoothing has been found in current research with pressure array monitoring. However, least square fitting of a combined respiratory and BCG signal

has been done in order to remove the respiratory component [25].

3.3 Frequency Estimation Algorithms

Frequency estimation techniques are useful for pressure sensor array analysis in the estimation of respiratory rates and heart rates. Frequency estimation algorithms may be done by temporal techniques, spectral techniques, and techniques that incorporate both dimensions.

3.3.1 Zero Crossing / Peak Detection

The simplest temporal analysis method may be peak detection. Peaks in the signals are found and the frequency of the signal is determined to be the inverse of the period between peaks.

Noise in the signal can cause extra peaks to occur. To protect against choosing peaks caused by noise, a few steps can be taken. Firstly, the peak must be located between two zero crossings. Secondly, each peak must be a minimum distance away from the previous peak. This second requirement ensures that noise around the zero crossing does not cause detected peaks. Signal enhancement and noise cancellation also protect against these spurious peaks. This method of respiratory rate estimation by peak detection has been employed for respiratory rate estimation from impedance sensing chest-belts [80].

3.3.2 Autocorrelation

Autocorrelation is a second method of frequency estimation by temporal analysis. The autocorrelation sequence provides a metric of how well a delayed version of a

signal matches the original signal. The equation for the autocorrelation sequence, R_{xx}, of a discrete variable at a given delay, τ is as follows [74]:

$$R_{xx}[\tau] = \sum_{k=-\infty}^{\infty} x[k]x[\tau + k] \tag{3.36}$$

where $x[\tau + k]$ is the original signal delayed by τ.

For periodic signals, the autocorrelation of the signal at a delay equal to the period of the signal produces a peak. The diagram in Fig. 3.11 shows the autocorrelation of a 0.5 Hz sine wave with lags from -2 times its period to +2 times its period. The

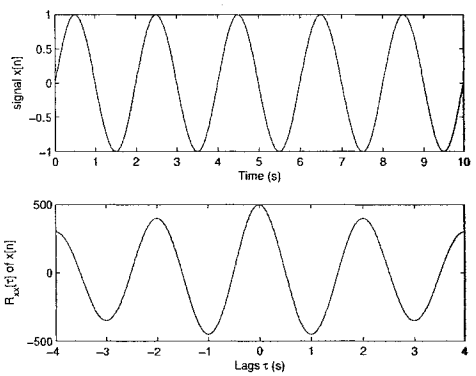

Figure 3.11: The autocorrelation sequence of a 0.5 Hz sinusoid

frequency of a signal can then be found by finding the location of the first peak after $R_{xx}(0)$ and taking the inverse of the lag at this point. In Fig. 3.11, the first peak is at 2 seconds, and thus the period is calculated as $\frac{1}{2s} = 0.5Hz$.

The frequency detected by the autocorrelation method has a precision based on the sample rate of the original signal. A high sample rate can give it a greater precision. However, since the frequency is the inverse of the lag, the precision of the sequence is on an inverse scale, with greater precision offered for a lower frequency than a higher frequency, assuming a constant sampling rate.

Since in practice, signals are of finite length and finite sampling rate, the autocorrelation's range of possibly detected frequencies is finite and related to the sample

frequency and the length of the signal. Assume a signal of length M and sampling frequency f_s. To properly detect a peak, a valley followed by a peak must be formed and so the lowest detectable frequency is $\frac{f_s}{L}$. The highest frequency that could be detected would occur at the second delay sample so that a valley is formed at the first sample and it would therefore be $\frac{f_s}{2}$.

3.3.3 Fourier Transform

The Fourier transform of the autocorrelation sequence is the power density spectrum. The area under the curve of a certain frequency band of the power density spectrum is the mean square value of the input in that frequency band [74]. Thus, by finding the peaks in the power density spectrum, the frequency ranges of the constituent input frequencies can be found.

Instead of calculating the power spectral density from the autocorrelation function, a fast Fourier transform (FFT) of the input signals can be found. The square of the magnitude of the Fourier transform of a signal is its power spectral density.

The spectrum is made up of bins that cover a range of frequencies, f_s/L wide, where L is the length of the input data sequence [81]. This is the available resolution of the spectrum. While it is possible to interpolate the frequency spectrum by padding the input data with zeros, this will not improve the resolution since the lobe width does not decrease [81].

The lowest frequency that can be estimated from the power spectrum density is $\frac{f_s}{L}$. Since the spectrum is symmetric across $f_s/2$, the highest frequency that can be estimated is $\frac{f_s}{2}$. These work out similarly to the autocorrelation sequence's frequency estimation limits.

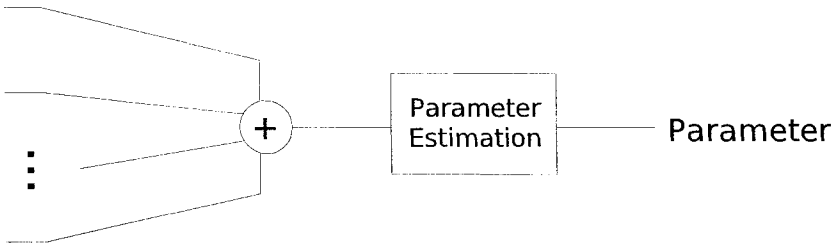

Figure 3.12: Data fusion by pre-summation

3.3.4 Use in Literature of Pressure Array Monitoring

Peak to peak detection has been used to determine breath rate from bed-based sensors. For instance, Harada et al. found two consecutive peaks of an 'activity score' to correspond to one breath [46]. Valley to valley detection has been also reported [32]. A method of peak to peak detection using the zero crossings of the differentiated signals has also be used for pulse rate estimation [33].

Autocorrelation has been used for analysis of heart rate from BCG signals [25] while Fourier spectrum peak detection has been used by a variety of researchers to estimate respiratory rates [42], [35] and heart rates [35]

3.4 Sensor Array Data Fusion

A sensor array allows redundant data for better measurement accuracy. To fuse the data from multiple sensors a method of data fusion must be chosen. Pre-summation, post-summation, and reference sensor(s), are all methods of data fusion that have been used with pressure array monitoring.

Pre-summation, shown in Fig. 3.12 sums all sensor outputs prior to processing.

Post-summation uses the mean value of a parameter calculated by data from multiple sensors. A weighted mean may also be employed. This weighting could be probability of the sensor's accuracy based on its previous track record.

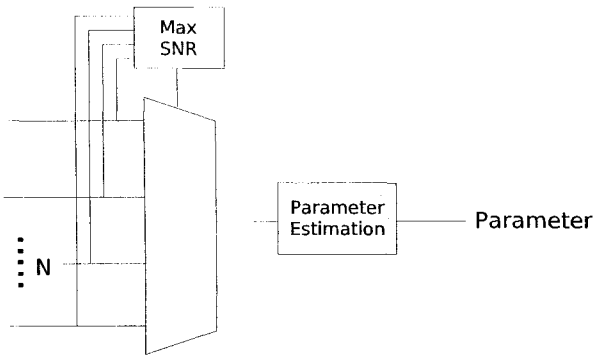

Figure 3.13: Data fusion by reference sensor selection

The reference sensor method finds the sensor displaying the best desired characteristics and chooses parameters based on processing of the signal from that sensor.

3.4.1 Use in Literature of Pressure Array Monitoring

Pre-summation has been used by a number of researchers to simplify data fusion [48], [44], [51]. Harada et al. proposed an activity score, $E_a[n]$, as the sum of pressures times the difference squared [48]:

$$E_a[n] = \sum_i x_i[n](\dot{x}_i[n])^2 \tag{3.37}$$

where $x_i[n]$ denotes the ith sensor output at sample time n and $\dot{x}_i[n]$ is its time derivative. Nishida et al., phase aligned the signal prior to summation. Sensor outputs were flipped according to correlation values to align the respiratory signal phases for respiratory rate estimation [44].

Van der Loos used the sensor of interest method to choose respiratory and heart rate by focusing on the sensor with the best frequency characteristics in the band of interest [19].

3.5 Validity Evaluation

Once a parameter has been estimated, it may be important to know how good that estimate is. For instance, a respiratory rate of 15 bpm that suddenly shoots up to 50 bpm may signal a problem, but if the 50 bpm respiratory rate is actually an inaccurate estimate due to signal noise, a false alarm could be activated. Validity evaluation examines the accuracy or reliability of an estimate.

3.5.1 Use in Literature of Pressure Array Monitoring

Watanabe et al. [35] used a breathing rate and respiratory rate reliability metric from the signal to noise ratio (SNR) in the frequency spectrum using the fast Fourier transform (FFT). A threshold of 12 - 13 dB was used to separate unreliable estimates from reliable ones based on examined results [35]. Harada et al. [48] used a similar metric.

Chapter 4

Experimental Setup

This chapter describes the steps that were necessary to allow processing experiments to be run using sensor data and simulated data. Computer simulations were undertaken, therefore a description of simulated data creation is included. Data from a pressure sensor array was acquired. Included here is a description of both the data acquisition setup as well as the data acquisition methodology. Additionally, the process of merging the data and performing annotations is described. Finally, a synopsis is provided of a database of respiratory signals that was created for simplicity and rigour in respiratory signal processing and rate finding experiments.

As part of the data acquisition, two experiments were undertaken with human participants. These were an observed experiment and a nocturnal experiment. Ethics approval was obtained prior to experimentation with human participants from the Carleton Research Ethics Committee. Ten adult volunteers, five women and five men, took part and performed either one or both experiments. Participants ranged in height from 162 cm to 193 cm and weight from 56 kg to 105 kg.

4.1 Computer Simulation

A computer simulation of data pressure sensors was created to help evaluate potential algorithms. A MATLAB script was written and run with MATLAB version 7.0 to create a simulated pressure signal. The signal consisted of a concatenation of simulated movement segments followed by restful segments. The restful segments were made up of either a noisy breathing signal or just noise. The noise was additive Gaussian noise with a variance of $\sqrt{2}$ counts^2. This is a conservative noise power as it is higher than the expected noise on the pad. To simulate saturation, any signal levels above 1750 counts, which is the average saturation level from the pressure pads in experimental use, were set to that constant saturation level.

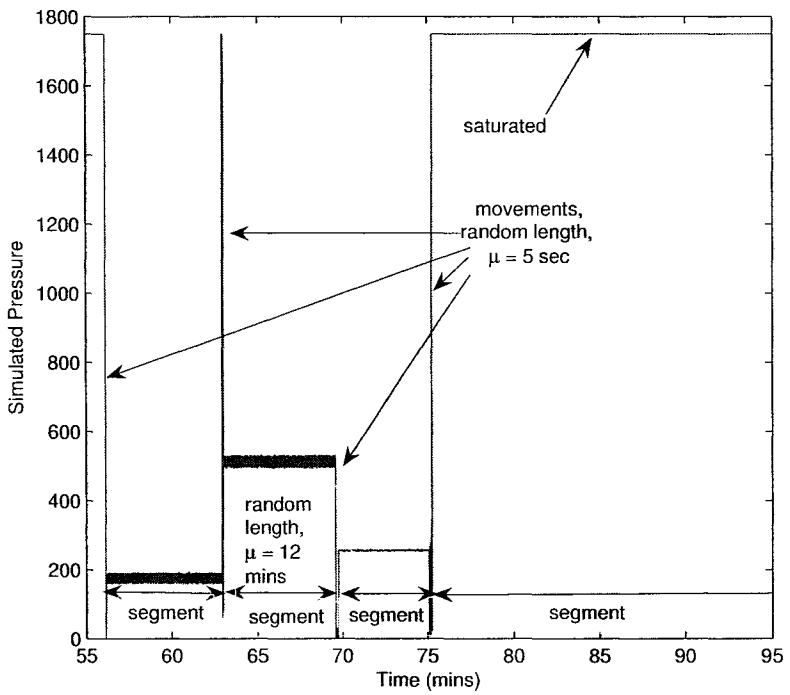

Figure 4.1: Forty minutes of simulated data

The length of a segment was randomly chosen from an exponential distribution

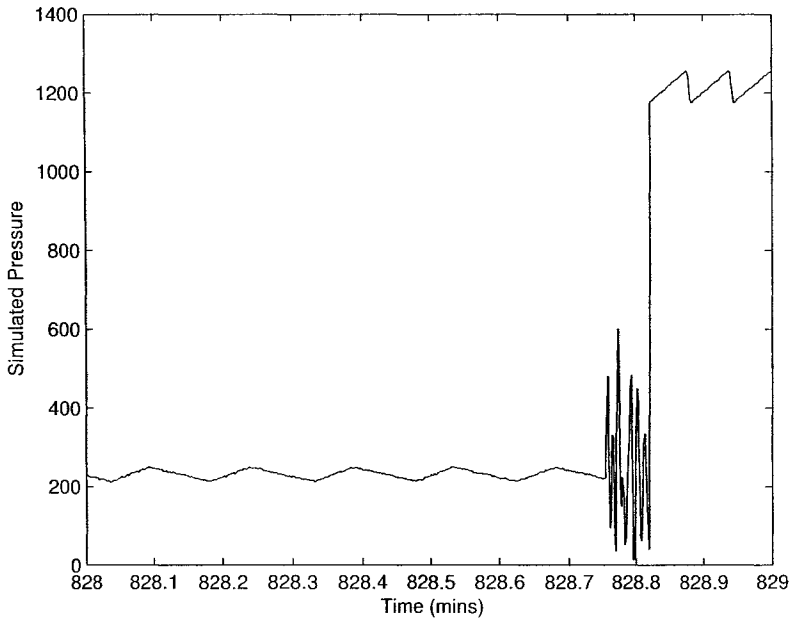

Figure 4.2: Simulated movement and breathing

with a mean of 12 minutes, while the length of movement within the segment was also chosen from an exponential distribution, this time with a mean of 5 seconds. Fig. 4.1 presents a few of these segments during forty minutes of simulated data.

Movement was simulated as a random process, uniformly distributed between zero and a maximum amplitude. The random process was filtered through a lowpass filter to better match actual movement signals. This maximum amplitude is picked for each movement from a Gaussian distribution with a variance of 1000 counts^2. Fig. 4.2 presents a simulated movement between two breathing signals.

Breathing was simulated as a periodic sawtooth wave, using a random breathing rate for each segment. This rate was chosen from a normal distribution with a mean of 15 bpm and a variance of 6 counts^2. A random duty cycle was also chosen from a uniform distribution between 0 and 100%. The amplitude of the breathing was also random, from a gamma distribution ($\alpha = 2, \beta = 3$) with a mean of 30 counts

and a variance of 112 counts^2. The gamma distribution was chosen since it weighs more heavily on lower values and breathing signals are generally observed to have low amplitudes with a small number of high amplitude signals.

The sawtooth model was chosen by observation of the breathing signals. Triangle waves have also been used as a respiratory model by other researchers [25]. Fig. 4.3 shows a simulated breathing signal and its derivative superimposed on top of participant sensor data of a breathing signal.

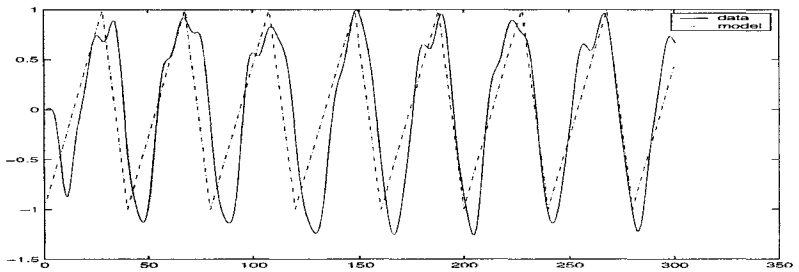

(a) Simulated and Actual Breathing Signal

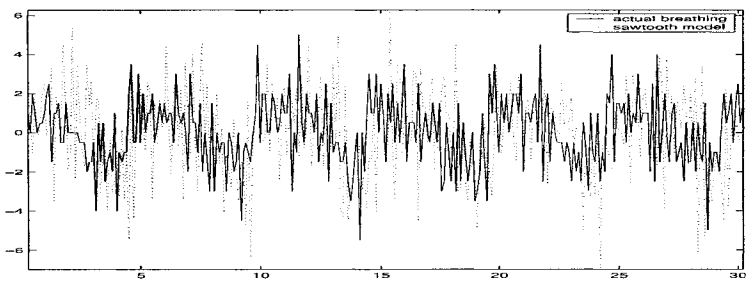

(b) Derivative

Figure 4.3: The sawtooth model of a breathing signal

Breathing signals longer than a consecutive 10 minutes were injected with a small movement, occurring anywhere within the 10 minutes and lasting an average of 1 second.

4.2 Data Acquisition Setup

The experiments use the Tactex Bed Occupancy Sensor (BOS), with a resolution of 10 cm. Data from the BOS was sent by serial port to a laptop computer and captured by the Tactex 'CCL Data Acquisition' software. This software logged the pressure array element data to an ASCII comma delimited file. The sampling rate was set to 10Hz via an initialization file.

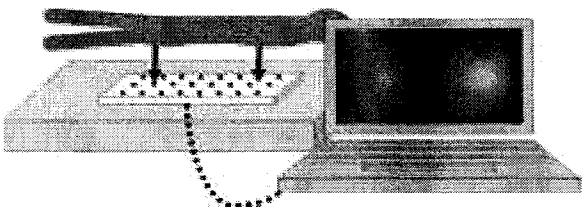

Figure 4.4: Data acquisition setup

The ASCII comma delimited file was converted in MATLAB to a binary '.mat' MATLAB data file. See Section 4.5 for more information about the conversion and data merging process.

4.3 Observed Data Acquisition Experiment

The protocol that was followed for the observed experiment is outlined here. During each experiment, the researcher logged comments to a file to aid in future data annotation. Logging software was developed so that timestamps were added to the log comments for future merging with sensor data.

Although what follows is a description of the protocols followed for the experiments, in reality the protocols were flexible to allow the participants the right to choose what parts they preferred to complete or to not complete. Any deviation from the written protocol was noted in the log comments.

The protocol of each upcoming experiment was reviewed for participants prior to undertaking each experiment. They were then asked if they felt comfortable completing this experiment. No abstentions actually occurred at this point. The fourth experiment was not completed for two participants due to time restrictions or equipment availability.

During the experiments, an actigraph watch was worn. Since actigraphy is an accepted method of home monitoring, future research may wish to compare results derived from the processing of pressure sensor array data with results derived from accepted standards of actigraphy processing.

4.3.1 Experiment Descriptions

Four experiments were observed. In each of the experiments, a pressure sensor pad was placed on top of the bed, directly under the participant. The experiments were:

- Experiment 1: Bed Entry / Bed Exit
- Experiment 2: Position and Movement
- Experiment 3: Breathing
- Experiment 4: Ballistocardiogram / Heart Rate

The exact protocol of each experiment can be found in Appendix A. A synopsis of each experiment is provided here.

4.3.2 Experiment 1 - Bed Entry / Bed Exit

Approximate time to complete:	5 minutes
Placement of pad:	aligned to side of the bed
Experimental goal:	To acquire data from a participant's position when entering or exiting the bed. Data may be used for analysis of bed entry or exit. For instance, pressure put on hands could be uncovered.

Participants got in and out of bed six times, staying in bed for 20 seconds before exiting. Likewise, participant stayed out of bed for 20 seconds before entering again.

During the first three iterations, participants were asked to get out of bed naturally. During the last three iterations, participants were requested to use their hands to push themselves out of bed.

Experiment 2 - Position and Movement

Approximate time to complete:	20 minutes
Placement of pad:	aligned horizontally to middle of pillow
Experimental goal:	expected to be used for movement algorithm validation, position analysis, and movement classification

Participants started in bed in any position (on of front/back/right/left). They lay still for a minute until the observer instructed when the minute was up and requested

a position change. Participants chose which position they moved to. Participants were also requested at some points to cough or move without position change instead of changing positions.

Experiment 3 - Breathing

Approximate time to complete:	30 minutes
Placement of pad:	aligned horizontally to middle of pillow
Experimental goal:	allow for comparison to breathing detection and respiratory rate estimation

Participants were instructed to breath normally unless told otherwise. The observer went over this experiment in detail with the participant before undertaking it. This experiment involved lying still for three minutes followed by quick and shallow breathing for 30 seconds, normal breathing for 30 seconds, deep breathing for 30 seconds, normal breathing for 30 seconds, apnea for up to 30 seconds, and normal breathing for 30 seconds. This pattern is repeated for each of three positions: back, front and right or left side.

Participants were instructed that breathing changes could be dangerous and to only do those that they feel comfortable with, only to the degree that they feel comfortable. In particular, for breath holding, they were instructed to breath again as soon as they felt like a breath was needed. The thirty second limit was only imposed to make sure that their breath wasn't held too long. Additionally, the participants were requested to start holding their breath only once they felt comfortable to do so.

In later experiments, participants were requested not to take a deep breath before holding their breaths. It was noted in the first few experiments that participants

wanted to prove they could hold their breath for the entire 30 seconds (even after instruction that the 30 seconds limit was only to ensure that the breath wasn't held for too long), and so a large gasp of air was usually taken prior.

Since this is not generally what would be expected of subjects who stopped breathing during the night, a more natural cessation of breathing was requested. Participants were told that holding their breath after this natural cessation would be more difficult and to not go the entire 30 seconds without breathing. Additionally, data often showed breathing-like movement before a breath was actually taken as the participant's central nervous system tried to restart the breathing.

Many participants found this experiment quite restful and up to half of the participants actually fell into a light sleep during the experiment.

In addition to logging comments about the participants position and movement, breaths taken by the participant were also logged. By logging the letter 'b' to the timestamped logging file every time the participant breathed, a record was made of the participants' breathing. Breath times were determined by observation of the participants' chest and body movements. Logging was done at the most obvious movement time, usually just after the peak of inhalation.

Since it was not possible to simultaneously log a movement event and the breaths that occurred during the logging of that movement, there were some missed breaths. Moreover, the observer sometimes missed logging a breath or accidentally logged two during one respiratory period. This happened rarely but these mistaken annotations should be found and fixed before data use.

Experiment 4 - Ballistocardiogram / Heart Rate

Approximate time to complete:	5 minutes
Placement of pad:	aligned horizontally to middle of pillow
Experimental goal	to be used for comparison to heart rate estimation methods and for ballistocardiogram detection

Participants put on a heart rate monitor strap and were requested to do some light exercise. Some of the activities chosen by participants were walking down and up a flight of stairs, knee bends, jogging in place, and jumping jacks.

The participants then got into bed, usually lying on their front and their heart rate was recorded continuously. Heart rates were logged while the heart rate descended and for a couple minutes after it stabilized at a resting heart rate. Participants were then asked to hold their breath again for up to 30 seconds so that a recording of the BCG could be made without respiratory interference. After normal breathing commenced again, heart rates were recorded for another minute or so.

Initially, participants were not requested to hold their breath during the experiment, but after data from the first few participants during Experiment 3 showed a clear BCG during breath holding, this part was added to the experiment.

4.4 Nocturnal Data Acquisition Experiment

The nocturnal experiment takes an overnight recording of bed pressure over two nights. Two nights are used to guard against the first night effect. The participant is not observed during this time, but answers a questionnaire before bed and a second

one upon waking in the morning. The questions are adapted from the Pittsburgh Sleep Diary and are available in Appendix B. This experiment is designed to test the feasibility of nocturnal and bed-based monitoring in the home and so the participant is free, and requested, to go about their sleep and wake routines as usual.

Data recording is started either by the participant or by the researcher. The participant is shown how to turn off the logging and is advised that he or she may do this at any time. Data recording is stopped in the morning and started again just before going to bed on the second night.

The sensor arrays were placed under the top mattress for all participants, as the sensor array currently in use would not be comfortable enough to allow extended use on top of a mattress. Future nocturnal experiments may use a more comfortable sensor mat that can be placed on top of the mattress.

4.5 Data Merging and Annotation

Data was merged into two MATLAB data files, one for sensor data and one for annotations, using a MATLAB script. Time stamps in the files were used for data alignment.

The original annotations were created from the experiment log file which was written by the observer as the experiment took place. Breaths, which were logged during the experiment using the character 'b', are separated into a breaths variable that holds all of the recorded breaths. Since the observer missed a number of breath observations, this variable needed to be checked and annotations added manually.

Fig. 4.5 shows the GUI that was created to help annotate the data.

Using this interface, the researcher can load data points and create multiple annotation variables (e.g. one for breaths, another for movement). Annotations can be

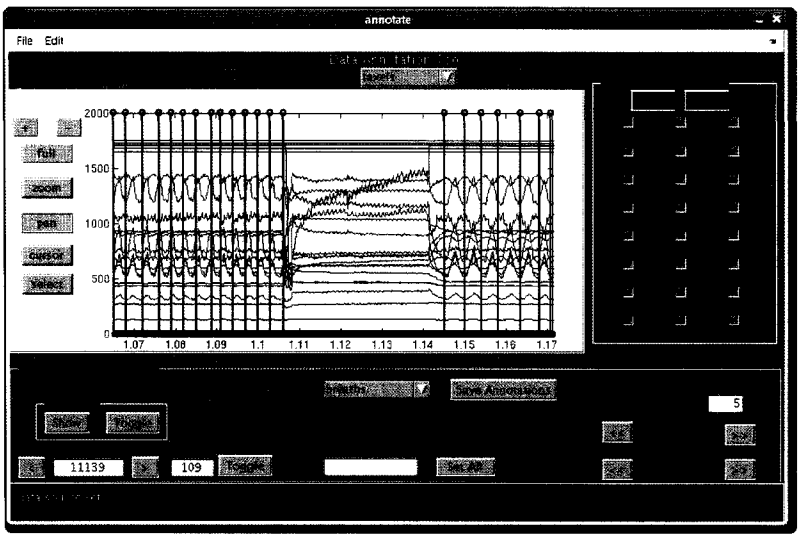

Figure 4.5: Screenshot of the MATLAB annotation GUI

added, removed, and shifted.

4.6 Breathing Signal Identification

It was hypothesized that the periodic signals throughout the data originated from the breathing of the participants lying on the pressure sensor array. These signals exhibited a periodic wave motion in the frequency band of interest, had diverse amplitudes ranging from less than 10 counts to over 200 counts, and were often displayed by several sensors simultaneously, albeit with different wave shapes and phases ($\pm 180°$) at each sensor.

To test the hypothesis, the data and corresponding logged breath annotations of Experiment 3 were loaded into the annotation GUI. It was determined that these logged breaths lined up with these periodic signals. Additionally, it was seen that when the participant was asked to stop breathing, the periodic signals disappeared but started again once breathing resumed. No similar signals were discovered that

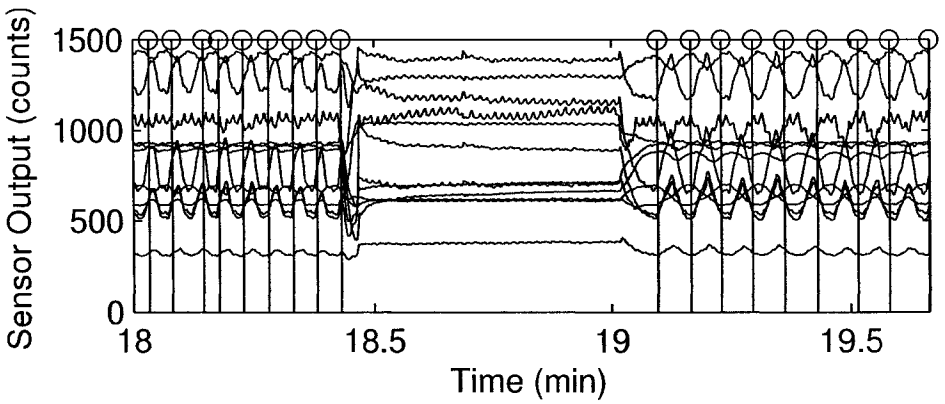

Figure 4.6: Correlation of breaths to breathing signals

could not be explained by these logged breaths. Other periodic signals were seen, but these signals had a small amplitude of less than 5 counts and a frequency higher than 0.8 Hz. They were likely BCG signals.

The breathing signals, overlayed by the logged breath annotations, can be seen in the data that is shown in the annotation GUI of Fig. 4.5. Another instance of this overlay is shown in Fig. 4.6. The data here comes from 10 sensors that display the breathing signals. Normal breathing is followed by stopped breathing, which is followed by normal breathing again. The vertical bars and attached circles show the moments that breaths were independently logged by the observer.

4.7 Respiration Signal Database

Using the logged breaths times and data from Experiment 3, a collection of respiration signals was created. At least twenty breathing signal segments, each 30 seconds long, were identified through manual examination of the data from each of 5 participants. A total of 116 breathing signals made up the database. Respiratory rates for each of the signals were calculated from the locations of the logged breath times as the mean time between breaths.

Table 4.1 outlines the types of respiratory signals that were included. For each type, two breath signals were chosen from each participant. Breath signals from a given participant came from as many different sensor locations in the sensor array as possible, with sensor repetitions minimized.

Of the ten participants who took part in the research, eight took part in Experiment 3. The five participants that were included in the database were the first five participants to complete this experiment. The respiration signal database can be updated to include the three newer participants and any future participants in the experiment.

Table 4.1: Types of respiration signals

Number	Description	Descriptor
10	Low amplitude	LA
10	Medium amplitude	MA
10	High amplitude	HA
10	Low frequency	LF
10	High frequency	HF
10	Changing frequency	CF
10	Small movement included	SM
10	Large movement at beginning	MB
10	Large movement in middle	MM
10	Large movement at end	ME
10	Half respiration and half BCG only	RB
6	Half respiration and half constant	RC
116	Total Number of Respiration Signals	

Where possible, the description of the respiration signal type is used, but space and clarity constraints may require the descriptor to be employed.

Chapter 5

Segmentation

This chapter presents the results of applying abrupt change detection segmentation methods to pressure pad signals in order to detect movement. A portion of these results have been published at the 2006 IEEE International Workshop on Medical Measurement and Applications (MeMeA 2006) under the title "Identifying Movement Onset Times for a Bed-Based Pressure Sensor Array" [2].

During a night, a person will change position every so often. Between position changes, signal means are relatively stable and respiration rates and ballistocardiograms are detectable, but during position changes these signals are disrupted. Smaller movements than position changes may also disturb the signals, so that respiratory or pulse rate measurements yield inaccurate results.

Three segmentation methods are investigated: segmentation by Shewhart control limits, single model with CUSUM, and a two model test using GLR. All of these algorithms require either Gaussian inputs or the error from an adaptive filter as the input, so each algorithm received the same inputs from an autoregressive (AR) adaptive filter of order 4. The whitened signal comes from the residual error of the AR filter's output.

5.1 Methods

A control limit movement detector is proposed and will be compared to other movement detection schemes.

5.1.1 Control Limit Movement Detector

The control limit movement detector is proposed in Fig. 5.1. This version of control limit testing sets the group size, p, to one and tests if each new point fits within control limits calculated from a sliding reference window. The control limits are updated at every point based on the mean and variance of a sliding window of the previous L samples. Since the system is designed to be a combined segmentation and movement detector that only produces new segments when movement is detected to start or stop, it may not necessarily detect changes in other parameters. Movement onset is detected as two consecutive points that are outside the control limits. Since the model rapidly adjusts the control limits as movements are sampled, the movement offset point is detected as the point when control limits drop again after rising to accomodate the movement.

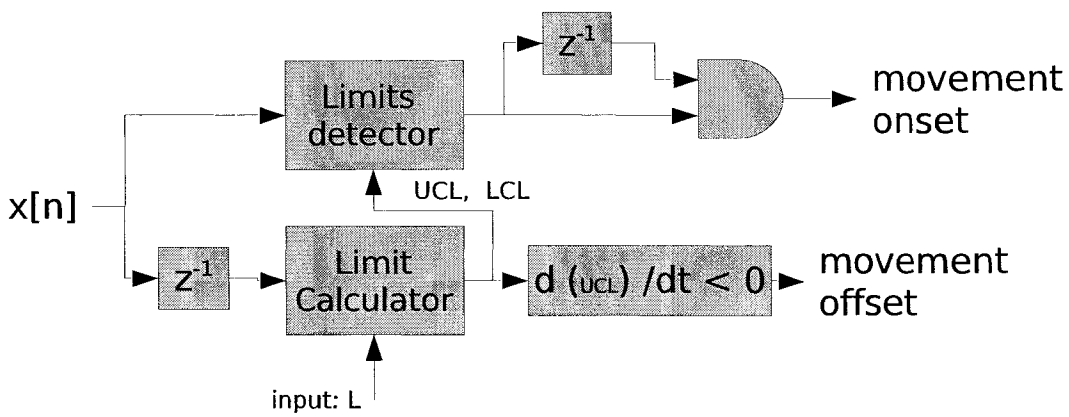

Figure 5.1: Control limits movement detection scheme

Fig. 5.1 shows the movement detector. The sliding reference window length, L, can be input to the detector. A one-sample delay (z^{-1}) is added before the control limit calculator to allow for testing of two points in a row before the limits adapt to the variance of these new points. The limit detector outputs a logic 1 if $x[n]$ is outside of the calculated upper control limit (UCL) and lower control limit (LCL). This result and the previous result (output of z^{-1}) are put through an AND operation. Movement onset is determined to have occured if the result is a logic 1. The movement offset time detector outputs a logic 1 once the derivative of UCL is negative. At this point, movement is determined to have ceased.

5.1.2 Two Model Control Limits

The classic control limits method is essentially a two model detector. It requires knowledge of the mean and variation of the data from a reference model estimated during processing by calculating the mean and variation from the data. The reference model parameters are fixed at the beginning of each segment based on the first L samples of data. Each point m_k on the chart is calculated from the mean of p consecutive samples, $[x[n-p+1] \ldots x[n]]$, which becomes the test model.

Fig. 5.2 shows the system. Normalized least mean squares (NLMS) is used as a whitening filter at the input of the detector. The filter model was an AR model of order 4. The filter was adapted by the error, $e[n]$. The control limits, UCL and LCL, are calculated at the beginning of each segment by the control limit reference. A moving average of p samples of the whitened input is tested against the control limits. When the output, a_n, is a logic 1, then a segment boundary is deemed to have occurred.

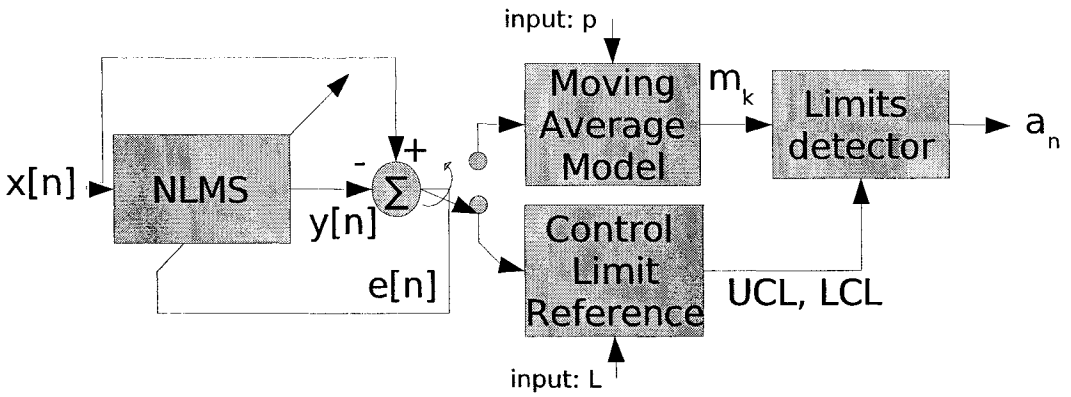

Figure 5.2: Two model control limits detection scheme

The limits detector takes the distance measure at sample time n as:

$$d_{n_{UCL}} = -UCL + \sum_{k=n-p+1}^{p} y[k] \tag{5.1}$$

$$d_{n_{LCL}} = LCL - \sum_{k=n-p+1}^{p} y[k] \tag{5.2}$$

where the control limits, UCL and LCL are calculated as in Eq. 5.3 and Eq. 5.4.

$$UCL = \hat{\mu} + 3\frac{\hat{\sigma}}{\sqrt{p}} \tag{5.3}$$

$$LCL = \hat{\mu} - 3\frac{\hat{\sigma}}{\sqrt{p}} \tag{5.4}$$

The alarm is raised when the test model roams outside the control limits:

$$a_n = (d_{n_{UCL}} > 0) \quad || \quad (d_{n_{LCL}} > 0) \tag{5.5}$$

The averages and variations were calculated as in Eq. 3.4 and Eq. 3.5.

5.1.3 One Model CUSUM

The AR model with 4 taps was chosen as a single model with its residual error passed to the CUSUM algorithm. Fig 5.3. shows the detection scheme for this method,

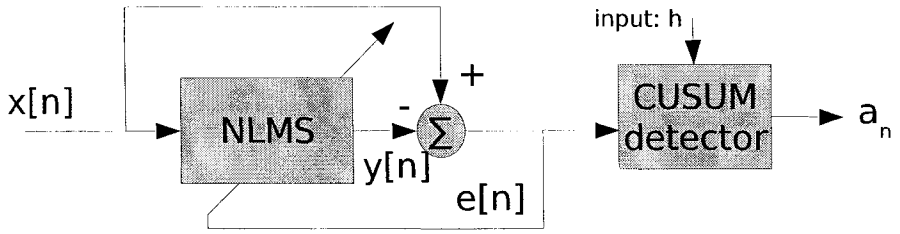

Figure 5.3: One model with CUSUM detection

where $e[n]$ is the residual error. CUSUM takes a threshold, h, as an input. Differing values of h were evaluated.

5.1.4 Two Model Generalized Likelihood Ratio (GLR) Test

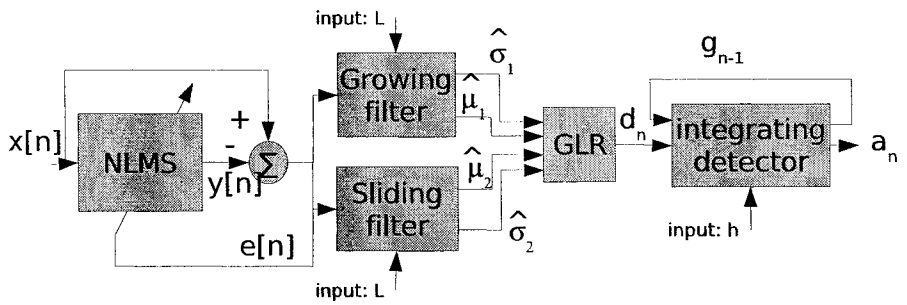

Figure 5.4: Two model GLR detection

The method of GLR outlined as 'Brandt's GLR' in [64] was implemented. Fig. 5.4 is the block diagram of this test. This method estimates statistical parameters, $\hat{\sigma}_1$, $\hat{\mu}_1$, $\hat{\sigma}_2$, and $\hat{\mu}_2$, from the given data using a sliding window of length L. The detector is an integrating detector with threshold h. Differing values of h and L were evaluated.

5.2 Evaluation

The methods were applied to the computer simulated data described in Section 4.1. They were evaluated based on detection delay, false alarms, and missed detections. The control limits method used here gives differing results depending upon the length of the estimation window, L, and the number of samples per estimation, p. Results were evaluated using differing values of L and p. The one model CUSUM method has only one degree of freedom in the choice of the threshold, h. Results were evaluated for the one model CUSUM method using differing values of h. For the GLR method, the two independent parameters, h (threshold) and L (sliding window size), were varied and the results were evaluated.

The methods were also applied to participant data from a single sensor during an overnight experiment and evaluated subjectively.

True positives are defined as locations where segment boundaries were determined to begin within 10 seconds (100 samples) of the actual segment boundary. For the GLR method, which is considers a segment boundary occurring at L samples before the current sample boundary, detection times were allowed to be up to $L+100$ samples late. False alarms were classified as locations where a boundary were signaled, but no segment boundary actually existed.

5.3 Results

The results of the methods applied to inputs from a simulated signal are described in Sec. 5.3.1, while the results of the methods applied to a real overnight signal are described in Sec. 5.3.2

5.3.1 Computer Simulation Results

First, the described methods were evaluated using a simulated sensor signal. The simulated signal had known movement times and segment boundaries were considered as the beginning and end of each of the simulated movements.

Fig. 5.5 is the receiver operating characteristic (ROC) of the methods, which plots the probability of a true positive (detecting a segment boundary accurately) with respect to the probability of a false alarm (detecting a segment boundary where no boundary exists) for each of the examined methods. Fig. 5.5 can also be used to obtain the possible detection rates for a given false alarm rate.

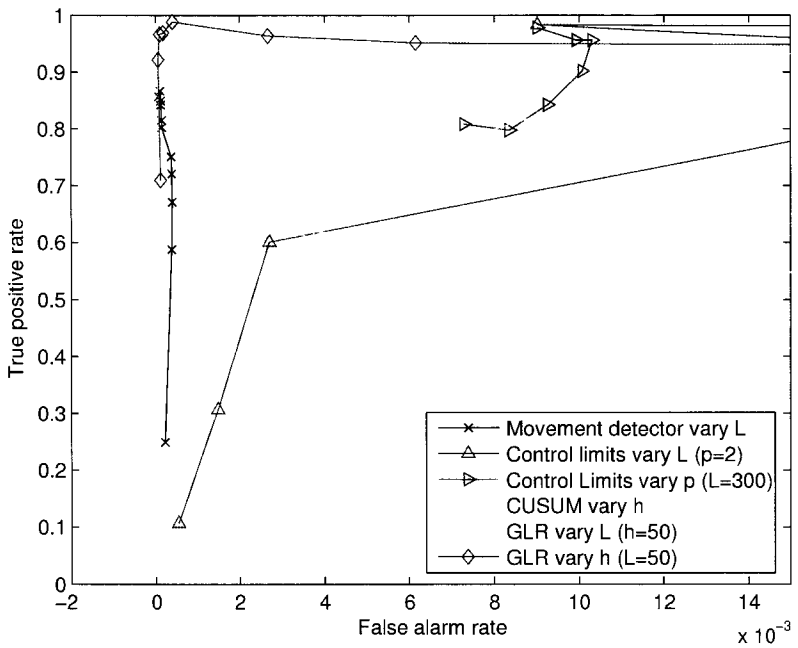

Figure 5.5: True positives in relation to false alarms

In Fig. 5.5, we see that the proposed control limits method provides a very low false alarm rate for any given true positive rate, but fails to reach the high true positive rate (> 0.9) of the other algorithms. The classic control limits method shows

a higher false alarm rate for a given reference window length, L, and a given test window length, p, but does manage to positively identify almost all segments, with a true positive rate near 1 where the two control limits lines intersect. CUSUM follows the classic shape of an ROC curve, where higher true positives can be attained at the expense of higher rates of false alarms. However, for a constant false alarm rate, there is always at least one other algorithm that misses less segment boundaries. GLR is very dependent on the window length, L, for good results, with certain window lengths showing higher detection rates together with less falsely detected segments. Varying the threshold, h, allows more fine-grain control of true positives to false alarm rate.

To examine the goal of minimizing time to detection at a given false alarm rate [64], Fig. 5.6 presents the time to detection as a function of false alarm rate, in logarithmic form for better viewing of these results over the area of interest. Fig. 5.6 suggests

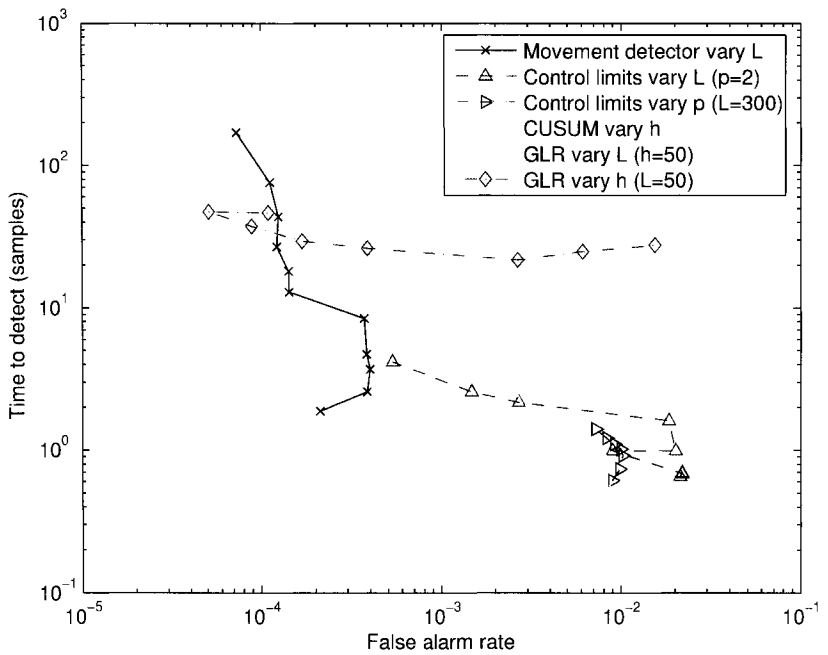

Figure 5.6: Logarithmic plot of detection time vs false alarms

that the lowest time to detection can be achieved by the CUSUM method. The control limits method can also provide low detection times, and varying the test window length, p, provides a means to finely control the detection time at a nearly constant false alarm rate. GLR has a rather high constant time to detect at any given threshold, h, when the length of the test window (L) is 300. However, similar to the control limits method, the length of the test window, L, can be used to decrease the time to detection. Varying the reference window length, L, of the proposed movement detector method shows that detection time is related to this length. The lowest false alarm rates can be achieved with this method, but at the expense of higher detection times.

A false alarm rate near 0.003 may be used to examine segmentation results at a similar false alarm rate. This is a convenient rate as it is near the middle of the scale and practical for obtaining results from each of the methods. The results shown in Table 5.1 were obtained for test results near this rate.

Table 5.1: Segmentation results near a 0.003 false alarm rate

Test	Parameters	False Alarm Rate	True Positive Rate	Delay to Detection (s)
Movement detector	L = 42	0.0004	0.67	0.37
Two model control limits	L = 75, p=2	0.0027	0.6	0.22
CUSUM	h = 500	0.0035	0.69	0.18
GLR	L = 4, h=50	0.0036	0.62	0.15
GLR	L = 50, h=10	0.0027	0.96	2.1

Table 5.1 shows that although the false alarm rate is low, the positive detection

rates are also on the most part low. Except for GLR with $L = 50, h = 10$, all true positive rates are in the range of 0.6 - 0.7. GLR stands out here for the best true positive rate at this false alarm rate. However, it also has the highest delay to detection. The movement detector has the second highest delay to detection, while CUSUM, two model control limits and GLR with $L = 4, h = 50$ show low delays, near two tenths of a second. To design for minimized delay, any of these three methods would be appropriate.

Requiring instead that true positives are taken into account yields results according to Table. 5.2. The results in Table 5.2 require the true positive rate to be

Table 5.2: Results for true positive rate > 0.90

Test	Parameters	False Alarm Rate	True Positive Rate	Delay to Detection (s)
Movement detector	L = 500	0.0001	0.87	7.6
Two model control limits	L = 300, p=2	0.009	0.98	0.061
CUSUM	h = 100	0.013	0.92	0.034
GLR	L = 50, h=50	0.0004	0.99	2.6
GLR	L = 50, h=200	0.00009	0.97	3.7

greater than 0.9, while also minimizing the false alarm rate. The movement detector is not quite able to reach this threshold, showing a maximum rate of 0.87. However, it offers one of the lowest false alarm rates, rivaled only by the GLR method with $L = 50, h = 200$. It is the slowest to react to a change. The second slowest, GLR, still offers a low false alarm rate, but with a very high true positive rate, especially with $L = 50, h = 50$ where the true positive rate is 0.99. CUSUM shows the quickest

reaction to changes in the signal, but its false alarm rate is the highest. The two model control limit could be used instead if delay to detection is paramount. Its false alarm rate is a bit lower while adding more true positives. Delay to detection still averages less than a tenth of a second, which means that most segments are detected within the first sample of change, since the period between samples is 0.1 seconds.

Examining the results from the individual methods demonstrates how the variable inputs affect the results. To demonstrate the performance of each method, the

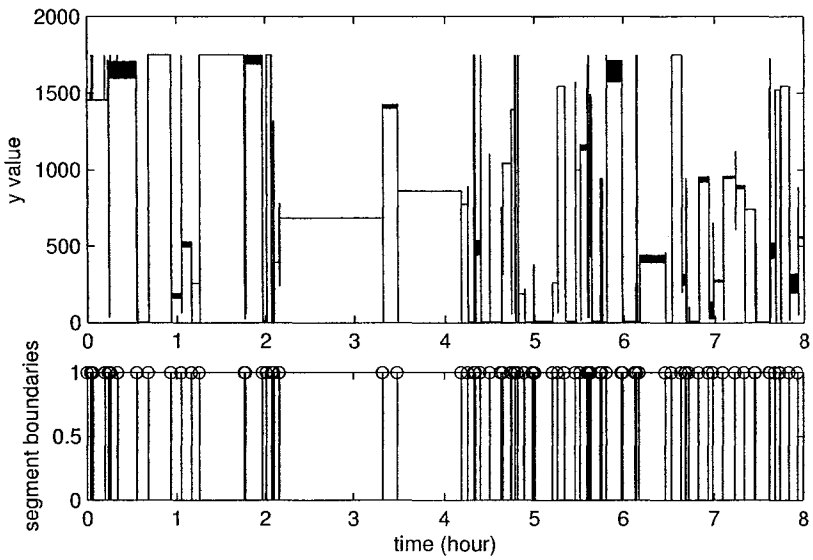

Figure 5.7: Expected segmentation points

boundaries detected by the method from a sample simulated eight-hour signal will be presented. The signal and the expected segmentation boundaries are shown in Fig. 5.7, where boundaries can be seen to line up with the spikes in the data. Additionally, true positive rate, the false alarm rate and the mean time to detection will be plotted as a function of the input variables available to each method.

Control limit movement detector results

Plots in Fig. 5.8 show the true positives, false alarms, and the mean time to detection for differing values of L. For this detector, the false alarm rate initially increases

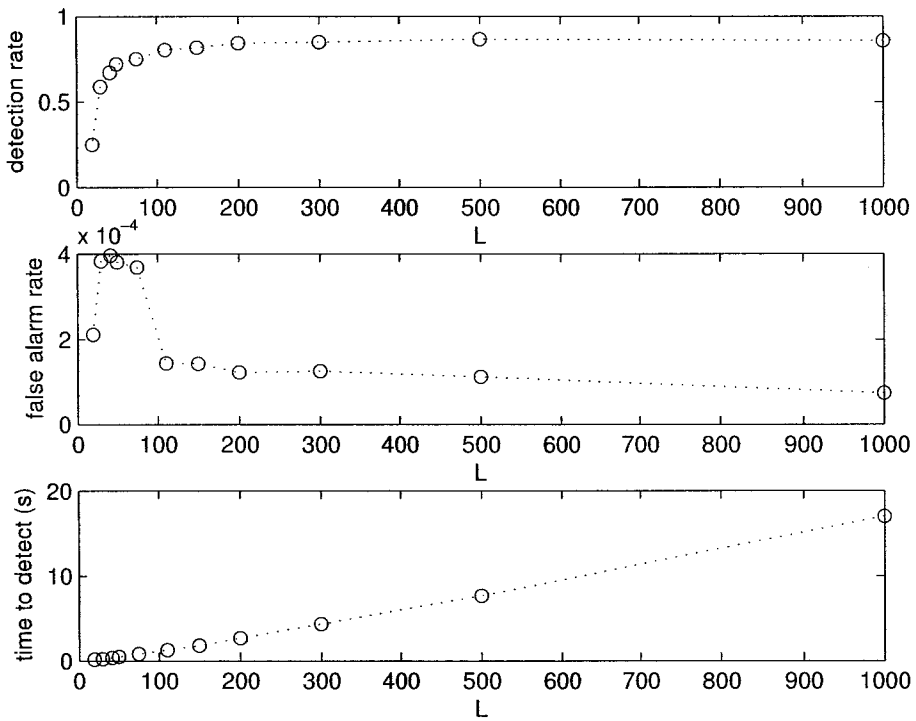

Figure 5.8: Control limits movement detector: varying L

with a longer L, but then drops, even as the true positive rate continues to increase. Therefore, optimizing for false alarm rate also optimizes for true positives. The trade-off is seen instead in the delay to detection, which rises linearly with an increasing L. A good operating point may be with $L = 300$. This point allows for almost as many true detections as $L = 500$, but at almost half the delay to detection. This detection delay is 4.3 seconds instead of 7.6 seconds at this fixed reference window length.

The segment boundaries expected and detected by the movement detector are shown in Fig. 5.9. While false alarms can be seen in a few places as heavy vertical lines, the number of these false alarms does not overshadow the true detections.

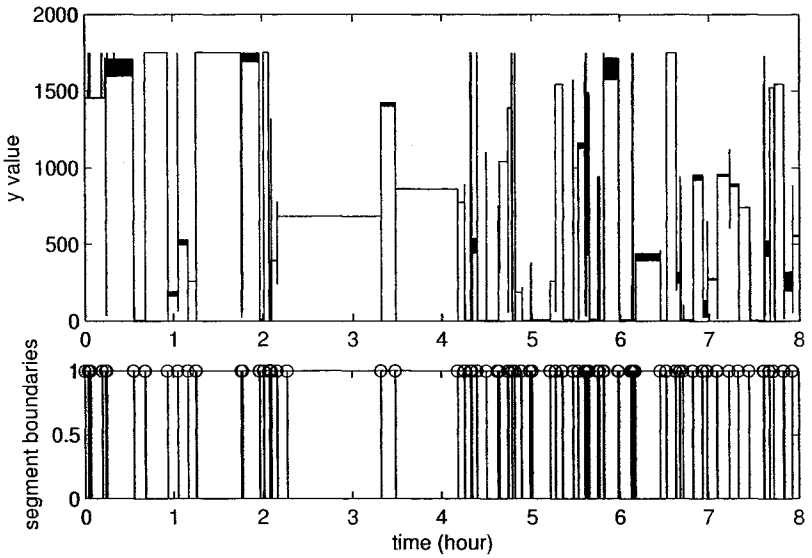

(a) Control limit, L=300

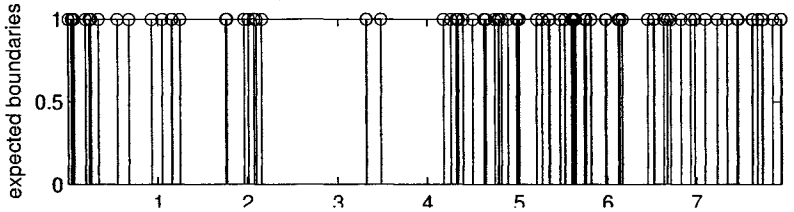

(b) Expected Boundaries

Figure 5.9: Proposed movement detector boundaries

For instance, just prior to the second hour, there is an extra detection during the movement. Another extra detection occurs at around 10 minutes past the second hour. No signal types are especially prone to false alarms, except perhaps movement signals, which might be expected as their mean could be constantly shifting.

Two model control limit results

Plots in Fig. 5.10 and Fig. 5.11 show the true positives, false alarms, and the mean time to detection for differing values of reference window length L and test window length p.

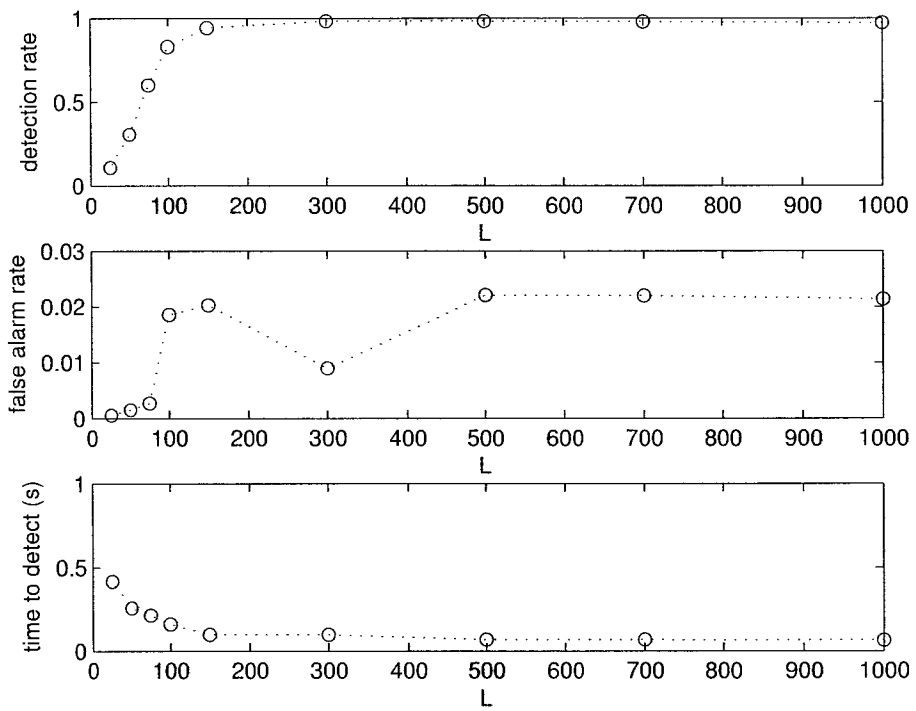

Figure 5.10: Control limits (p=2): varying L

In Fig. 5.10, the detection rate climbs steadily and plateaus at a 98% rate of detection at a steady p when L is increased. Once at this plateau, a small decrease can be seen in the detection rate, possibly due to boundaries occuring within the

reference window time. The false alarm rate remains quite steady at 0.02 over most values of L, but dips down at $L = 300$ and is even smaller at values of $L < 100$. As L increases, time to detection decreases. Optimally, L should be set at 300 to take advantage of the false alarm dip and top detection rate.

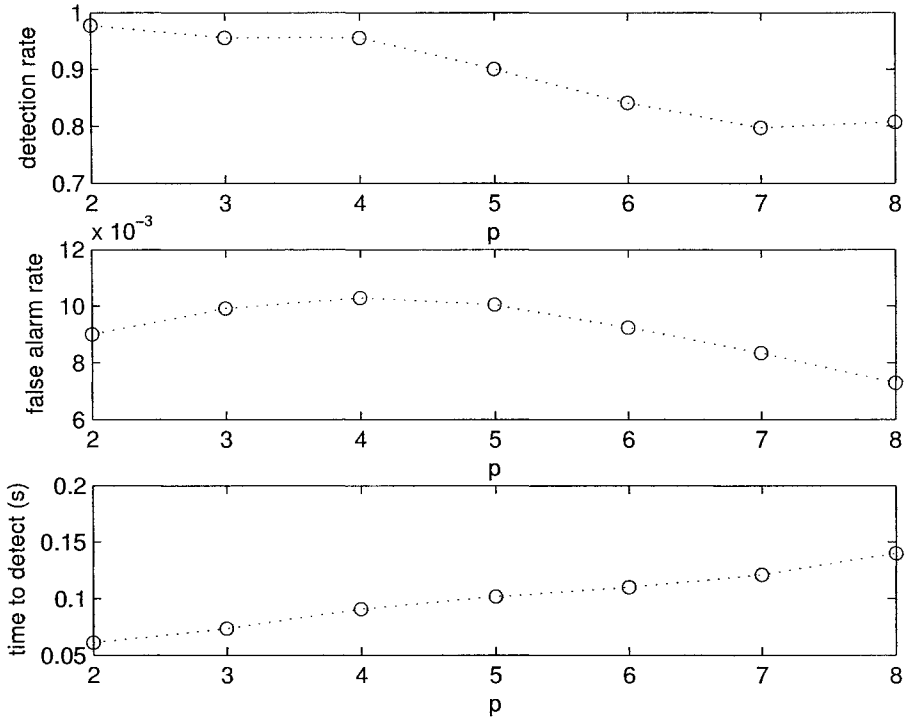

Figure 5.11: Control limits (L=300): varying p

When changing p, the best detection rates occur with low values, while the false alarm rate climbs and peaks at $p = 4$. Time to detection rises linearly with p. This is due to larger values of p that include more past samples, and thus giving less initial weight to a change in the data. The optimal p would be 2 to take advantage of high detection rates, low time to detections, and false alarm rates that are lower than the peak value.

The segment boundaries expected and detected by control limit tests, with $L = 300$ and $p = 2$, are shown in Fig. 5.12. Although the optimum values of $L = 300$ and

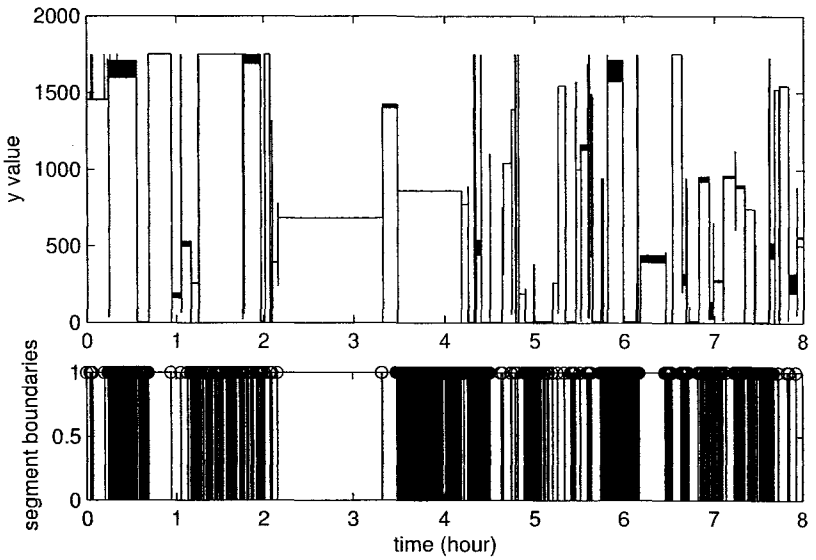

(a) Control Limit, L=300, p=2

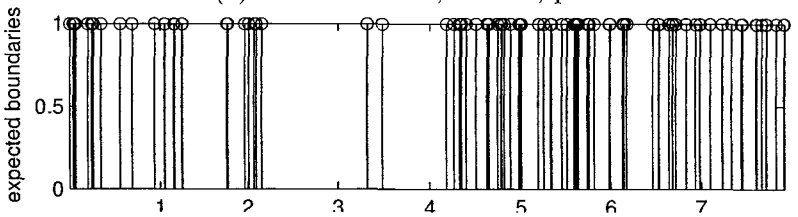

(b) Expected Boundaries

Figure 5.12: Control limits boundaries

$p = 2$ seem promising, Fig. 5.12 shows many false alarms across the eight hours of data. The length, L could be decreased below $L = 100$, but at this point too many missed detections are likely to occur.

One model CUSUM results

Fig. 5.13 plots the true positives, false alarms, and the mean time to detection for differing values of h when the CUSUM method is employed. As the threshold, h, is

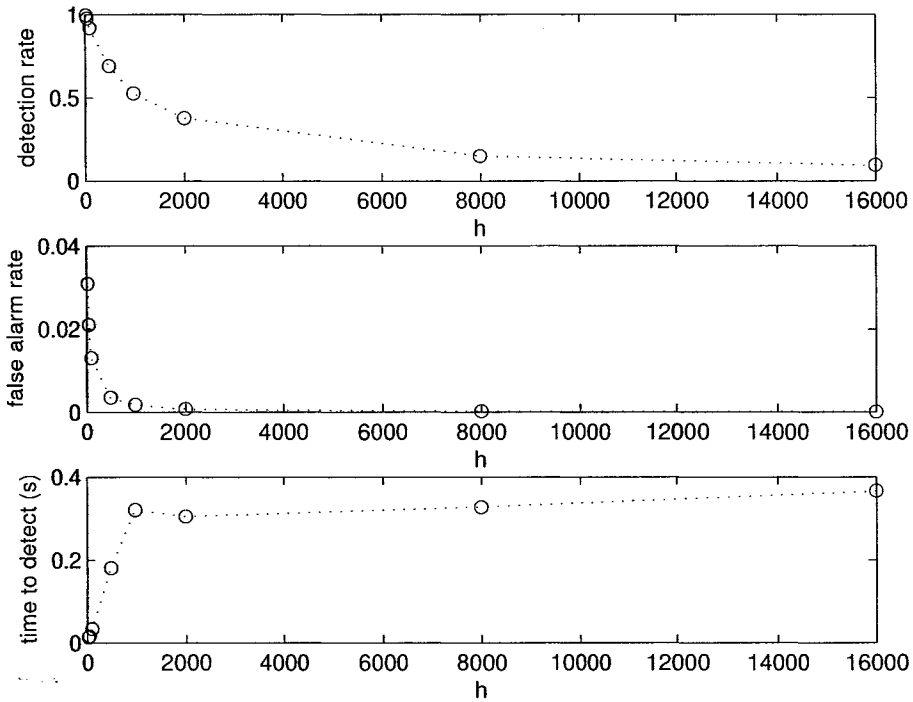

Figure 5.13: CUSUM: varying threshold h

increased, less segments are found and higher delays to detection result. However, at low h, false alarms are quite high. An optimal h threshold may be at $h = 100$, where detection rate is still over 90%, and the false alarm rate has fallen slightly. The time to detection is also minimized at this threshold.

The segment boundaries expected and detected by one model CUSUM, with $h =$

100, are shown in Fig. 5.14. During the first half of the data, the CUSUM method

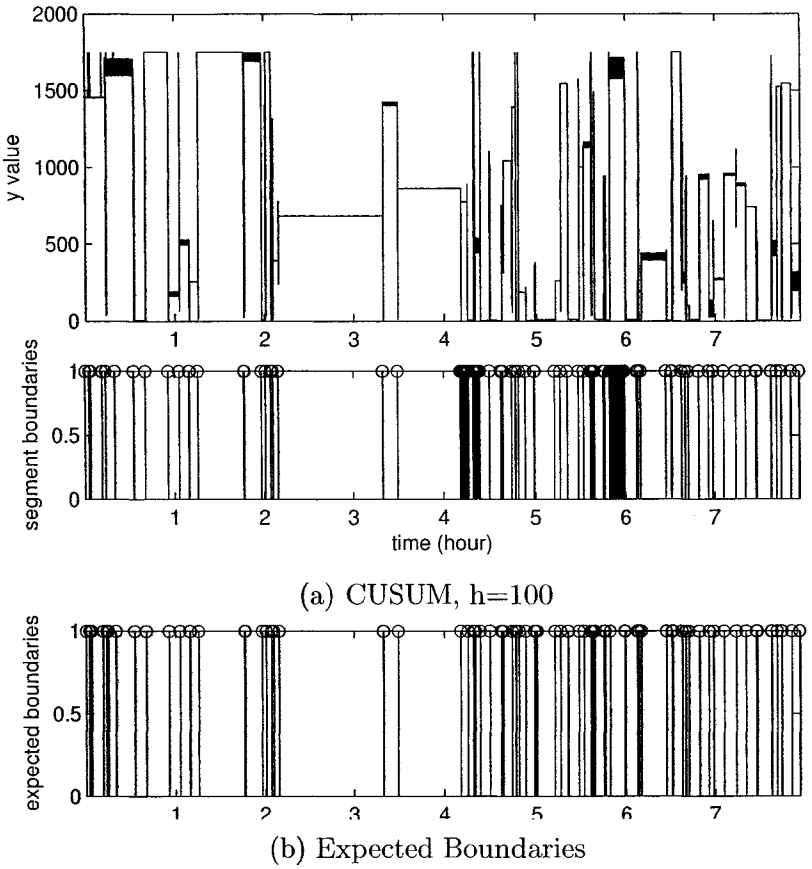

(a) CUSUM, h=100

(b) Expected Boundaries

Figure 5.14: CUSUM boundaries

lines up well with the expected boundaries. However, some noise during the fourth hour results in a number of false alarms. A breathing signal during the sixth hour is also picked up by the detector. Both of these areas can be seen by the thick black vertical lines in the segment boundaries plot. Some missed detections during the fifth hour are also noticed.

Two model GLR results

Fig. 5.15 plots the true positives, false alarms, and the mean time to detection for differing values of the threshold h, while Fig. 5.16 plots the same variables for differing values of the window size, L. In Fig. 5.15, we can see that low values of h result in a

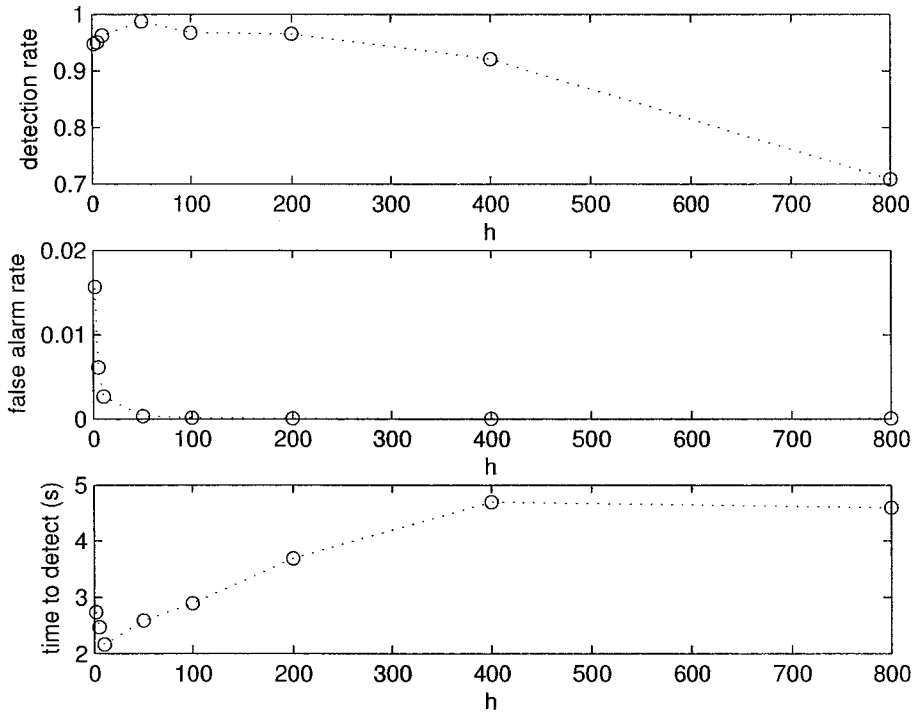

Figure 5.15: GLR: varying threshold h (L=50)

high number of correctly identified segment boundaries. At values of $h < 50$, the true positive rate drops slightly, while the false alarm rate rises sharply as h is decreased. The time to detection rises linearly with an increase in the threshold, plateaus at $h = 200$, and then drops after $h = 400$. An optimal value of h would be $h = 50$, to optimize for high detection rate, low false alarms, and low time to detection.

Fig. 5.16 shows that detection rate increases with L, but then drops off when the test window length (L) gets too long. This could be due to missed detections during the start of a segment, before the full test window length is available. This same

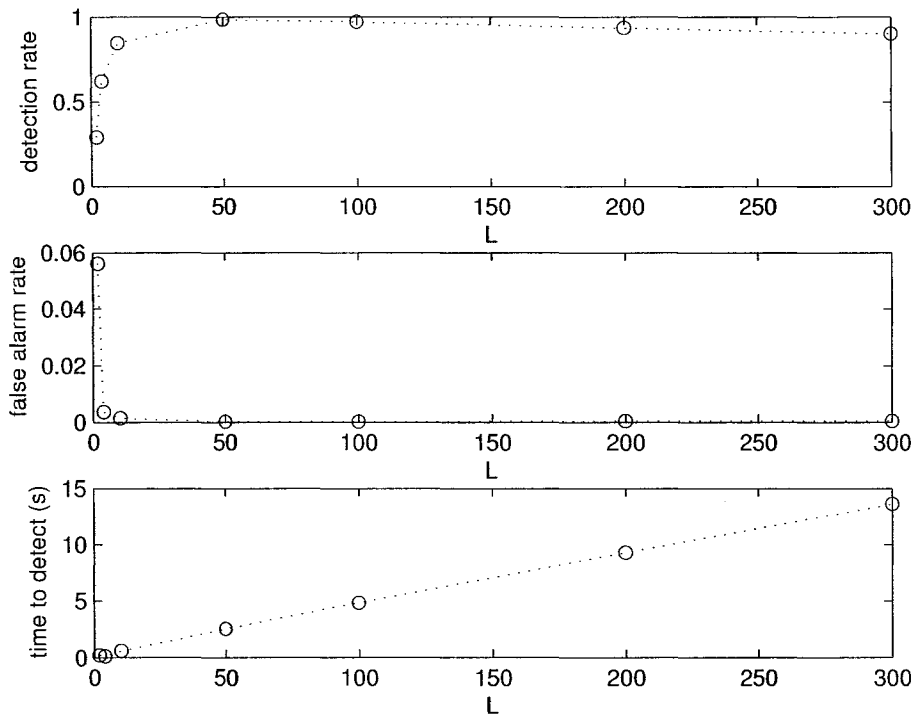

Figure 5.16: GLR: varying window size L (h=50)

phenomenon was seen in the control limits method, but in that method, it was the reference window length that had to be a fixed L samples long. False alarm rates also decrease with higher values of L, while time to detection rises linearly with L.

After closer observation of the segment timing, it was discovered that it usually takes one sample to detect movement onset, but close to L samples to detect offset. This means that the method would not show symmetric detection. The difference in detection time is reflected in the time to detections, since this time is close to 0.5 times the window size and it was seen that every second window takes close to the full L samples prior to detection. Recalling that the sampling rate is 10 Hz, an $L = 200$ would be 20 seconds long, and we can see it results in a mean of 10 seconds to detection.

The segment boundaries expected and detected by two model GLR, with $h = 50$

and $L = 50$ are shown in Fig. 5.17. Although this figure seems to produce more

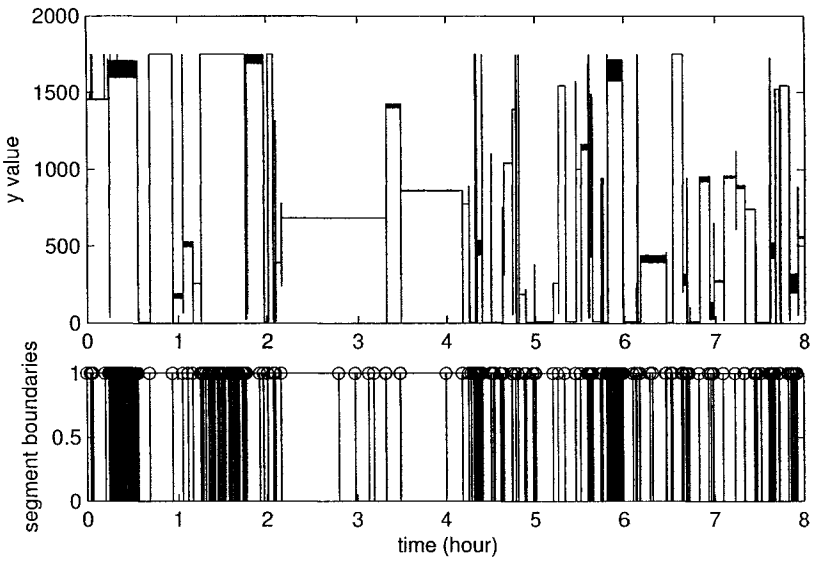

(a) GLR, h=50, L=50

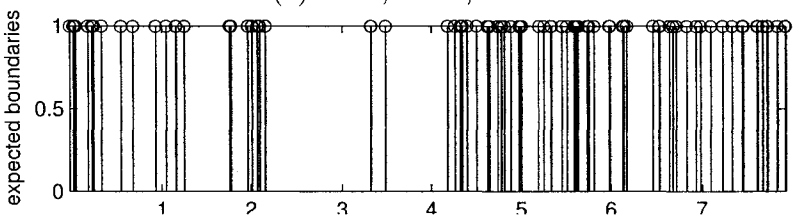

(b) Expected Boundaries

Figure 5.17: GLR boundaries

false alarms than the CUSUM method, as evidenced by the thick black areas, in fact, only 339 segments are represented here. The CUSUM segmentation, shown in Fig. 5.14 resulted in 4512 segments. The CUSUM false alarms are much more highly concentrated than those of GLR, and thus are not as visible.

5.3.2 Overnight Results

When segmenting real signals, such as EEG data, it is hard to determine if segmentation yields correct results, except by subjective means [68]. This is because the

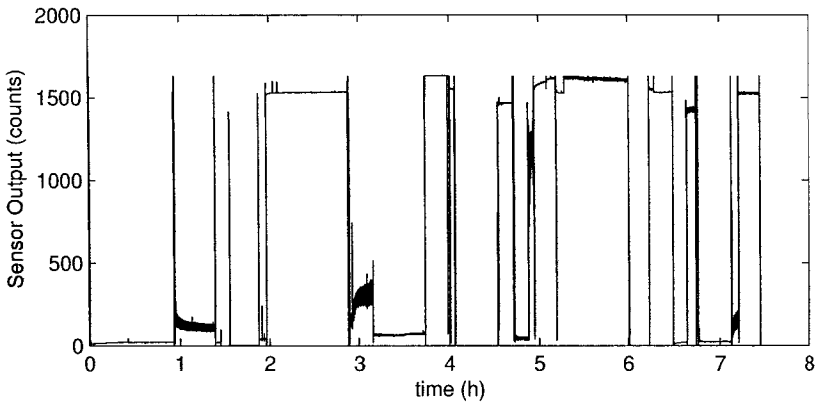

Figure 5.18: Overnight data from a single sensor

algorithms may detect changes that are not obvious by observation of the data. For instance, shifts in means due to slow baseline drift may result in a segment boundary. Changes in breathing patterns, such as in amplitude or frequency, may also be picked up.

To evaluate the use of the methods as movement-based segmentation methods, the number of expected movements can be compared to the number of segments detected. The number of expected movements can be hypothesized by observation of the number of visible spikes in the data. Processing time is a second metric for objective comparison.

Fig. 5.18 presents the data that will be segmented by each of the algorithms. This data is from a single sensor that was located near the chest/abdomen area, during a single night of monitoring a participant from bed entry to bed exit. 25 locations are counted where the mean changes around an activity spike in the data. These locations are likely position changes, where loading on the sensor changes during and after movement. 24 locations of smaller movement spikes, without mean changes around them, were identified. Additionally, at least two locations were found where no movement spike occurred, but the mean during breathing abruptly changed. In

total, 49 possible movement areas were identified, which would be expected to result in 98 segment boundaries.

Table 5.3 summarizes the results of segmentation for each algorithm, including number of detections and processing time requirements.

Table 5.3: Overnight segmentation

Type	Parameters	Number of Segments	Processing Time (s)
Movement detector	L=300	275	1.2
Two model control limits	L=300, p=2	2171	29
Two model control limits	L=75, p=2	1242	17
CUSUM	h=100	684	0.033
GLR	h=50, L=50	208	26
GLR	h=200, L=50	109	46

As shown in Table 5.3, the method that resulted in the number of segments closest to the expected value was GLR. However, GLR also took the longest to process the data, clocking in at three quarters of a minute. The fastest method was CUSUM, which barely took 3/100 of a second to calculate its 684 segmentation points. This is more than six times as many points as expected. By increasing processing time to just over a second, the movement detector can be employed, cutting back down the number of segments to 275. The two model control limits method took nearly as long to process the data as GLR, but likely shows many false alarms as it found over 1000 segments when $L = 75$ and over 2000 when $L = 300$.

The overnight results can also be evaluated by subjective observation. The following plots show the segmentation of the data from the sensor with the given segmentation methods.

The first plot is of the results from segmentation with the movement detector, were $L = 300$. The segments found look like they line up well with the spikes in the

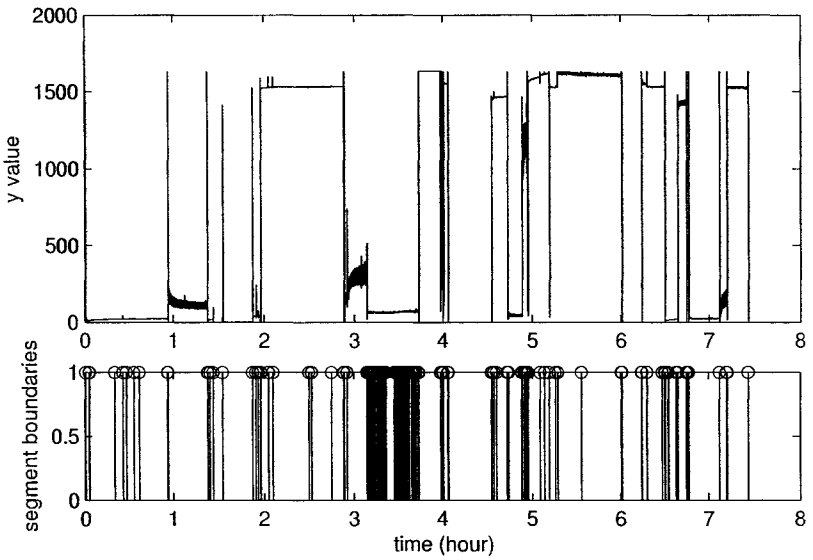

Figure 5.19: Overnight data segmented with movement detector (L=300)

data. During the third hour, many segments were found. These were false alarms, caused by a low-amplitude breathing signal with a wandering baseline and sharp wave peaks. Inspection of the rest of the night's segmentation points reveal some clustering of extra boundaries around movement. No obvious segment boundary is missed, however and many small movements are picked up.

Fig. 5.20 demonstrates the segmentation of the data by means of the control limits algorithm, with $L = 300$ and $p = 2$. It is expected from the number of segment boundaries found by this method that there will be a number of false alarms occurring. Looking at Fig. 5.20, this hypothesis can be accepted. Some parts of the night are free from false alarms, such as the time between the fourth and fifth hour, but much of the night, especially when the sensor was loaded, includes a high rate of segment boundaries.

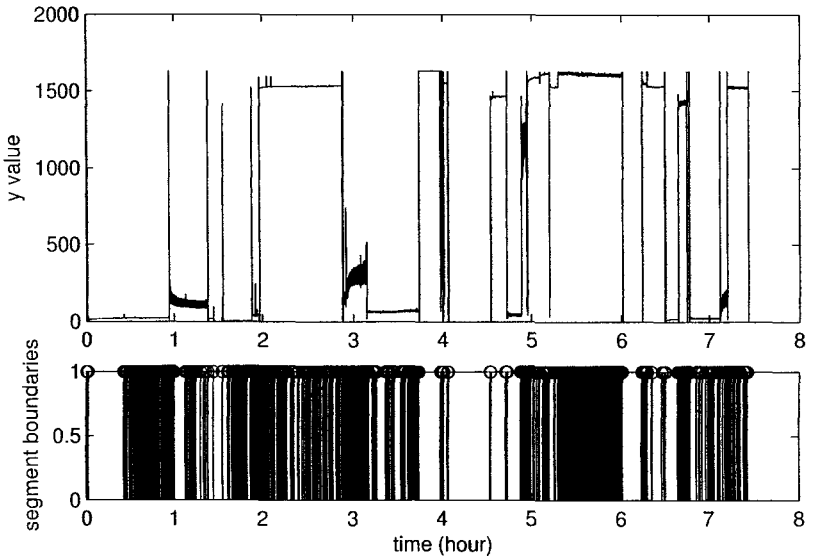

Figure 5.20: Overnight data segmented with control limits (L=300, p=2)

By decreasing the reference window length, L, it may be possible to reduce these false alarms. Fig. 5.21 shows the night's segmentation with $L = 75$. Again, we see in

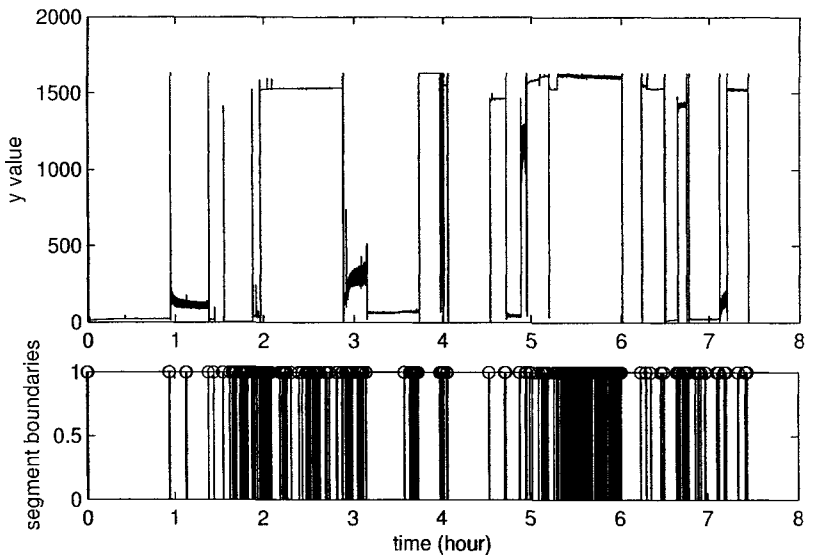

Figure 5.21: Overnight data segmented by control limits (L=75, p=2)

Fig. 5.21, that many areas of the night are thick with segment boundaries, but the width of these areas has decreased. However, there are some missed detections that are visible. A small spur occurs at the first half hour mark, and does not result in a boundary. A change in the mean happens at around 4h45min and no boundary is declared. Since there are both missed detections and many false alarms, the value of this method for segmentation is in doubt.

Fig. 5.22 shows the results of CUSUM segmentation. After viewing the results

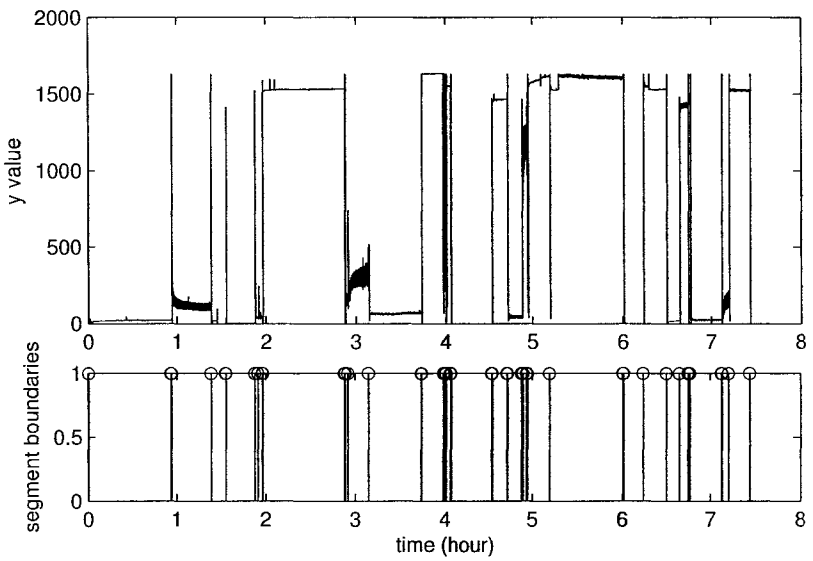

Figure 5.22: Overnight data segmented with the one model CUSUM test (h=100)

of the control limits segmentation, the sparseness of the boundaries detected by the CUSUM method is welcome. Fig. 5.22 shows that CUSUM picks up all major movement spikes. However, a number of smaller spikes remain undetected. These are visible from 1h00 to 1h15 and from 2h00 and 2h15. As in the simulation, there are many false alarms around the true positives at movement boundaries.

Fig. 5.23 shows the results of segmentation with two-model GLR, when $h = 50$ and $L = 50$. These parameters were shown to detect a high rate of true positives during

simulation. As is seen in Fig. 5.23, segment boundaries are detected throughout the

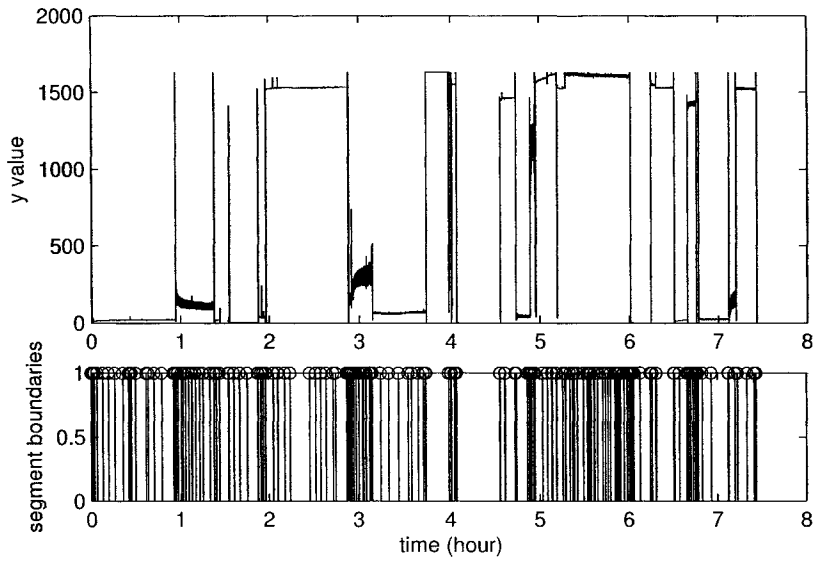

Figure 5.23: Overnight data segmented with GLR (h=50, L=50)

night. While it seems to provide more boundaries than the CUSUM algorithm, the boundaries themselves rarely include multiple false alarms surrounding them as they do with CUSUM. For each spike, a single boundary on each side is usually seen. The segments that are picked up during the night often show subtle changes that are not immediately obvious. For instance, a very small (< 5 count) change in the mean was picked up during breathing just after the first hour. This segment was not included in the original count as it was too subtle to be easily observed.

By raising the threshold, h, it is expected that less boundaries will occur, and those that do will be due to less subtle changes. Fig. 5.24 shows the results of GLR segmentation with $h = 200$ and L kept at 50. In Fig. 5.24, some of the boundaries shown in Fig. 5.23 remain, but the number has been cut down considerably. In Table 5.3, the number of boundaries was shown to be cut down to close to half of those found with $h = 50$. As expected, the boundaries that are left occur during movement

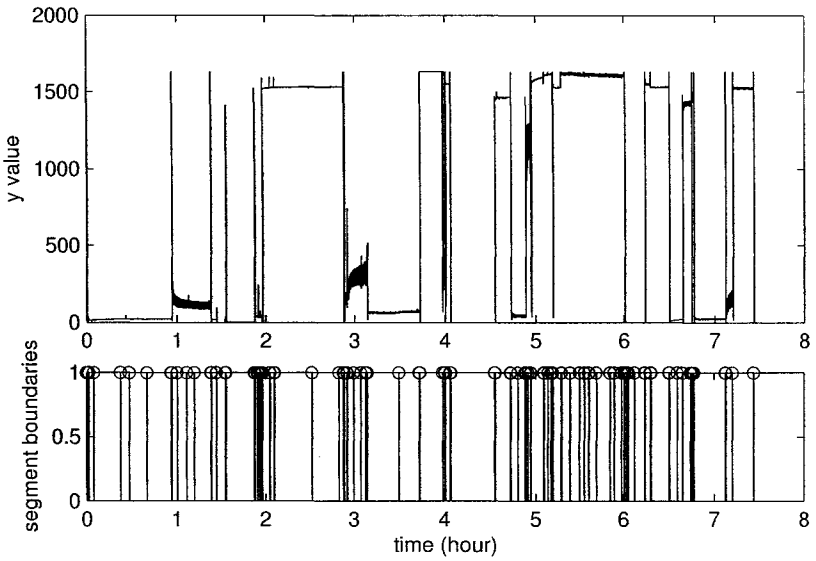

Figure 5.24: Overnight data segmented with GLR (h=200, L=50)

spikes and are less likely to occur because of small changes to the signal mean. There were no missing boundaries detected at this threshold level.

5.4 Discussion

The choice of optimal segmentation method revolves around the requirements for time to detection, true positive rate, false negative rate, and processing complexity. By analysis of the results in Tables 5.2 and 5.3, and subjective observation of the segmentation boundaries located by each method for a given dataset, we can evaluate the performance of the individual algorithms with these requirements.

When time to detection is important, the CUSUM algorithm delivers the lowest delay. For true positive rates at low false negative rates, the GLR algorithm showed up to 99% of simulated movements to be detected with a rate of less than 0.04% false alarms. It was also able to detect subtle changes in the mean of a breathing signal

from real experimental data.

Should false alarms be undesired, GLR offers a relatively stable detection of segment boundaries, for a wide range of threshold values. Reducing threshold values can help to minimize alarms that are the result of subtle changes, without sacrificing detection of the movement-related boundaries. For overnight segmentation, it produced the number of segments that was closest to the expected number.

The delay to detection for GLR could be more than a few seconds, especially during the change from a movement signal to a resting signal. However, methods have been introduced that allow repositioning of the boundaries after change detection [1], [52] in order to ensure that segment boundaries are correct even though detection is late. Additionally, the longer processing times related to GLR could be reduced. In [70], Brandt presents a recursive algorithm that could be implemented to speed up processing.

The proposed movement detector, with a sliding window length of $L = 300$, stuck a balance between all of the requirements, allowing less than five seconds to pass on average before detecting a change, but producing one of the lowest false alarm rates, and detecting most of the segment boundaries that occurred. Moreover, it had one of the fastest processing times. When processing actual data, it was affected by noisy breathing at one point, but was able to process most breathing without raising false alarms.

On the other hand, the close cousin of the proposed movement detector, the control limits detector, was not found to be suitable for segmentation of the pressure signals. It incurred too many false alarms without detecting the smaller changes. It was also one of the slower algorithms in terms of processing speed.

The CUSUM method requires far less processing time than the other algorithms, completing a full overnight segmentation more than 35 times faster than the next

fastest method. Its segmentation of overnight data produced more segment boundaries than the GLR or the proposed movement detector, but segments were dense around areas of movement and much of the night was undisturbed by false alarms. It may be possible to eliminate these false alarms when boundaries are detected within a specified number of samples of a previous alarm.

When movements occur frequently, the size of fixed-length reference windows becomes important, since these become dead zones for detection. This was shown to occur for both the GLR and control limits methods. A size of 300 samples was shown to be a good window size for both of these algorithms. 300 samples works well with breathing signals, since the lowest detectable respiratory rate should be 2 bpm, or one cycle every 300 samples. For a person with a very low breathing rate, reference windows less than 300 samples may result in segmentation occurring due to a single breath.

For all methods applied to real data from an overnight experiment, there were false alarms, although the term false alarm could be disputed. Actual breathing signals are much less stable or stationary than the simulated signals and so a number of the algorithms picked up changes based on these non-stationarities. False alarms may not necessarily be a problem, since segments could be recombined later where necessary [1].

Diagnosis or classification of segment data has been done in this chapter, except through the movement detector's classification of movement versus restful segments. Through classification, false alarms could be identified. This would reduce the negative effects of a false alarm. For instance, if the number of segments during the night is used as a restlessness detector, false alarms would artificially increase the calculated restlessness. By removing the false alarms, the restlessness scale would better reflect the actual restlessness of the individual. It has been argued that false alarms

are not as important for segmentation applications compared to other applications of change detection [52], due to the possibility of segment recombination. However, recombining segments due to false alarms would slow down processing speed.

Chapter 6

Source Extraction

This chapter examines the extraction of individual source components from the sensor signal. Current methods of signal extraction were evaluated and a method was proposed based on a combination of two of these methods. All methods were evaluated by application to the extraction of breathing signals from the data.

Respiratory signals suffer from noise due to the ballistocardiogram, systemic Gaussian noise, and aperiodic movements. Five methods were compared for respiratory signal extraction using the respiratory signal collection outlined in Sec. 4.7:

- movement suppression
- digital filtering
- wavelet filtering
- adaptive smoothing
- a proposed two stage cascade combination of the above

6.1 Method

The database of respiratory signals were loaded, and segmentation for movement detection was performed according to the movement detection algorithm presented in Chapter 5 and published in [2]. The mean was subtracted from the signals and the algorithms under test were used to extract the breathing signals. Results were evaluated as described in the next section.

The movement suppression algorithm first sets all points where movement was detected to zero. Next, it subtracts the mean from all the points where movement was not detected.

$$s_i[n] = \begin{cases} x_i[n]_{m_i[n]=0} - E[x_i[n]_{m_i[n]=0}] & \text{for } m_i[n]=0 \\ 0 & \text{for } m_i[n]=1 \end{cases} \tag{6.1}$$

Digital filtering was applied to attenuate the frequencies that are out of the expected respiratory frequency range. Each respiration signal was input to a digital bandpass filter FIR filter with cutoff frequencies of 0.033Hz and 0.833Hz, created using the MATLAB 'fir1' function. An IIR Butterworth filter was also applied using the MATLAB 'butter' function. The effect of changing the filter orders was investigated.

A third type of digital filtering is through discrete wavelet transforms (DWTs). The DWT was used to decompose the respiration signal into detail and approximation coefficients. The detail coefficients whose scale fit within the frequency band from 0.03 Hz to 0.8Hz were used to reconstruct the signal. This method of decomposition reconstruction was reviewed in Sec. 3.2.1, and has been previously used for source extraction of respiration signals from a pressure sensor [33]. The maximum decomposition level was the first level at which the approximation coefficients occupied frequencies below 0.03 Hz. If the approximation coefficients occupied the band

below 0.03 Hz and also up to near 0.8 Hz, then only the approximation coefficients were used for the reconstruction.

The effect of changing the filter order of the DWT was tested by trying different levels of Daubechies mother wavelets, from Daubechies 1 (also called the Haar wavelet) to Daubechies 8. The frequency band for each detail coefficient level and approximation coefficient level were calculated at run time based on the sampling rate (10 Hz), the length of each signal window (300 samples) and the mother wavelet's center frequencies.

Adaptive filtering was applied using the normalized least mean square algorithm (NLMS). A smoothing configuration was investigated. This configuration uses the adaptive algorithm to smooth the signal by applying the expected output as a delayed version of the input.

Combining these algorithms together could result in better signal extraction than one method alone could provide. The proposed system is to combine the previous techniques through a cascade of movement suppression and filtering. Here, DWT filtering will be used at the filtering stage.

6.2 Evaluation

The results of these methods were evaluated by comparing the signal energy at the frequency of interest in the spectrum of the output signals. A signal to noise ratio (SNR) measure was made for the signals by taking the ratio of signal energy in the frequency bin of interest to the total signal energy in the spectrum up to the Nyquist rate. Improvement was measured by a ratio of the new SNR to the old SNR and comparisons were made regarding the dB improvement. This was called the 'SNR improvement'.

Although this provides a good method for comparison, there is also interest in knowing how the signal energy in the frequency bin compares with the peaks in the signal. Ideally, this extraction would allow respiratory rate estimations based solely on the highest peak in the spectrum. Therefore, a second metric was evaluated from the ratio of the signal energy at the frequency of interest to the highest peak in the rest of the spectrum. This is called the spurious free dynamic range (SFDR). The ratio of the extracted signal's SFDR to the original signal's SFDR was measured as the 'SFDR improvement'.

The SNR and SFDR improvements were measured in decibels (dB). The aim of the analysis is to discover which algorithms resulted in high positive values for each of these metrics. Algorithms that provided negative improvements were considered to deteriorate the extracted signal rather than improve it.

6.3 Results

The first results presented are comparisons of how each of the algorithms fared in the testing. Details regarding the results of each of the methods are shown next.

6.3.1 Comparison of Extraction Algorithm Performance

For most of the algorithms presented here, parameters could be chosen that would improve their performance. The following results use parameters for each algorithm that were chosen to show good results. These results will be shown in Sec. 6.3.2 to Sec. 6.3.6.

Fig. 6.1 presents a resume of the mean improvement to all of the signals in the database by method. Each of the algorithms has shown a marked SNR improvement over the original. SFDR improvement was lower, but was positive for all algorithms.

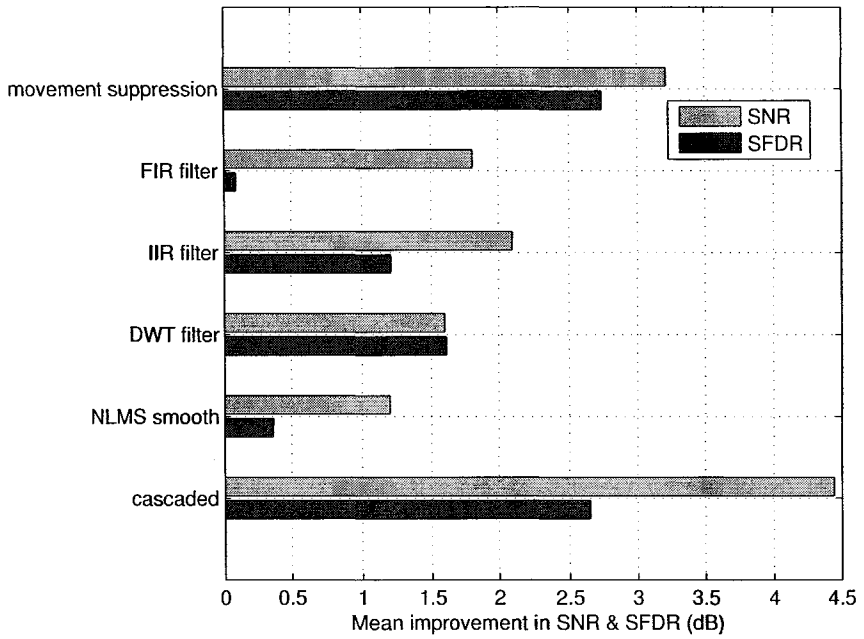

Figure 6.1: Mean enhancement by algorithm

The movement suppression algorithm had the highest improvements of all single-stage extraction methods. The cascaded method leveraged this result together with the improvement offered by the DWT filter, to give the highest SNR improvement, but was not able to further improve the SFDR. While both the FIR filter and the NLMS smoothing method showed an increase in SNR, SFDR was only slightly improved. All other algorithms increased both SNR and SFDR by at least 1 dB.

Fig. 6.2 breaks down the SNR improvement for each method by type of signal. In the first three signal types of Fig. 6.2, SNR is improved in inverse relation to the amplitude of the signal. This is because the original SNR is lower at lower amplitudes and an equal suppression in noise will improve the SNR of low amplitude ratios the most. For these three signal types, which are at regular breathing frequencies with

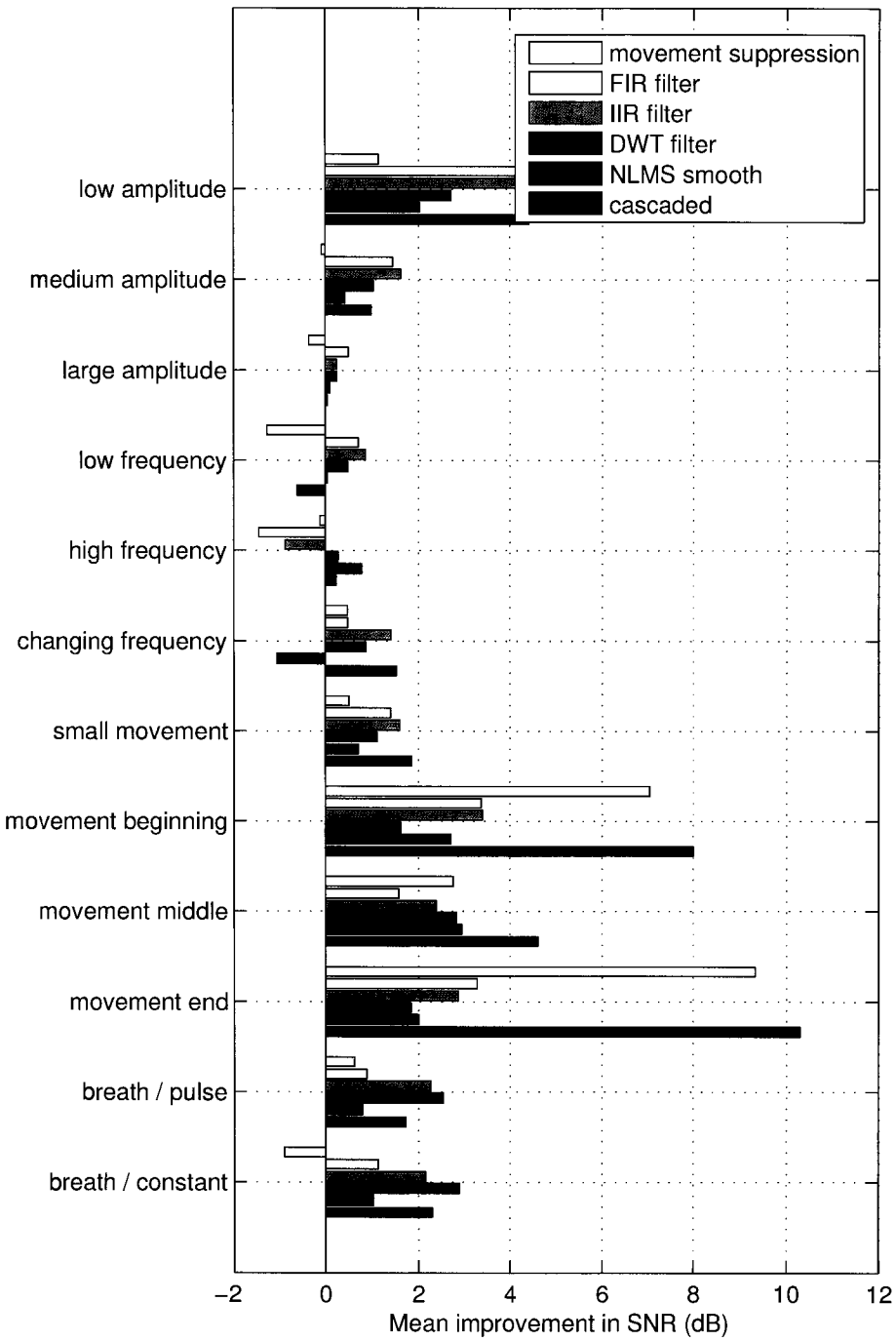

Figure 6.2: Mean SNR enhancement by algorithm and type

medium amplitudes and no movements, FIR and IIR filtering offer the best single-stage SNR improvement.

These two filter types were not as good for high frequency breathing signals as they actually degraded the SNR on those signals. This was was investigated and it was found that some of the high frequency breathing occurs with frequencies exceeding the highest expected rate (> 0.8 Hz) and thus past the cutoff frequency of the filters.

All signal extraction methods improved the SNR of breathing signals that included movement by an average of around 3 dB. Movement signals occupy a wide frequency bandwidth and so filtering methods can improve SNR by reducing the noise power due to movement that is out of band.

Fig. 6.3 displays SFDR improvement by signal type. Fig. 6.3 shows that the amplitude of the breathing signal only negligibly affects the SFDR improvement and that high frequency breathing signals are once again degraded by the digital filters. SFDR was improved the most for signals with movement or that change from including breathing to not including breathing (breath/constant and breath/pulse) half-way through.

The SFDR of breath signals with a frequency change are degraded on the most part by filtering. This might be a function of the fact that the breath rate of these signals is a mean value and may not be located on a peak of the spectrum. After filtering, the peaks may be stronger, reducing the SFDR at the spectral location of the mean frequency.

The next sections (Sec. 6.3.2 to Sec. 6.3.6.) will provide an examination of the results of individual methods.

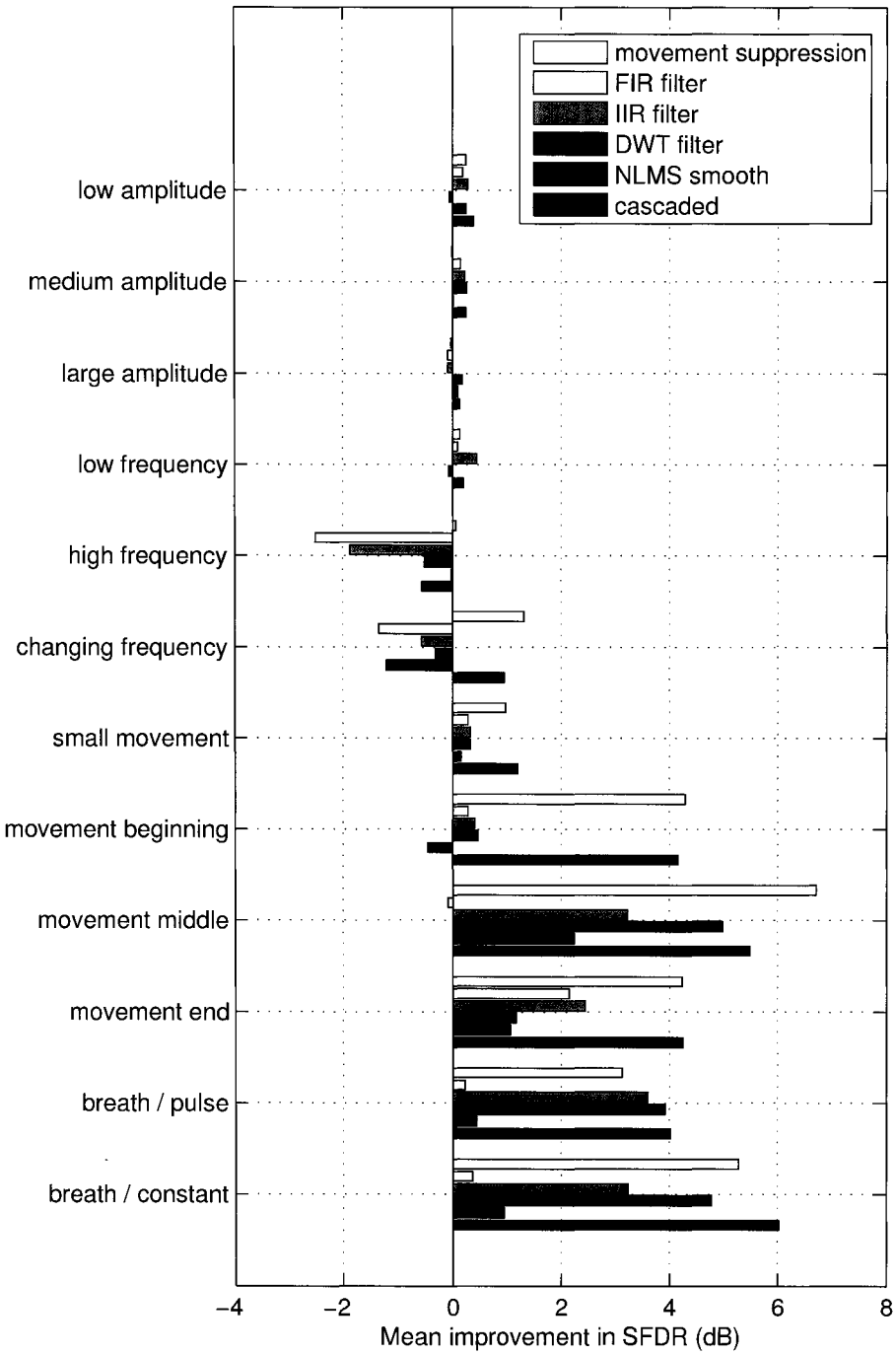

Figure 6.3: Mean SFDR enhancement by algorithm

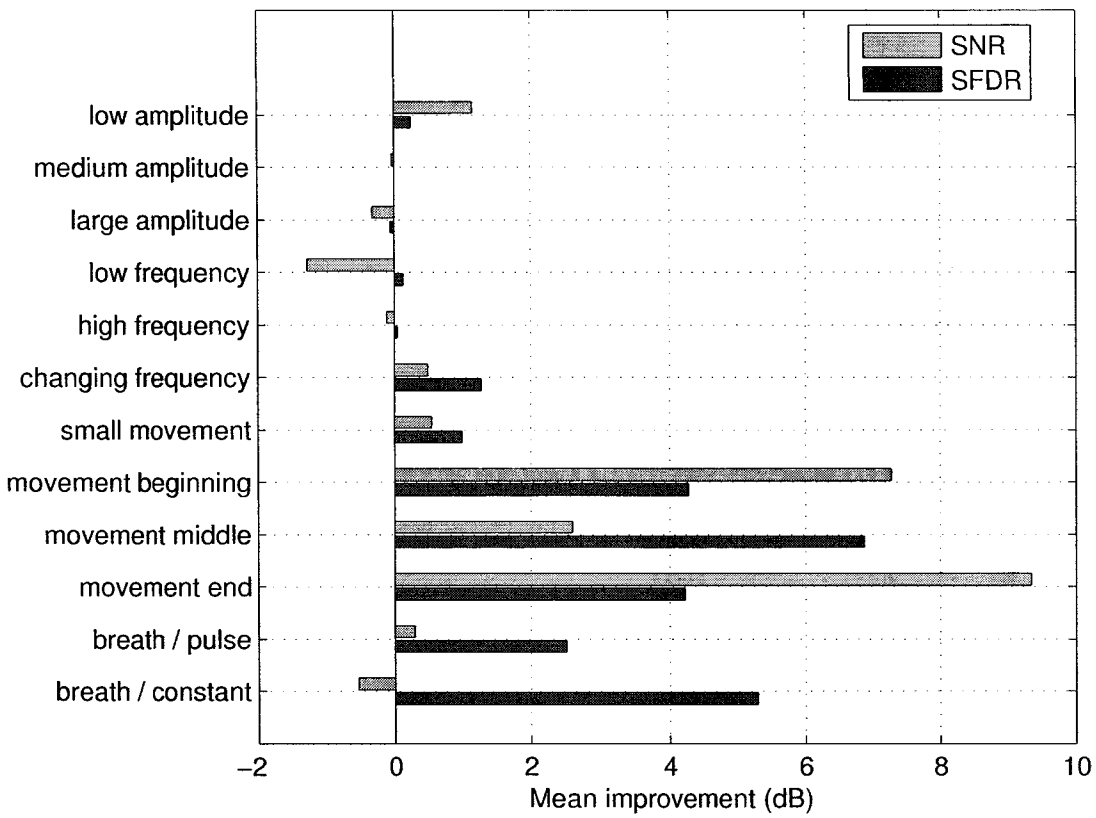

Figure 6.4: Respiration signal enhancement by movement suppression

6.3.2 Movement Suppression

Fig. 6.4 shows the signal enhancement for different respiration signal types with the movement suppression algorithm.

Movement suppression improved the SNR of breathing signals that included movement at the beginning or end by over 7 dB. Movements in the middle of the breathing signal were not as improved by movement suppression. This may be due to the fact that a change in output level often occurs after a movement and this output level change is not suppressed by the movement suppression algorithm, creating a sharp edge in the signal. Although the SNR didn't improve as much for signals with

movement in the middle, the SFDR did improve. The SFDR for all large movement-corrupted signals improved by more than 4 dB through the use of movement suppression. Since there is sometimes a movement when a breathing signal changes to a constant signal, SFDR is also improved by movement suppression of in half breathing / half constant signals.

6.3.3 Digital Filtering

Designing a digital passband filter for the area of interest is not a trivial task. The lower passband frequency cutoff is relatively close to zero and the passband itself is relatively narrow. This difficulty has been previously reported [33]. Creation of an IIR filter proved to be difficult for orders past 6 since unstable filters resulted, with poles placed outside the unit circle. These poles were due to the low-frequency cutoff which required zeros at zero and strong poles to offset these near 0.033Hz.

Fig. 6.5 shows the mean signal enhancement by filter order for a FIR filter. Higher filter orders improve both the SFDR and SNR. SNR shows the fastest rate of improvement for filter orders up to around 10. Past this point, dB improvement becomes more linear, with some small dips. SFDR actually degrades on average at low filter orders, but shows a linear upwards trend at 15 taps and up. After 30 taps, SFDR starts to show improvement rather than degradation.

Fig. 6.6 shows the signal enhancement for different respiration signal types due to FIR filtering. As shown in Fig. 6.6, low amplitude signals showed the best SNR improvement due to FIR filtering. However, marked SFDR improvement was only shown for breathing signals corrupted by movement.

Fig. 6.7 shows the mean signal enhancement due to IIR filtering by filter order. Again, higher filter orders improved both SNR and SFDR. Unlike FIR filtering, all filter orders produced SFDR improvement. At filter orders of 4 and above, SNR

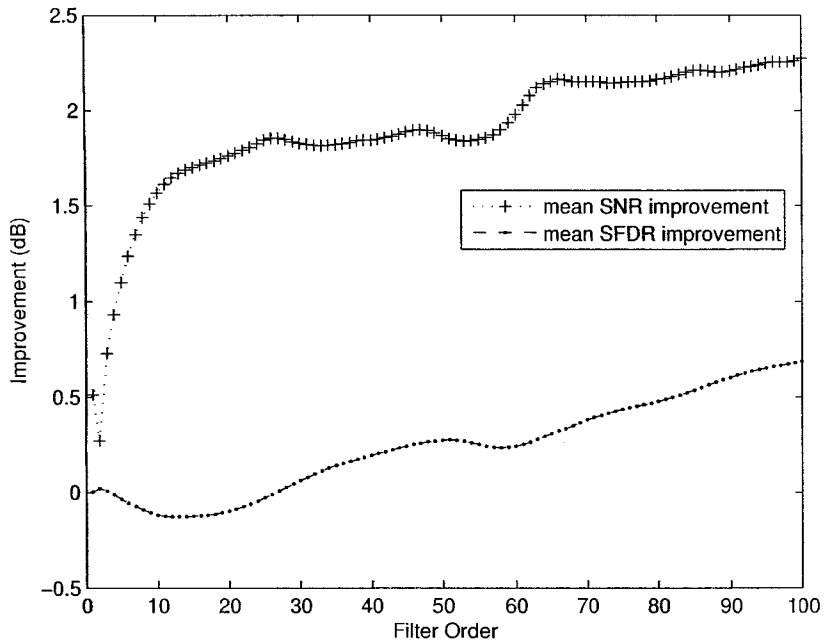

Figure 6.5: Enhancement as a function of FIR filter order

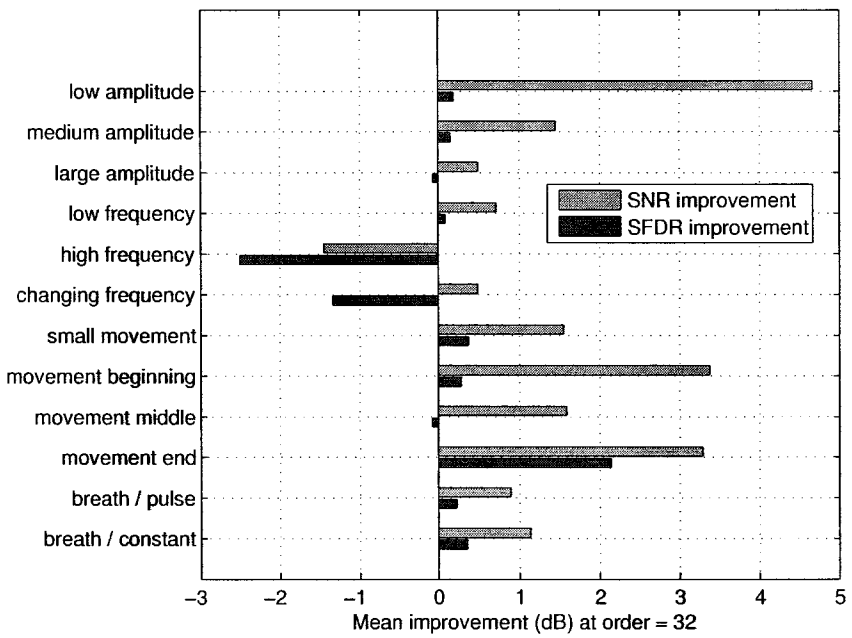

Figure 6.6: Respiration signal enhancement by FIR filtering at order = 32

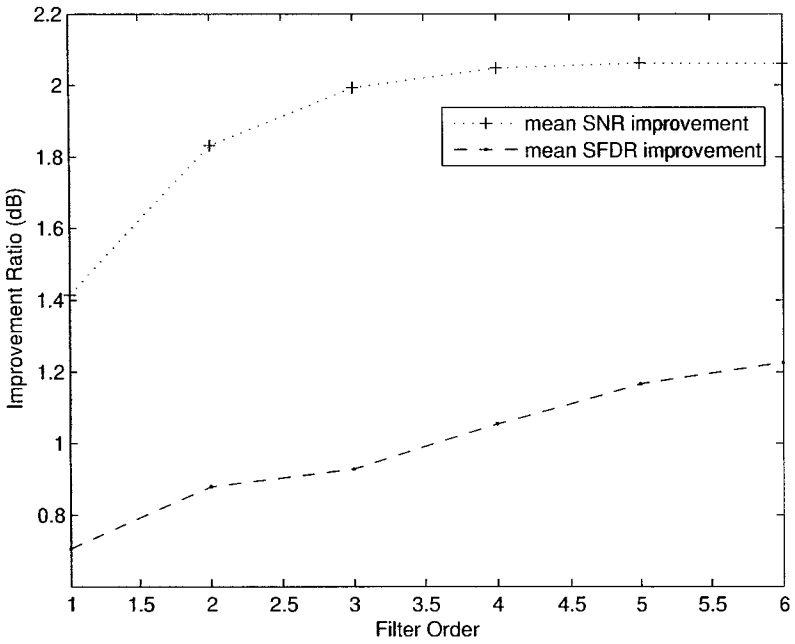

Figure 6.7: Enhancement as a function of IIR filter order

improvement leveled off, but SFDR continued to improve. A filter of order 6 is optimal as it allows maximum SNR and SFDR performance.

Fig. 6.8 shows the signal enhancement for different respiration signal types due to IIR filtering. These results are quite similar to those reported for FIR filtering for the first 8 signal types. However, IIR filtering showed much higher improvements for both SNR and SFDR for the last 4 signal types.

Although Fig. 6.8 indicates that IIR filtering does a good job at extracting the breathing signal during movement, inspection of the extracted signals with movement show that it is actually doing a good job at transforming the movement into a breathing-like signal. The breathing signal preceding or following the movement is not enhanced and may in fact be lost in the extracted signal.

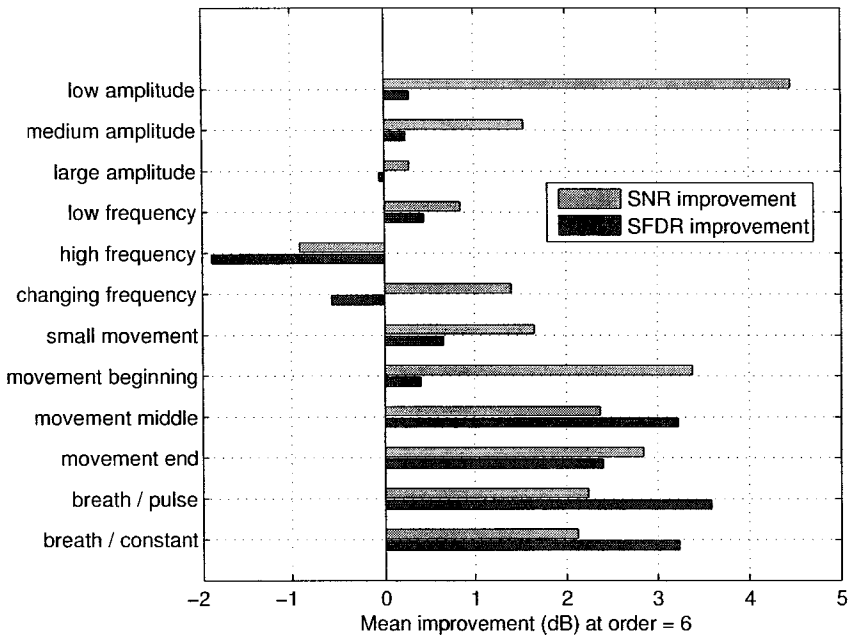

Figure 6.8: Respiration signal enhancement by IIR filtering

6.3.4 Discrete Wavelet Transform Filtering

Table 6.1 summarizes the maximum levels of DWT decomposition that were performed according to filter order. The coefficients levels used to reconstruct the signals are listed, along with the estimated frequency band they occupy. A_3 stands for approximation coefficients from level 3 and D_7 for detail coefficients from level 7. From the frequency bands listed in the table, one can see that most reconstructions occupied a slightly larger bandwidth than the 0.033 Hz to 0.8 Hz of the FIR and IIR filters.

Fig. 6.9 shows the mean signal enhancement by filter order due to extraction from recomposition levels shown in Table 6.1. The Haar mother wavelet (filter order = 1) did not allow appreciable SNR improvement and degraded the SFDR. However, for filter orders greater than 1 (Daubechies mother wavelets 2 - 7), both SFDR and SNR

Table 6.1: Decomposition coefficients used for reconstruction

Order	Maximum Level	Coefficients	Frequency Band (Hz)
1	3	A_3	0.000-0.623
2	7	$D_3 - D_7$	0.026-0.833
3	7	$D_3 - D_7$	0.031-1.000
4	7	$D_3 - D_7$	0.028-0.893
5	7	$D_3 - D_7$	0.026-0.833
6	7	$D_3 - D_7$	0.028-0.909
7	7	$D_3 - D_7$	0.027-0.865
8	7	$D_3 - D_7$	0.026-0.833

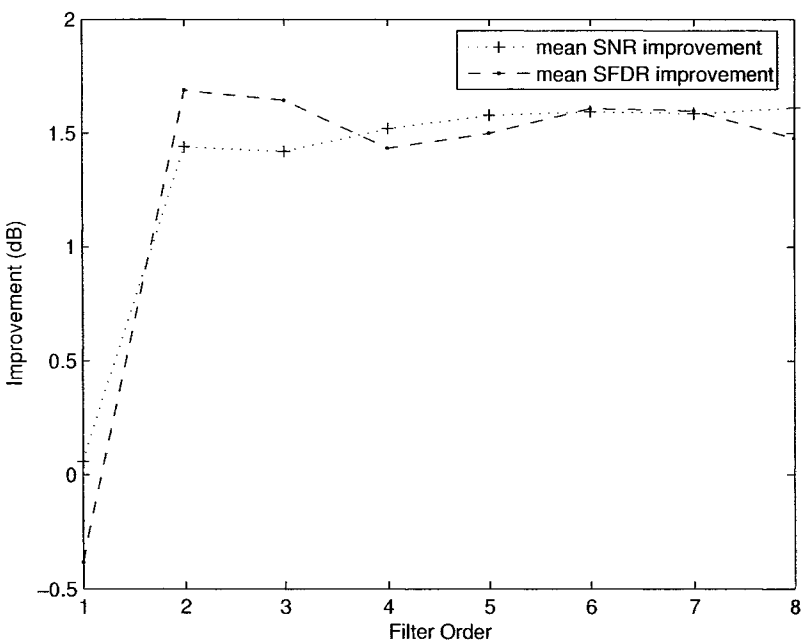

Figure 6.9: Enhancement as a function of DWT filter order

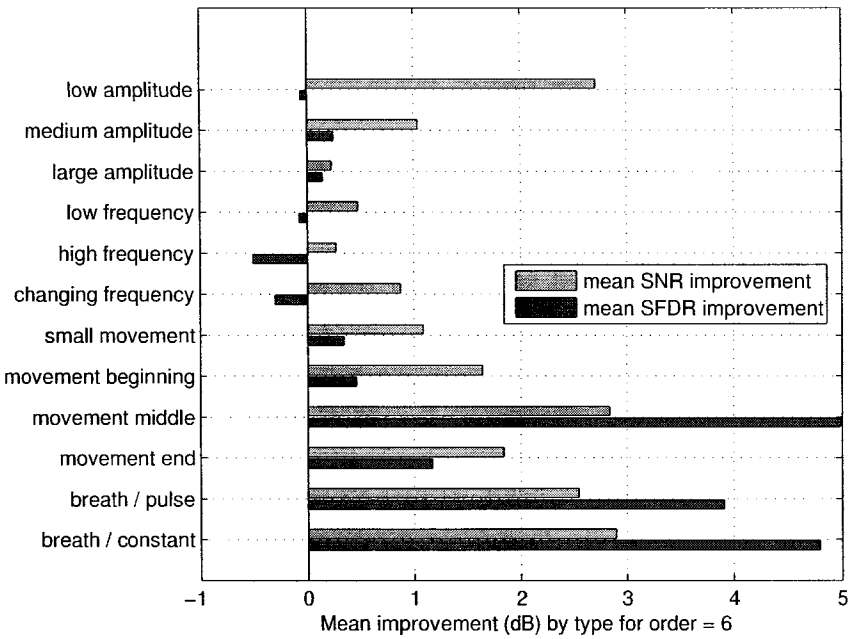

Figure 6.10: Respiration signal enhancement by DWT filtering

improved by around 1.5 dB. Filter orders 6 and 7 may be the optimal orders, where both SNR and SFDR is maximized to be above 1.5 dB.

Fig. 6.10 shows the signal enhancement for different respiration signal types due to DWT filtering. These results are similar to the results shown for IIR filtering, even though the DWT filters use FIR filtering. The best improvements occur for movement corrupted signals, where SFDR is improved by as much as 5 dB and SNR by almost 3 dB. Like most filtering methods, low amplitude breathing signals are also some of the most improved by this filtering method.

6.3.5 Adaptive Smoothing

The delay between input and output is what creates the smoothing effect of the adaptive smoothing filter. Fig. 6.11 shows the mean signal enhancement performance

as a function of the delay, where β is 0.4 and the filter is a moving average (MA) filter of order 10. Long delays were shown in this figure to decrease signal quality.

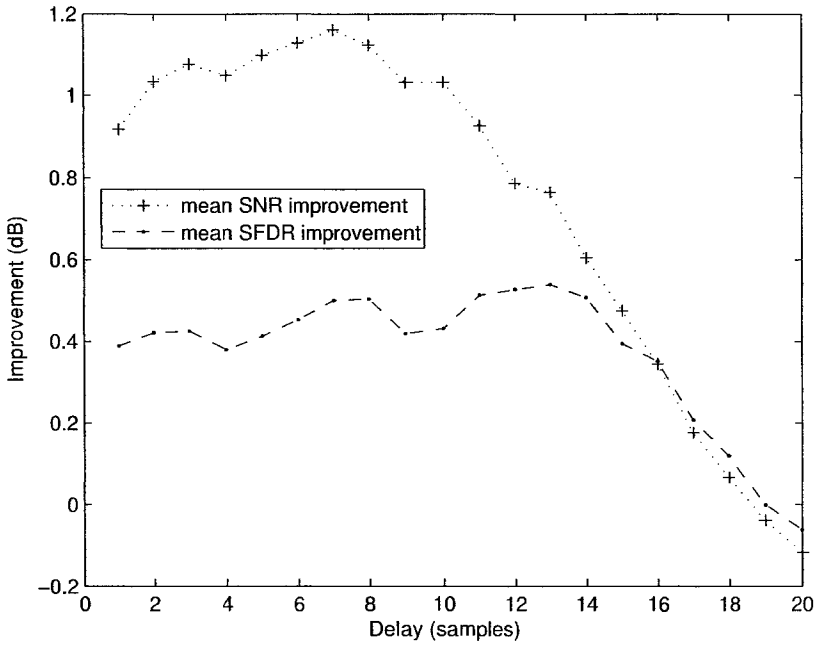

Figure 6.11: Adaptive smoothing enhancement as a function of delay

For SNR, this decrease began after 7 samples of delay. For SFDR, the decrease began a little later, after 14 samples of delay. Using a delay of 7 samples may be optimal.

Fig. 6.12 shows the mean signal enhancement performance as a function of a variable β. This parameter controls how fast the adaptation will converge but faster convergence is a trade-off with steady state error swings. In fact, lower betas (and therefore slower convergence) show better SNR improvements. SNR improvement decreases linearly with higher beta, while SFDR remains somewhat constant, with a slightly negative slope. While lower β values result in better performance, the delay to convergence is expected to be longer with a small β.

Fig. 6.13 shows the delay to convergence with respect to β. As expected, lower

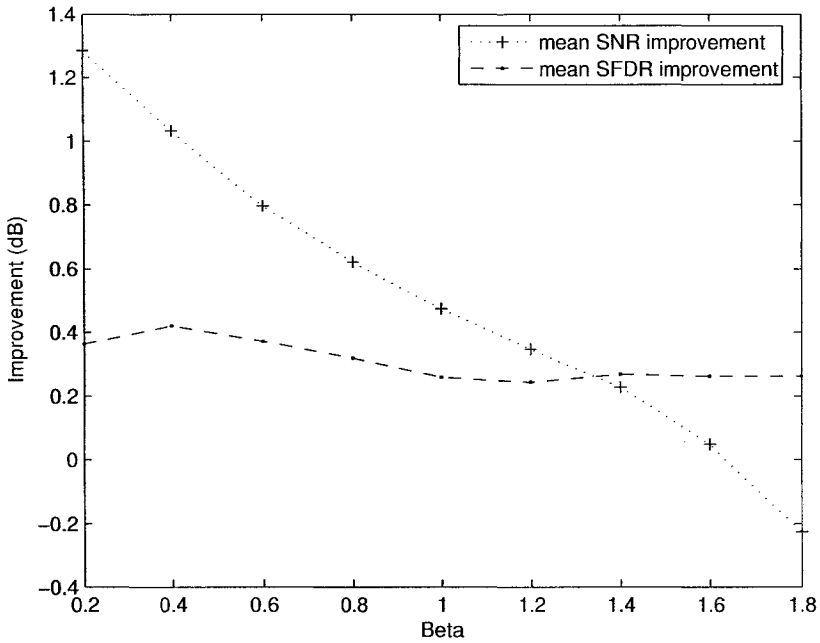

Figure 6.12: Adaptive smoothing enhancement as a function of β

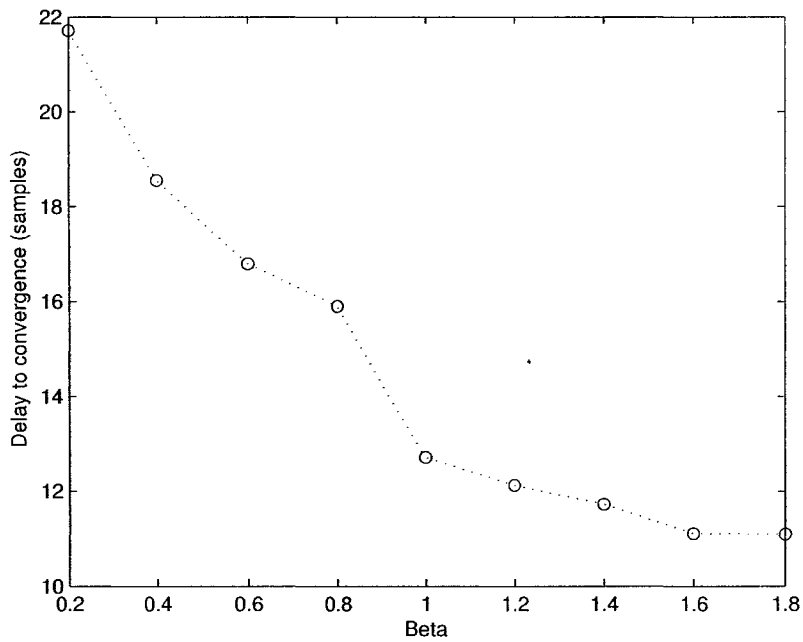

Figure 6.13: Delay to convergence as a function of β

betas take longer to converge. However, the gains in SNR and SFDR with the slower convergence may be worth it. The slowest convergence is only just over 2 seconds, or 1/15 the size of the 30-second data window used for source extraction.

The type of filter used and its order also plays a part in the performance of this algorithm. Fig. 6.14 demonstrates that an autoregressive filter is not the best choice

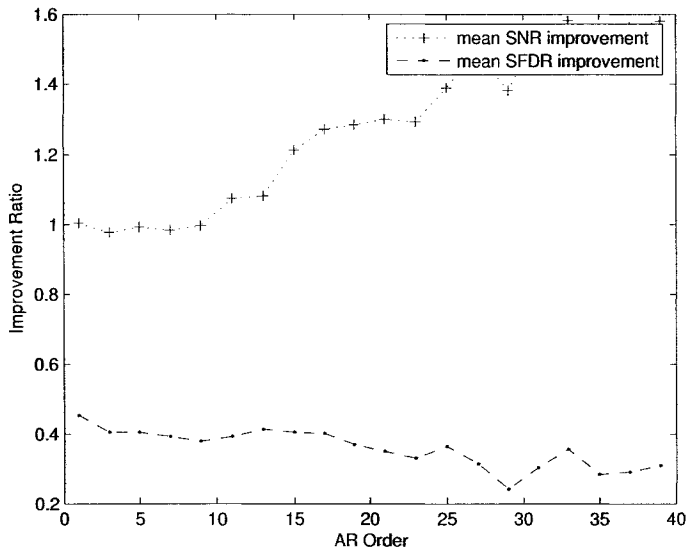

Figure 6.14: Adaptive smoothing enhancement by differing AR filter orders

if a low filter order is desired, while Fig. 6.15 demonstrates how a moving average filter can produce enhanced results at low orders. This is intuitive as the smoothing filter's required output is a delayed version of the input and the AR filter ignores the input for its calculations, thus negating the benefit of the delay between the delayed and undelayed signal.

Fig. 6.16 shows the signal enhancement for different respiration signal types due to adaptive smoothing using parameters chosen through analysis of the previous results. Adaptive smoothing is one of the only algorithms to provide SNR improvement to high frequency breathing signals. Since the smoothing is not limited by a frequency

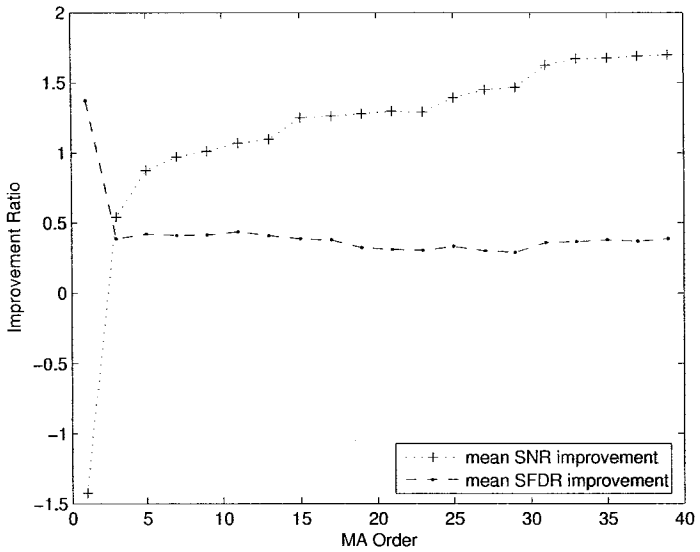

Figure 6.15: Signal enhancement by MA filters, by filter order

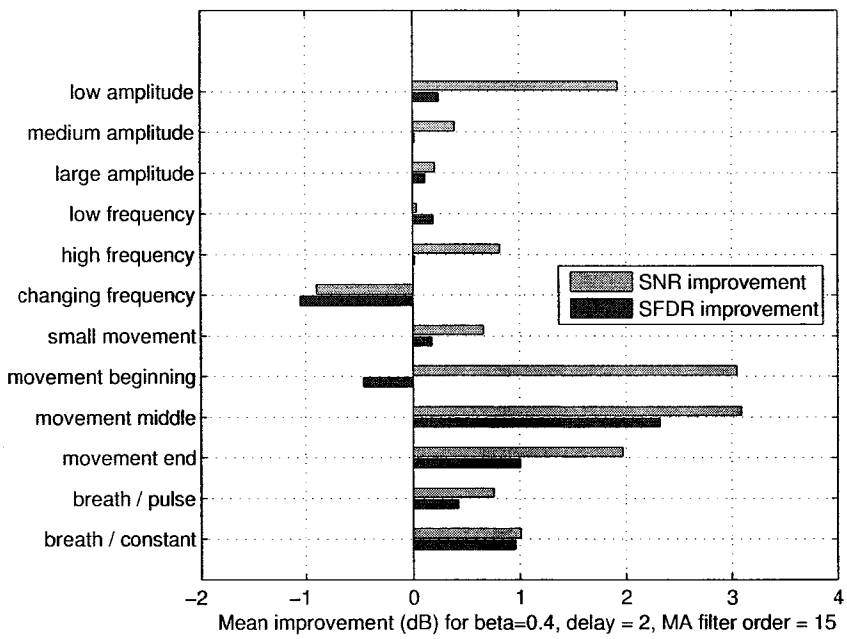

Figure 6.16: Adaptive smoothing enhancement by signal type

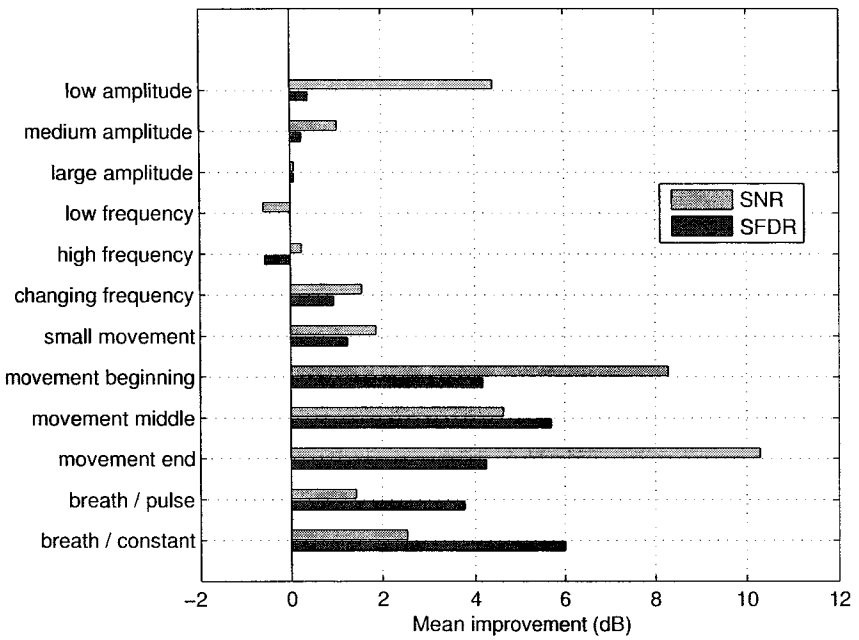

Figure 6.17: Cascaded enhancement by signal type

band of interest, it can follow high frequency breathing signals better than FIR, IIR, and DWT filters. Movement at the beginning of a breathing signal is detrimental to the SFDR, perhaps because it attempts to adapt to this movement at first. However, SNR is still improved since it will smooth out this movement as well as the breathing signal.

6.3.6 Cascaded Enhancement

By choosing parameter values from the previous results and cascading together the movement suppression and DWT filtering superior performance should result. Fig. 6.17 demonstrates the signal enhancement performance of the cascaded system by breathing signal type. This system shows SNR and SFDR improvements greater than 4 dB for all signals with movements in differing locations. The only signals that

are not improved in either SNR or SFDR are the high frequency signals that have been previously reported to be problematic for the DWT filter and the low frequency signals which were also problematic for the movement suppression algorithm. The cascade of movement suppression and DWT can improve the SNR of breathing signals that are corrupted by movements at the signal's end by more than 10 dB. This is the best improvement seen thus far across all signal types and extraction methods.

6.4 Discussion

The evaluation method used concentrated on the spectrum in the area of the frequency of the respiratory rate. However, a breathing signal is not a sinusoid and the best methods of extraction found here could ignore the shape of the input signal in favour of producing a sinusoidal output. The results for IIR extraction show that this evaluation method does not tell the whole story when movement is involved. A better evaluation method would be to compare the source breathing signal with the extracted signal, although this would require either the source breathing signal or a manually constructed one.

Of the sources of noise, movement can be perhaps the most destructive for respiration rate estimation. However, movement suppression actually reduces the quality of the extracted signal for some signal types due to false alarms in movements, i.e. signals are suppressed that are not movement. However, the added strength of movement suppression could be argued to outweigh the small performance loss due to false alarms.

FIR filters should be built with at least 30 filter taps to ensure both SFDR and SNR improvement, while IIR filters with 6 filter taps showed the best results. It may be useful to investigate higher order lowpass filters that can avoid the problem of the

low frequency bandpass cutoff point which makes filter design difficult.

The use of DWT for noise reduction, especially with non-stationary signals is popular. The results shown in Fig. 6.10 agree with this popularity as the DWT transform resulted in good improvement for both SNR and SFDR in a wide variety of signal types.

The cascaded method proposed here showed consistently good result for most signal types,as seen in Fig. 6.17. High frequency breathing and low frequency breathing were the exceptions to this. For signal types where it was not the best method of extraction, it was usually second best. On average, it improved the signal SNR by 4.45 dB and SFDR by 2.65 dB. Adding to the cascade with more filtering methods could further improve results. For instance, the output of the DWT stage could be input to an adaptive filter. However, as more stages are added, processing time would suffer.

The high respiratory rates encountered from the 'high rate' type in the respiration database were found to be problematic as all filter designs were created with the expectation that rates would not be that high. While these respiratory rates were not from natural breathing rates but rather from forced hyperventilation, it is important to note that it is possible for people to breath at a higher rate than the 50 bpm that is used as the top end of the scale.

Chapter 7

Data Fusion

This chapter proposes a method of data fusion and applies it to respiratory rate estimation. This proposed method was presented at the 2005 Conference of the Canadian Association on Gerontology in October 2005, in Halifax, Nova Scotia under the title "Nocturnal Monitoring of Elderly Patients with a Bed-Placed Pressure Pad" [3].

Previous research has used the sum of all sensor activity as a single extracted signal [48], or has picked a reference sensor with the highest frequency score [44], [19]. That is, the sensor that exhibits the maximum ratio of in-band spectral energy to out-of-band energy.

Herein, a method is investigated that selects signals from sensors that demonstrate a variance above the instrument's noise threshold. This does not require the calculation of the Fourier transform for each sensor and will allow for post-processing data fusion. This is expected to be more robust in the presence of localized movements.

7.1 Method

Three methods of data fusion were compared: a pre-summation method, a reference sensor method and a proposed method. These methods were applied both to the respiratory database signals and to the overnight participant data of 4 subjects.

Breathing signals were extracted from each data segment by the cascaded extraction method introduced in Chapter 6. All breathing frequencies were estimated by finding the delay to the first peak in the autocorrelation sequence.

7.2 Pre-Summation Method

At each sample time, samples from each sensor were summed to create a single signal. Breathing signals were extracted prior to summation, using the given extraction method. The respiratory rate was estimated from the summed signal.

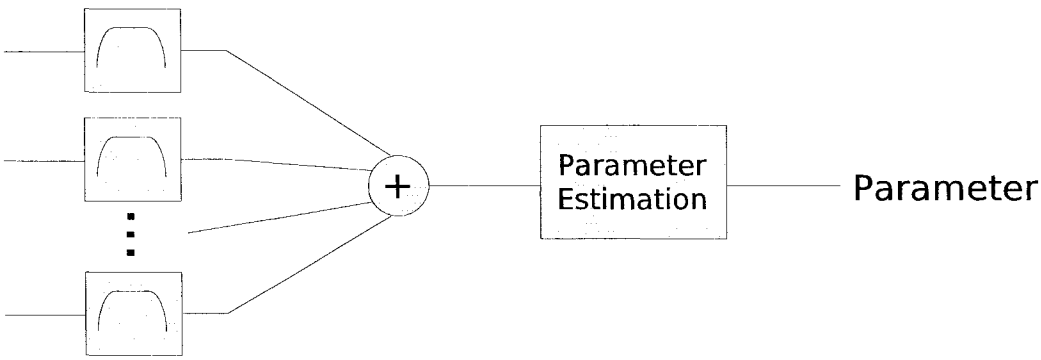

Figure 7.1: Pre-summation data fusion

7.3 Reference Sensor Method

A reference sensor was chosen for each data segment according to which sensor had the most energy in the band of interest. For each respiratory rate estimation, a 1024-point FFT from zero-padded data was taken. A score was assigned to each sensor based on its SNR of spectral power between 0.03 Hz and 0.8 Hz to total spectral power. The respiratory rate was estimated from the sensor with the highest score.

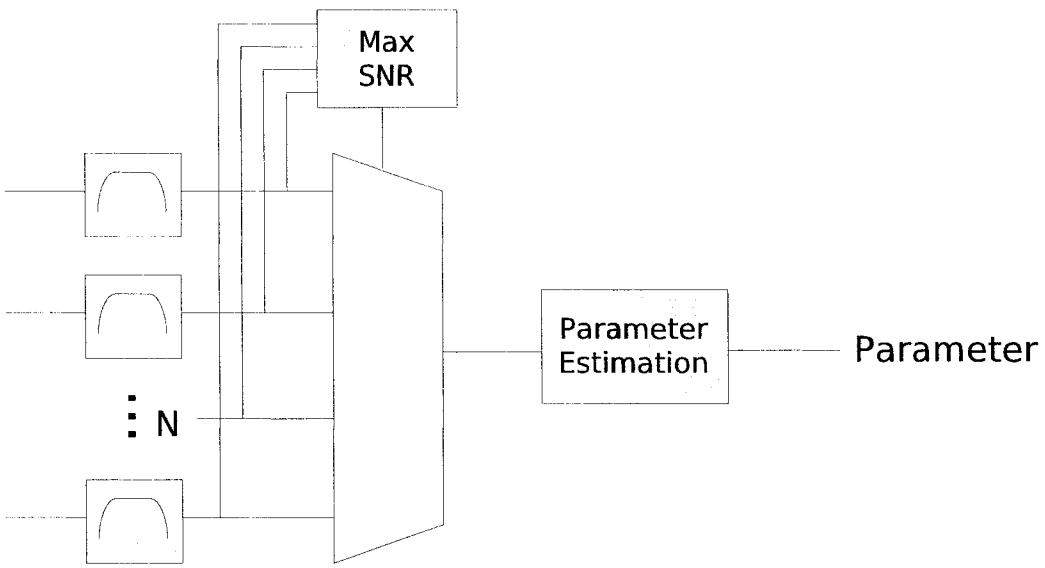

Figure 7.2: Reference sensor data fusion

7.4 Proposed Method

Fig. 7.3 shows a flow chart of the proposed fusion method. The proposed method employs both a sensors of interest and a weighted voting scheme for data fusion. A block diagram is shown in Fig. 7.4. 30-second signals were extracted from each sensor. Sensors that were not likely to contain breathing signals were eliminated by choosing the sensors of interest. Frequency estimation occurred for the signals from

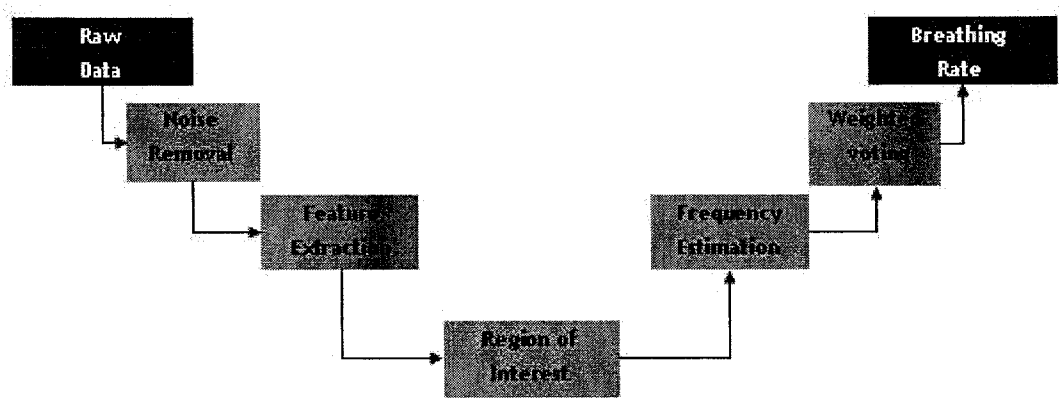

Figure 7.3: Flow chart of proposed method

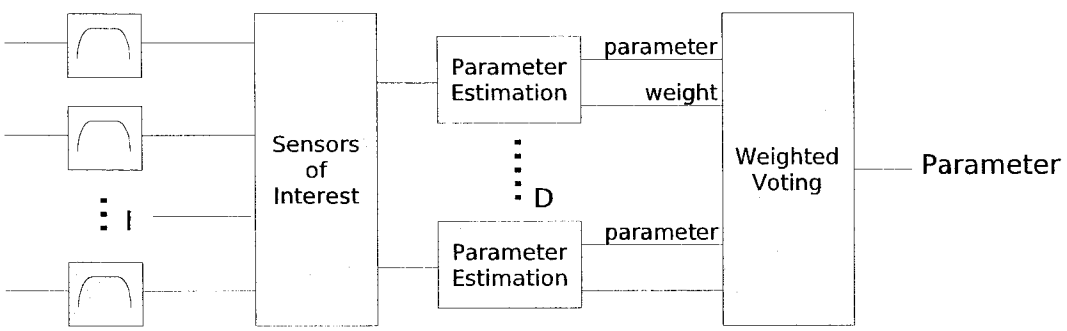

Figure 7.4: Proposed method of data fusion

just the chosen sensors. A weighting was given to each estimate which was used in a weighted voting scheme to choose the the best frequency estimate. output.

The sensors of interest were found by extracting the variance of all the signals and choosing only sensors with variances greater than 3. This eliminates both saturated sensors and sensors with just noise and no breathing signals. Movement was also taken into account at this step and sensors that reported more than 25% of the current samples as corrupted by movement were eliminated.

Fundamental frequency estimation was applied using autocorrelation. The delay to the first peak of the autocorrelation sequence was considered the period of the signal. A weight for this estimation is also calculated from the ratio of the value at that peak to the value at delay = 0.

At this point, multiple estimations are available from sensors showing characteristics of breathing signals. A cluster-based voting method is used to choose the final estimated respiratory rate. Candidate rates are grouped and the cluster with the highest weighting is chosen. The equation for the weighting of each cluster is given in Eq. 7.1.

$$Wc_k = \sum_{n_c=0}^{I_c} W_{k,i_c} \tag{7.1}$$

with i_c is the i_cth sensor in the cluster of size I_c. The subscript k refers to the kth estimation. Clustering reduces the impact of incorrect estimates from noisy sensors. The final estimation is the weighted mean of the rates given by the sensors in the chosen cluster.

Each sensor is added to the cluster with mean rate closest to its reported rate. If no cluster exists within 1 bpm of the reported rate, a new cluster is started. The weighted voting takes into account not only the weighting, but also the number of sensors reporting that weight. The final estimation is a weighted average of all reported rates in the cluster with the highest weighting.

7.5 Evaluation

The proposed method is evaluated by calculating the mean square error (MSE) of the calculated breathing rates for both the method of a single sensor of interest and a pre-summation of sensor outputs using the known frequencies in the database of respiratory signals.

For overnight processing, respiratory rates are unknown, therefore the variance of the resulting frequency was used as a measure of how consistent the results were. Processing time was also evaluated for each method.

7.6 Results

Table 7.1 lists the mean square error between proposed methods, found by comparing the expected respiratory rate in the respiration signal database to the estimated rates. The processing time required to process all of the signals from the respiratory signal database is also listed.

Table 7.1: A comparison of MSE and processing time by data fusion method

Method	MSE	Processing Time (s)
pre-summation	434.5	0.37
reference sensor	410.9	1.05
proposed	287.1	2.81

Fig. 7.5 shows an example of the respiratory rates found by each of the compared methods during one night. The pre-summation method has respiration rates that are quite variable, often choosing lower than expected rates. This happens particularly during movement corruption. The reference sensor improves the signal, but between hour 3 and 4 it is possible to see that it consistently reports a high rate, at double

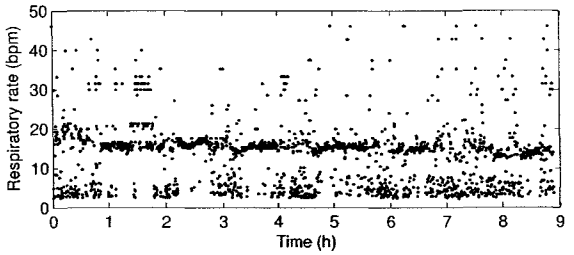

(a) Pre-summation

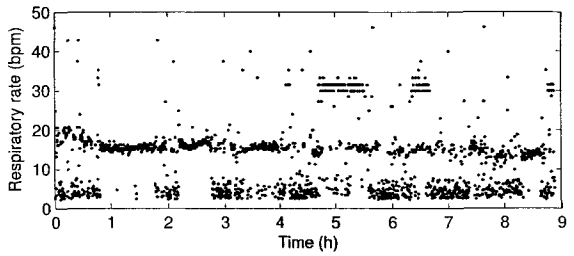

(b) Reference sensor

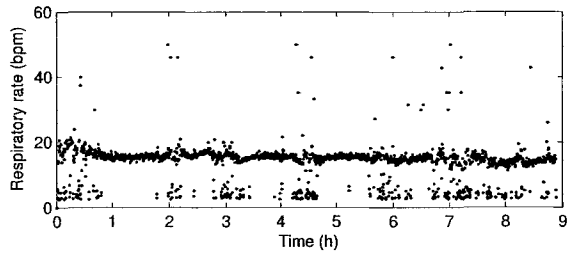

(c) Proposed method

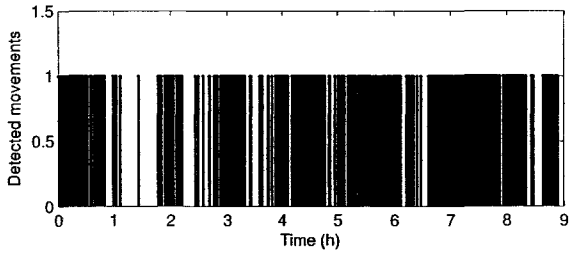

(d) Detected movements during the night

Figure 7.5: Example of nocturnal breathing rates results with compared data fusion methods

Method	Mean σ^2	Normalized Processing Time (s)
Pre-summation	83.58	0.0031
Reference sensor	104.93	0.0089
Proposed method	47.29	0.0115

Table 7.2: Comparison of overnight results by data fusion method

the expected rate. The proposed method results in the most clean estimation plot. With a few overestimated estimates and a number of underestimated rates, grouped together and occurring especially during movements.

Table 7.2 presents the mean variance of the breathing rates calculated by each method. Mean processing time is also shown, normalized prior to mean calculation by the number of estimations.

7.7 Discussion

The pre-summation method, while it can be a way to improve SNR, can actually decrease SNR when respiratory signals with opposing phases cancel each other out. Additionally, movements from just one sensor can drown out the breathing signals from all other sensors. This could be seen from the high rate of respiratory rate estimate corruption. However, the pre-summation method is the fastest method. The reference sensor method strikes a balance between accuracy and time processing, however when accuracy is important, the proposed method shows the best mean square error when compared to known rates and lowest variance during overnight tests. This method is also not much slower than the reference sensor method.

Chapter 8

Validity Evaluation

This chapter proposes a validity evaluation technique and evaluates its performance. This proposed method has been published at IEEE 2006 International Conference of the Engineering in Medicine and Biology Society (EMBC 2006) in New York, USA, with the title "Reliable respiratory rate estimation from a bed pressure array" [4].

8.1 Methods

In examining the respiratory rate estimations produced by the system, it would be a simple method of validity evaluation to determine if the given estimation is within the range of frequency estimations expected for that individual. However, this validity measure would mask the situation of a change in breathing patterns, which is certainly something that should be detected. Instead, we must look towards validity evaluations based on the quality of input data and not perhaps the output parameters.

Researchers have suggested the use of the signal to noise ratio at the frequency of interest as a metric for data reliability [48], [35]. This thesis proposes the use of a similar metric that incorporates both signal to noise ratio and movement information since one of the most corruptive elements in breathing rate estimation is movement.

In some instances, movement occupies the same frequency range as breathing [82], producing perhaps a solid SNR, but an inaccurate estimate.

The autocorrelation sequence is used for rate estimation, and not a Fourier transform, so a weighting measure from the autocorrelation sequence is taken instead of a spectrum-based signal to noise ratio. This weighting is calculated by taking the ratio of the peak value to the value of the autocorrelation at $\tau = 0$. To ensure that peaks located on the main lobe of the autocorrelation function do not get artificially heavy weightings, the difference between the peak and the previous valley is taken. The weighting, W, of the kth estimate for sensor i becomes:

$$W_{(k,i)} = \frac{(R_{xx(k,i)}(\tau_{peak}) - R_{xx(k,i)}(\tau_{valley})}{2 * R_{xx(k,i)}(0)}, \tag{8.1}$$

and produces an output between 0 and 1.

A reliability metric is proposed that is defined as this weighting multiplied by the percentage of samples that do not contain movement. This gives a reliability between 0 and 100 for each sensor.

$$G_{(k,i)} = W_{(k,i)} * M_{(k,i)} \tag{8.2}$$

$G_{(k,i)}$ is the reliability metric using $M_{(k,i)}$, the percentage of samples in the kth segment at sensor i that are not corrupted by movement.

8.1.1 Data Fusion

In the previous chapter, a data fusion method was presented. The same fusion method is proposed here with a small adjustment. The fusion weighting is updated to include reliability information and the probability that a given sensor contains respiratory rate information.

This probability is calculated similarly to the probability estimate given in [83].

$$P_{(k,i)} = \frac{1}{N} \sum_{j=k-J-1}^{k-1} D_i[j] \tag{8.3}$$

Here, $D_i[k]$ is defined as one if sensor i was chosen during the jth of last J rate estimates and zero otherwise.

A cluster's weighting score is updated from Eq. 7.1 to Eq. 8.4 to take advantage of the reliability information.

$$Wc_k = \sum_{i_c=0}^{I_c} G_{k,i_c} * P_{k,i_c} \tag{8.4}$$

A final single 'estimate reliability' is defined as the mean of the reliability metrics from sensors in the chosen cluster.

A block diagram of the proposed system is shown in Fig. 8.1. The variable x refers to input data after source extraction and choice of sensors of interest, μ refers to detected movements, W is the autocorrelation weighting as calculated from Eq. 8.1, G is the estimate reliability, $E[G]$ is the expected value of G, or the mean of G, and f is the estimated respiratory rates from all sensors of interest.

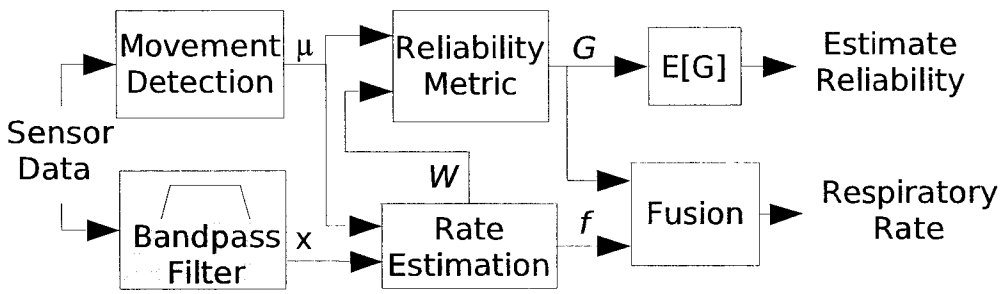

Figure 8.1: Block diagram of rate estimation and reliability metric

8.2 Evaluation

The proposed method was evaluated using nocturnal experiment data from five participants. The breathing signal database will not be used since the probability of previous sensor use can not be extracted from it. Respiratory rates were calculated every fifteen seconds from a sliding 30 second window according to the algorithm proposed in the preceding chapters: movement detection, source extraction, and finally parameter estimation and data fusion. Since this segment size is larger than the update interval, segments will overlap and short movements can corrupt consecutive respiratory rate estimations.

To differentiate an accurate estimate from an invalid estimate, the reliability metric can be thresholded so that results with a reliability metric greater than the threshold can be considered as accurate estimates. A true positive is defined as an accurate estimate that is above the chosen threshold, while a false negative is an inaccurate estimate that is above the chosen threshold. The results from thresholding the reliability of signal to determine if an estimate is valid is examined for both reliability from just the autocorrelation weighting (similar to an SNR weighting) and for reliability calculated according to the proposed metric. The autocorrelation weighting is denoted as 'ACW' and the proposed movement corruption metric is denoted as 'MCM'.

To evaluate the results of thresholding for validity from the MCM and ACW, a range of valid respiratory rates is evaluated by observation of each participant's estimated rates. False positives and true positives are classified according to being outside or inside this limit. This method of evaluation is acceptable for the healthy adults participating in the study, but it would not be a good way to check validity results for people with high respiratory rate variance. In this case, it could be difficult

to find a range of frequencies that would include only correct estimates and exclude incorrect estimates. The method of validity thresholding from the reliability metric is still expected to be valid, but this method of evaluation would not be.

If a study is undertaken that includes participants with high respiratory rate variance, the evaluation of which estimates are accurate is difficult, unless respiratory rates are simultaneously gathered from a clinical respiration rate monitor. Alternatively, accuracy can be manually checked by visually evaluating the actual respiratory rates from the peaks and valleys in the data. This would be a very time consuming process, as a full night's data can include over 2000 estimated rates.

8.3 Results

Table 8.1 summarizes the movement corruption during the nocturnal monitoring. The 'Samples with movement' denotes how many samples out of the night were found to be corrupted by movement detected by the movement detector algorithm presented in Chap. 5. The 'Estimates with movement' denotes the percentage of estimates that were corrupted by at least five samples of movement. These results show that the number of estimates that include movement is almost four times higher than the percentage of samples that are corrupted by movement during the night.

An example nocturnal respiratory rate is shown in Fig. 8.2. Respiratory rates between the horizontal bands are considered to be accurate estimates, while those outside of the bands are considered to be inaccurate estimates. The reliability metrics for this same night are shown in Fig. 8.3. The two metrics look to give quite similar results, but the MCM metric is in fact lower in areas of movement corruption.

The ROC curves for aggregated results are presented in Fig. 8.4. These curves show the trade-off between the probability of classifying an estimate as invalid when

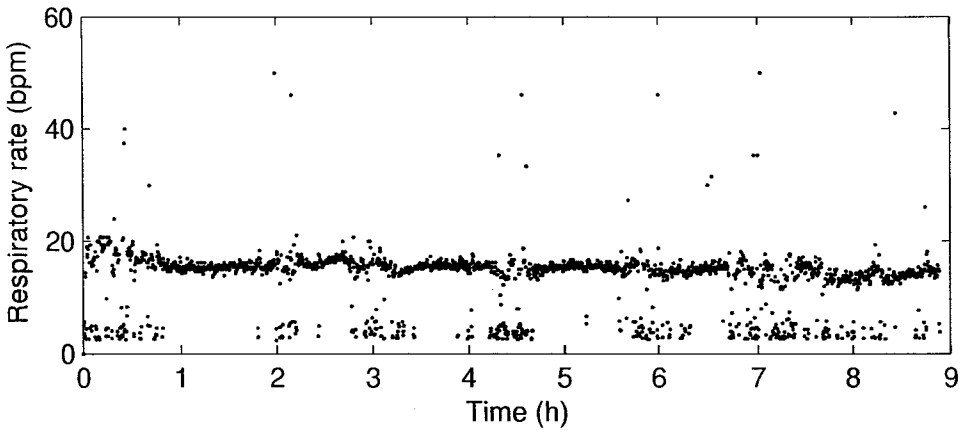

Figure 8.2: Example respiratory rate estimation prior to validity evaluation

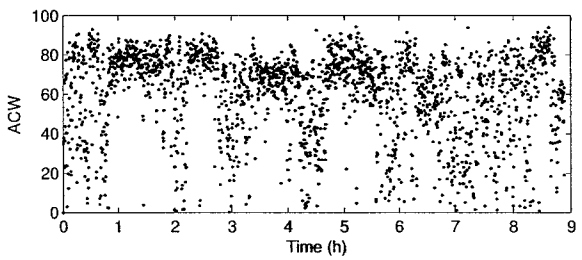

(a) ACW

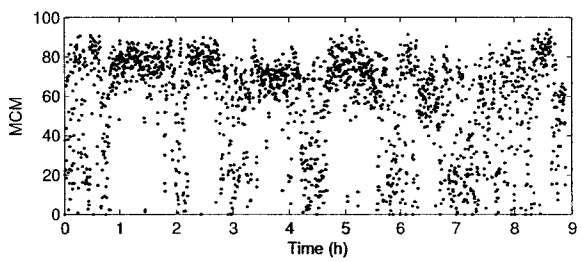

(b) MCM

Figure 8.3: Example reliability metrics

Table 8.1: Movement corruption estimates

Participant	Samples with movement (%)	Estimates with movement (%)
1	9.0	43.9
2	7.0	24.9
4	11.8	40.3
6	6.4	20.4
9	8.1	29.2
All	8.5	31.7

the estimate is indeed inaccurate (true positive) and classifying an estimate as invalid when the estimate is actually accurate (false positive).

Fig. 8.5 presents the true positives and false positives as a function of threshold value. From this figure, it can be seen that while the true positive rate is almost the same at each threshold level, the false positive rate is lower for MCM, especially for thresholds up to 50. Often, the thresholds for ACW at equivalent false positive rates to MCM must be set at levels over 10% higher. Overall, the MCM method improves the true positive rate compared to ACW by 6.55% across all threshold levels, at an equivalent ACW false positive rate.

A threshold of 50 was chosen as appropriate for validity evaluation through the MCM. At this rate, 80% of true positives are still considered valid, while only 1.7% of false positives remain. Fig. 8.6 presents the 'valid' rates, thresholded at MCM = 50, from the example nocturnal rates shown at the beginning of the results. The equivalent threshold for ACW, keeping the false positive rate the same is 61. At 61,

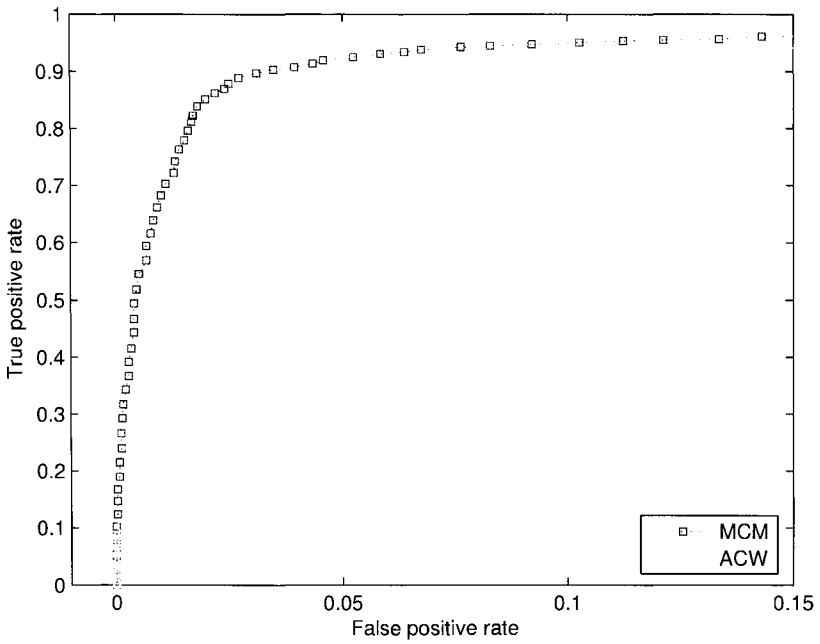

Figure 8.4: ROC curve for reliability metrics

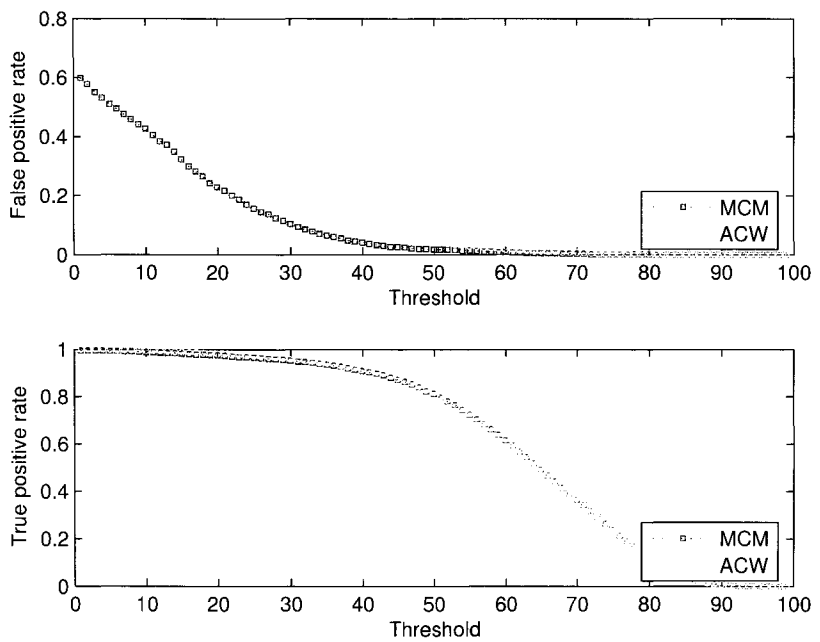

Figure 8.5: Thresholding: true validity and false validity

the true positive rate using ACW is just less than 60 %. For this example, 1568 of the

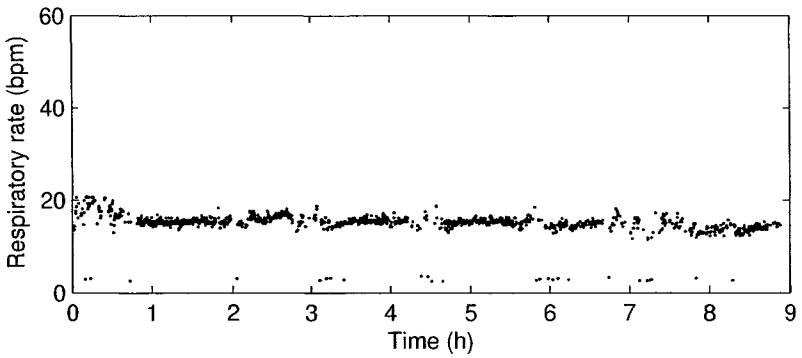

(a) Valid ACW rates: false positive rate < 1.8% (ACW > 61)

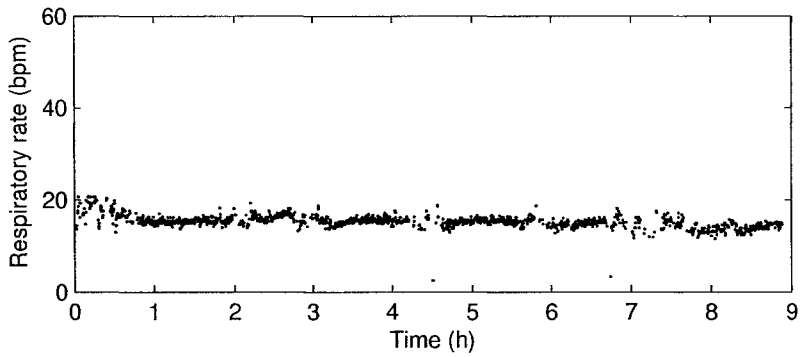

(b) Valid MCM rates: false positive rate < 1.8% (MCM > 50)

Figure 8.6: 'Valid' estimates: the example thresholded night

1961 original rate estimates remained for MCM, while only 1246 remained for ACW.

8.4 Discussion

Movement made up a significant portion of the night, affecting over 30% of rate estimations. While efforts at movement suppression during signal extraction have increased the signal to noise ratio, movement is still a significant corrupting factor, as was seen in the results of the previous chapter.

The use of post-processing data fusion was shown to be robust to movement

corruption, but during times of high movement, respiration signals are absent and these results should be invalidated. Invalidating results with estimate reliabilities lower than a threshold of 50 removed many false estimates. The threshold can be chosen depending on the application. It is possible to increase the required reliability metric threshold to ensure elimination of all false estimates, but this also results in the invalidation of estimates that are in fact valid, albeit at a lower reliability metric.

The MCM metric for reliability gives a modest improvement of the ACW metric. It could be possible to improve this further by improving the movement detector to ensure that the MCM catches all movements.

Since the reliability metric is related to the amount of movement during the night, it may also be used as a restlessness index, with lower metric values related to higher restlessness.

Chapter 9

Conclusions

A summary of presented results is listed here, along with suggestions for further research.

9.1 Summary of Results

For pressure array signal segmentation, the control limits movement detector proposed in Chapter 5 can detect 85% of signal changes, with less than five seconds delay to detection and a low false alarm rate. Additionally, it can classify each segment as containing movement or rest. If missing a segment boundary is important, GLR has been shown to recognize 99% of segment boundaries, albeit with a longer delay to detection and slower processing speed. Where processing speed is a factor, the one-model CUSUM segmentation algorithm is superior.

A cascade of movement suppression and DWT filtering was proposed as a method of signal extraction in Chapter 6 and was shown to be effective, increasing mean SNR by almost 4.5 dB and mean SFDR by over 2.5 dB. This method has been particularly beneficial in the extraction of breathing signals from movement. Where processing time is paramount, the movement suppression algorithm is effective at restoring the

spectrum of the original signal.

The mean square error of the data fusion method proposed in Chapter 7 applied to respiratory rate estimations showed a 33% improvement over the pre-summation method and a 30% improvement over the reference sensor method. However, this improvement came at the expense of processing time. Mean processing time increased by 267% compared to the pre-summation method and 30% compared to the reference sensor method. When applied to nocturnal data, the variance of the results decreased by 43 % over the pre-summation method and 55% over the reference sensor method.

Validity evaluation through a proposed reliability metric comprised of both parameter-focused signal to noise ratio and general movement level has been proven to provide valid estimates of respiration rates. Rates of true positives at a given threshold and false positive level improved by 6.55% over a reliability metric based solely on signal to noise ratio. The metric could also be used as an index of restlessness.

9.2 Recommendations for Further Research

The following sections make recommendations for further research, including additional experimental data to acquire, new data processing methods to investigate, and decision-making for autonomous monitoring.

9.2.1 Experimental Data Acquisition

Future experiments are needed to acquire data from both a broader population and a more targeted population. While data was acquired from 10 healthy young adult participants, testing the proposed methods with more participants would ensure that the methods have general application.

Data acquired from older adults may prove to include breathing patterns that

vary from the breathing patterns of the general population. It is recommended that experiments be conducted to acquire data specifically from older adults. The 'smart' apartment that has been set up through the Technology Assisted Friendly Environment for the Third Age (TAFETA) project would be a good location for this experiment.

9.2.2 Data Processing Method Investigation

Extracted data was segmented using a number of techniques, but classification of the segments was limited to whether the segment was active movement or rest. Classification of segments could give better illumination to a participant's actions. For instance, movement segments could be classified into position changes, leg movements, arm movements, head movements, and autonomous movements such as sneezes, coughs, or sighs. Additionally, rest segments could be classified by posture as either supine, prone, or side-lying. It is recommended that such classifications be researched in the future.

Source extraction methods outlined in the thesis included general filtering methods but did not include more sophisticated source separation methods. In particular, blind source separation techniques such as independent component analysis may yield improved performance.

9.2.3 Decision-Making

The thesis has examined how to reliably estimate parameters from a pressure sensor array, but has not examined when and how alarms could be set based on these parameters. For example, should a bed occupant not leave the bed for a long time, at what point should an alarm be raised to say that this is an abnormal event? With

the reliable extraction of human parameters via the pressure sensor array, decision-making based on these parameters will become important to produce meaningful results for care givers.

Chapter 10

Contributions

The following contributions were made during research for this thesis:

- Application of segmentation techniques to overnight monitoring was investigated and the results were presented here. As part of this analysis, a modified control limits algorithm for movement detection was proposed and published at the IEEE International Workshop on Medical Instrumentation and Applications 2006 (MeMea 2006) in Benevento, Italy, April 2006 [2]. The detection algorithm provides movement onset and offset detection with a low number of false alarms.

- Existing signal extraction methods were evaluated and a breathing signal extraction method was proposed based on these evaluations. The proposed method cascades a movement suppression algorithm with discrete wavelet transforms to create a mean 4.45 dB improvement in signal to noise ratio and 2.65 dB improvement in spurious free dynamic range.

- A method for data fusion of parameters estimated from an array of pressure sensors was proposed and compared to two fusion methods that have been in use in the field. This new method showed a marked improvement in mean square

error, with up to 33% reduction in this error. A poster presentation regarding this method was accepted and presented at the 2005 Conference of the Canadian Association on Gerontology in Halifax, Nova Scotia, October 2005 [3].

- Validity evaluation was investigated and a method for validity evaluation by a reliability metric was proposed and published at the EMBS 2006 Conference in New York, USA , September 2006 [4]. This metric improved the true positive rate by over 6%, compared to a standard reliability metric. The metric was also proposed for use as a restlessness index.

- Experimental evaluation required data collection. Data was acquired from experiments with ten participants. Four separate experiments were undertaken with participants under observation. Additionally, a nocturnal experiment acquired overnight data. A database of respiratory signals from multiple participants was created from the annotated observed experiments. These sources of data are useful not only for this thesis, but also for future work in this field.

- A MATLAB graphical user interface for sensor array data annotation was created. This interface enables fast and simple data annotation addition and correction.

List of References

[1] U. Appel and A. V. Brandt, "Adaptive sequential segmentation of piecewise stationary time series," *Information Sciences*, vol. 29, pp. 27–56, Feb 1983.

[2] M. Howell-Jones, R. Goubran, and F. Knoefel, "Identifying movement onset times for a bed-based pressure sensor array," in *Medical Measurement and Applications, 2006 IEEE International Workshop on*, pp. 111–114, 2006.

[3] M. Howell-Jones, F. Knoefel, and R. Goubran, "Nocturnal monitoring of elderly patients with a bed-placed pressure pad," in *2005 Conference of the Canadian Association on Gerontology*, 2005.

[4] M. Howell-Jones, R. Goubran, and F. Knoefel, "Reliable respiratory rate estimation from a bed pressure array," in *Engineering in Medicine and Biology Society, 2006.Proceedings of the 28th Annual International Conference of the IEEE*, 2006.

[5] Lexicle Limited, "Smart fridge." http://www.lexicle.com/smartfridge, 2004. Last accessed August 16, 2006.

[6] S. H. Park, S. H. Won, J. B. Lee, and S. W. Kim, "Smart home–digitally engineered domestic life," *Personal and Ubiquitous Computing*, vol. 7, no. 3, pp. 189–196, 2003.

[7] W. K. Edwards and R. E. Grinter, "At home with ubiquitous computing: Seven challenges," *Proceedings of the 3rd international conference on Ubiquitous Computing*, pp. 256–272, 2001.

[8] Seniorresource.com, "Aging in place." http://www.seniorresource.com/ageinpl.htm, 2006. Last accessed September 14, 2006.

[9] M. T. Smith and S. T. Wegener, "Measures of sleep: The Insomnia Severity Index, Medical Outcomes Study (MOS) sleep scale, Pittsburgh Sleep Diary (PSD),

and Pittsburgh Sleep Quality Index (PSQI)," *Arthritis care and research*, vol. 49, no. 5, pp. 184–196, 2003.

[10] R. D. Chervin, D. L. Murman, B. A. Malow, and V. Totten, "Cost-utility of three approaches to the diagnosis of sleep apnea: polysomnography, home testing, and empirical therapy," *Annals of Internal Medicine*, vol. 130, pp. 496–505, Mar 16 1999.

[11] O. L. Bon, L. Staner, G. Hoffmann, M. Dramaix, I. S. Sebastian, J. R. Murphy, M. Kentos, I. Pelc, and P. Linkowski, "The first-night effect may last more than one night," *Journal of psychiatric research*, vol. 35, pp. 165–172, May-Jun 2001.

[12] J. Kaartinen, I. Kuhlman, and P. Peura, "Long-term monitoring of movements in bed and their relation to subjective sleep quality," *Sleep and Hypnosis*, vol. 5, no. 3, pp. 145–153, 2003.

[13] M. Littner, C. A. Kushida, W. M. Anderson, D. Bailey, R. B. Berry, D. G. Davila, M. Hirshkowitz, S. Kapen, M. Kramer, D. Loube, M. Wise, S. F. Johnson, and S. of Practice Committee of the American Academy of Sleep Medicine., "Practice parameters for the role of actigraphy in the study of sleep and circadian rhythms: an update for 2002," *Sleep*, vol. 26, pp. 337–341, May 2003.

[14] A. Sadeh, P. J. Hauri, D. F. Kripke, and P. Lavie, "The role of actigraphy in the evaluation of sleep disorders," *Sleep*, vol. 18, pp. 288–302, May 1995.

[15] G. Jean-Louis, H. von Gizycki, F. Zizi, A. Spielman, P. Hauri, and H. Taub, "The actigraph data analysis software: II. A novel approach to scoring and interpreting sleep-wake activity," *Perceptual and motor skills*, vol. 85, pp. 219–226, Aug 1997.

[16] T. Someya, Y. Kato, T. Sekitani, S. Iba, Y. Noguchi, Y. Murase, H. Kawaguchi, and T. Sakurai, "From the cover: Conformable, flexible, large-area networks of pressure and thermal sensors with organic transistor active matrixes," *Proceedings of the National Academy of Sciences*, vol. 102, pp. 12321–12325, Aug 2005.

[17] D. Rosenbaum and H. Becker, "Plantar pressure distribution measurements. technical background and clinical applications," *Foot and Ankle Surgery*, vol. 3, pp. 1–14, Mar 1997.

[18] H. Morishita, R. Fukui, and T. Sato, "High resolution pressure sensor distributed floor for future human-robot symbiosis environments," in *Intelligent Robots and*

System, 2002.IEEE/RSJ International Conference on, vol. 2, pp. 1246–1251, 2002.

[19] H. F. Van der Loos, N. Ullrich and H. Kobayashi, "Development of sensate and robotic bed technologies for vital signs monitoring and sleep quality improvement," *Autonomous Robots*, vol. 15, pp. 67–79, Jul 2003.

[20] J. Paradiso, K. Hsiao, and E. Hu, "Interactive music for instrumented dancing shoes," *Proc.of the 1999 International Computer Music Conference*, pp. 453–456, Oct 1999.

[21] S. Urry, "Plantar pressure-measurement sensors," *Measurement Science and Technology*, vol. 10, no. 1, pp. R16–R32, 1999.

[22] R. Serway, *Physics for scientists and engineers with modern physics.* Saunders College Publishing Philadelphia, 3 ed., 1990.

[23] J. Alihanka, K. Vaahtoranta, and I. Saarikivi, "A new method for long-term monitoring of the ballistocardiogram, heart rate, and respiration," *The American Journal of Physiology*, vol. 240, pp. R384–92, May 1981.

[24] D. Pawluk, J. Son, P. Wellman, W. Peine, and R. Howe, "A distributed pressure sensor for biomechanical measurements.," *J Biomech Eng*, vol. 120, no. 2, pp. 302–305, 1998.

[25] B. H. Jansen, B. H. Larson, and K. Shankar, "Monitoring of the ballistocardiogram with the static charge sensitive bed," *Biomedical Engineering, IEEE Transactions on*, vol. 38, no. 8, pp. 748–751, 1991.

[26] R. D. Howe, "Tactile sensing and control of robotic manipulation," *Journal of Advanced Robotics*, vol. 8, no. 3, pp. 245–261, 1994.

[27] E. M. Reimer and L. H. Baldwin, "Cavity sensor technology for low cost automotive safety and control devices." http://www.canpolar.com/principles.shtm, 1999. Last accessed July 30, 2006.

[28] L. W. Chen and J. R. Lin, "Shape-memorized crosslinked ester-type polyurethane and its mechanical viscoelastic model," *Journal of Applied Polymer Science*, vol. 73, no. 7, pp. 1305–1319, 1999.

[29] D. V. Dounis and G. L. Wilkes, "Structure-property relationships of flexible polyurethane foams," *Polymer*, vol. 38, pp. 2819–2828, May 1997.

[30] Polyurethane Foam Association, "Examining viscoelastic flexible polyurethane foam." http://www.pfa.org/intouch/pdf/IntouchV11%5f1%5fread.pdf, Jun 2003.

[31] Polyurethane Foam Association, "Flexible polyurethane foam: a primer." http://www.pfa.org/intouch/new%5fpdf/lr%5fIntouchV1.1.pdf, Feb 1991.

[32] Y. Nishida and T. Hori, "Non-invasive and unrestrained monitoring of human respiratory system by sensorized environment," in *Sensors, 2002.Proceedings of IEEE*, vol. 1, pp. 705–710, 2002.

[33] W. Chen, X. Zhu, T. Nemoto, Y. Kanemitsu, K. Kitamura, and K. Yamakoshi, "Unconstrained detection of respiration rhythm and pulse rate with one under-pillow sensor during sleep," *Medical & Biological Engineering & Computing*, vol. 43, pp. 306–312, Mar 2005.

[34] L. Hernandez, B. Waag, H. Hsiao, and V. Neelon, "A new non-invasive approach for monitoring respiratory movements of sleeping subjects," *Physiological measurement*, vol. 16, no. 3, pp. 161–167, 1995.

[35] K. Watanabe, T. Watanabe, H. Watanabe, H. Ando, T. Ishikawa, and K. Kobayashi, "Noninvasive measurement of heartbeat, respiration, snoring and body movements of a subject in bed via a pneumatic method," *Biomedical Engineering, IEEE Transactions on*, vol. 52, no. 12, pp. 2100–2107, 2005.

[36] A. M. Adami, T. L. Hayes, M. Pavel, and C. M. Singer, "Detection and classification of movements in bed using load cells," in *Engineering in Medicine and Biology Society, 2005.IEEE-EMBS 2005.27th Annual International Conference of the*, pp. 589–592, 2005.

[37] P. Rey, P. Charvet, M. T. Delaye, and S. A. Hassan, "A high density capacitive pressure sensor array for fingerprint sensor application," in *Solid State Sensors and Actuators, 1997.TRANSDUCERS '97 Chicago., 1997 International Conference on*, vol. 2, pp. 1453–1456, 1997.

[38] Northwest Regional Spinal Cord Injury System, "Picture this... pressure mapping assessment for wheelchair users." http://depts.washington.edu/rehab/sci/pressure%5fmap.html, June 8 2004. Last accessed August 16 2006.

[39] Tekscan Inc., "Tekscan: Tactile pressure measurement, pressure mapping systems, and force sensors and measurement systems." http://www.tekscan.com/index.html, 2005. Last accessed August 16, 2006.

[40] J. G. Webster, *Medical Instrumentation: Application and Design.* New York: John Wiley and Sons, Inc., 3rd ed., 1998.

[41] I. Korhonen, R. Lappalainen, T. Tuomisto, T. Koobi, V. Pentikainen, M. Tuomisto, and V. Turjanmaa, "TERVA: wellness monitoring system," in *Engineering in Medicine and Biology Society, 1998.Proceedings of the 20th Annual International Conference of the IEEE*, vol. 4, pp. 1988–1991, 1998.

[42] W. B. Spillman(Jr.), M. Mayer, J. Bennett, J. Gong, K. E. Meissner, B. Davis, R. O. Claus, A. A. Muelenaer(Jr.), and X. Xu, "A smart bed for non-intrusive monitoring of patient physiological factors," *Measurement Science and Technology*, vol. 15, no. 8, pp. 1614–1620, 2004.

[43] T. Watanabe and K. Watanabe, "Noncontact method for sleep stage estimation," *Biomedical Engineering, IEEE Transactions on*, vol. 51, no. 10, pp. 1735–1748, 2004.

[44] Y. Nishida, M. Takeda, T. Mori, H. Mizoguchi, and T. Sato, "Monitoring patient respiration and posture using human symbiosis system," in *Intelligent Robots and Systems, 1997.IROS '97., Proceedings of the 1997 IEEE/RSJ International Conference on*, vol. 2, pp. 632–639, 1997.

[45] Y. Nishida, T. Mori, T. Sato, and S. Hirai, "The surrounding sensor approach - application to sleep apnea syndrome diagnosis based on image processing," in *Systems, Man, and Cybernetics (SMC), 1999. 1999 IEEE International Conference on*, vol. 6, pp. 382–388, 1999.

[46] T. Harada, A. Sakata, T. Mori, and T. Sato, "Sensor pillow system: monitoring respiration and body movement in sleep," in *Intelligent Robots and Systems, 2000.(IROS 2000).Proceedings.2000 IEEE/RSJ International Conference on*, vol. 1, pp. 351–356, 2000.

[47] T. Harada, T. Mori, Y. Nishida, T. Yoshimi, and T. Sato, "Body parts positions and posture estimation system based on pressure distribution image," in *Robotics and Automation, 1999.Proceedings ICRA '99 IEEE International Conference on*, vol. 2, pp. 968–975, 1999.

[48] T. Harada, T. Sato, and T. Mori, "Estimation of bed-ridden human's gross and slight movement based on pressure sensors distribution bed," in *Robotics and Automation, 2002.Proceedings ICRA '02 IEEE International Conference on*, vol. 4, pp. 3795–3800, 2002.

[49] T. Harada, T. Sato, and T. Mori, "Human motion tracking system based on skeleton and surface integration model using pressure sensors distribution bed," in *Human Motion, 2000. Workshop on*, pp. 99–106, 2000.

[50] T. Harada, T. Sato, and T. Mori, "Pressure distribution image based human motion tracking system using skeleton and surface integration model," in *Robotics and Automation, 2001.Proceedings of the ICRA '01 IEEE International Conference on*, vol. 4, pp. 3201–3207, 2001.

[51] A. M. Adami, T. L. Hayes, and M. Pavel, "Unobtrusive monitoring of sleep patterns," in *Engineering in Medicine and Biology Society, 2003.Proceedings of the 25th Annual International Conference of the IEEE*, vol. 2, pp. 1360–1363, 2003.

[52] M. Basseville and I. V. Nikiforov, *Detection of abrupt changes: theory and application.* Englewood Cliffs, N.J.: Prentice-Hall, Inc, Apr 1993.

[53] N. Nitanda, M. Haseyama, and H. Kitajima, "Accurate audio-segment classification using feature extraction matrix," in *Acoustics, Speech, and Signal Processing, 2005.Proceedings.(ICASSP '05).IEEE International Conference on*, vol. 3, pp. 261–264, 2005.

[54] M. Basseville and A. Benveniste, *Detection of Abrupt Changes in Signals and Dynamical Systems.* Springer-Verlag, 1986.

[55] A. Glavinovitch, M. N. S. Swamy, and E. I. Plotkin, "Wavelet-based segmentation techniques in the detection of microarousals in the sleep EEG," in *Circuits and Systems, 2005.48th Midwest Symposium on*, vol. 2, pp. 1302–1305, 2005.

[56] R. Agarwal, J. Gotman, D. Flanagan, and B. Rosenblatt, "Automatic EEG analysis during long-term monitoring in the ICU," *Electroencephalography and clinical neurophysiology*, vol. 107, pp. 44–58, Jul 1998.

[57] S. Charbonnier, G. Becq, and L. Biot, "On-line segmentation algorithm for continuously monitored data in intensive care units," *Biomedical Engineering, IEEE Transactions on*, vol. 51, no. 3, pp. 484–492, 2004.

[58] J. Shi and J. Malik, "Normalized cuts and image segmentation," *IEEE Transactions on Pattern Analysis and Machine Intelligence*, vol. 22, no. 8, pp. 888–905, 2000.

[59] X. Li, D. Eremina, L. Li, and Z. Liang, "Partial volume segmentation of medical images," in *Nuclear Science Symposium Conference Record, 2003 IEEE*, vol. 5, pp. 3176–3180, 2003.

[60] Z. Tao, C. C. Jaffe, and H. D. Tagare, "Tunnelling descent: A new algorithm for active contour segmentation of ultrasound images," *Inf Process Med Imaging*, vol. 18, pp. 246–257, Jul 2003.

[61] G. Bodenstein and H. M. Praetorius, "Feature extraction from the electroencephalogram by adaptive segmentation," *Proceedings of the IEEE*, vol. 65, no. 5, pp. 642–652, 1977.

[62] H. Zhang, A. Kankanhalli, and S. Smoliar, "Automatic partitioning of full-motion video," *Multimedia Systems*, vol. 1, no. 1, pp. 10–28, 1993.

[63] I. Koprinska and S. Carrato, "Temporal video segmentation: A survey," *Signal Processing: Image Communication*, vol. 16, pp. 477–500, 2001.

[64] F. Gustafsson, *Adaptive filtering and change detection.* Wiley New York, 2000.

[65] W. A. Shewhart, *Statistical Method from the Viewpoint of Quality Control.* Washington, USA: The Graduate School, The Department of Agriculture, 1939.

[66] J. Devore, *Probability and statistics for engineering and the sciences.* Duxbury Press Belmont, 1995.

[67] M. Basseville and A. Benveniste, "Sequential detection of abrupt changes in spectral characteristics of digital signals," *Information Theory, IEEE Transactions on*, vol. 29, no. 5, pp. 709–724, 1983.

[68] U. Appel and A. v. Brandt, "A comparative study of three sequential time series segmentation algorithms," *Signal Processing*, vol. 6, pp. 45–60, Jan 1984.

[69] D. Michael and J. Houchin, "Automatic EEG analysis: a segmentation procedure based on the autocorrelation function," *Electroencephalography and clinical neurophysiology*, vol. 46, pp. 232–235, Feb 1979.

[70] A. Brandt, "Detecting and estimating parameter jumps using ladder algorithms and likelihood ratio tests," in *Acoustics, Speech, and Signal Processing, IEEE International Conference on ICASSP '83.*, vol. 8, pp. 1017–1020, 1983.

[71] M. Khalil, J. Duchene, and C. Marque, "Generalized algorithm of detection and classification in uterine electromyography signal," in *Engineering in Medicine and Biology Society, 1998.Proceedings of the 20th Annual International Conference of the IEEE*, vol. 5, pp. 2658–2661, 1998.

[72] E. Munevar, J. A. Ramos, W. Gordon, M. Agnew, and W. Zhou, "Detection of abnormalities in the signal averaged electrocardiogram: a subspace system identification approach," in *Decision and Control, 1999.Proceedings of the 38th IEEE Conference on*, vol. 5, pp. 5094–5099, 1999.

[73] M. Bosc, F. Heitz, J. P. Armspach, I. Namer, D. Gounot, and L. Rumbach, "Automatic change detection in multimodal serial MRI: application to multiple sclerosis lesion evolution," *NeuroImage*, vol. 20, pp. 643–656, Oct 2003.

[74] A. Oppenheim and R. Schafer, *Discrete-time signal processing.* Prentice-Hall, Upper Saddle River, NJ, USA, 2nd ed., 1999.

[75] I. Daubechies, *Ten lectures on wavelets.* Society for Industrial and Applied Mathematics Philadelphia, PA, USA, 1992.

[76] C. Valens, "A really friendly guide to wavelets." http://perso.orange.fr/polyvalens/clemens/wavelets/wavelets.html, Feb 2004. Last accessed August 16, 2006.

[77] N. E. Huang, "The empirical mode decomposition and the hilbert spectrum for nonlinear and non-stationary time series analysis," *Proceedings: Mathematical, Physical and Engineering Sciences*, vol. 454, no. 1971, pp. 903–995, 1998.

[78] S. Mallat, "A theory for multiresolution signal decomposition: the wavelet representation," *Pattern Analysis and Machine Intelligence, IEEE Transactions on*, vol. 11, no. 7, pp. 674–693, 1989.

[79] M. Hayes, *Statistical Digital Signal Processing and Modeling.* John Wiley & Sons, Inc. New York, NY, USA, 1996.

[80] K. P. Cohen, W. M. Ladd, D. M. Beams, W. S. Sheers, R. G. Radwin, W. J. Tompkins, and J. G. Webster, "Comparison of impedance and inductance ventilation sensors on adults during breathing, motion, and simulated airway obstruction," *Biomedical Engineering, IEEE Transactions on*, vol. 44, no. 7, pp. 555–566, 1997.

[81] J. Proakis, *Digital communications.* McGraw-Hill New York, 1995.

[82] K. Cohen, Y. Hu, W. Tompkins, and J. Webster, "Breath detection using a fuzzy neural network and sensor fusion," *Acoustics, Speech, and Signal Processing, 1995. ICASSP-95., 1995 International Conference on*, vol. 5, 1995.

[83] D. Lo, R. A. Goubran, R. M. Dansereau, G. Thompson, and D. Schulz, "Robust joint audio-video localization in video conferencing using reliability information," *Instrumentation and Measurement, IEEE Transactions on*, vol. 53, no. 4, pp. 1132–1139, 2004.

Appendix A

Experimental Procedure for Observed Experiments

The experimental protocol followed for each experiment of the Observed Experiments is recorded here.

A.1 Protocol for Experiment 1 - Bed Entry / Bed Exit

	Participant Action	Logged Comments
	Stand beside bed	'start'
3x	Wait 20s	
	Enter bed	'M' before

continued on next page

(con't)	Participant Action	Logged Comments
(3x)	In bed	hand use may or may not be noted during bed entry
	Wait 20s	'right/left/back/front' position noted
	Exit bed	'M'
	Out of bed	Note use of hands if hands were used (assume no hands unless noted)
Instruct participant to use hands for bed exit		
3x	Wait 20s	
	Enter bed	'M' before
	In bed	hand use may or may not be noted during bed entry
	Wait 20s	'right/left/back/front' position noted
	Exit bed	'M'
	Out of bed	Note use of hands (assume hands used unless noted)

continued on next page

(con't)	Participant Action	Logged Comments
	Done	note finish

A.2 Protocol for Experiment 2 - Position and Movement

Participant Action	Logged Comments
Start on bed in any position	Note start with 's' or 'start', note back/front/left/right
Lie still 1 min	note any movement factors such as talking, laughing, sighs, twitches
Change position	'M' before, note back/front/left/right after
Lie still 1 min	note any movements
Change position	'M' before, note back/front/left/right after
Lie still 1 min	note any movements
Reposition (no change in position)	'M' before, note 'reposition'
Lie still 1 min	note any movements
Change position	'M' before, note back/front/left/right after

continued on next page

Participant Action (con't)	Logged Comments
Lie still 1 min	note any movements
Cough 1-2 times	'M' before, note 'cough' and # times
Lie still 1 min	note any movements
Change position	'M' before, note back/front/left/right after
Lie still 1 min	note any movements
Sigh	note sigh depth subjectively
Lie still 1 min	note any movements
Change position	'M' before, note back/front/left/right after
Lie still 1 min	note any movements
Move arm	'M' before, note how arm moved
Lie still 1 min	note any movements
Change position	'M' before, note back/front/left/right after
Lie still 1 min	note any movements
Twitch leg	evaluate leg twitch for depth subjectively and note
Lie still 20 sec	note any movements

continued on next page

Participant Action (con't)	Logged Comments
Twitch leg	evaluate leg twitch for depth subjectively and note
Lie still 20 sec	note any movements
Twitch leg	evaluate leg twitch for depth subjectively and note
Lie still 20 sec	note any movements
Change position	'M' before, note back/front/left/right after
Lie still 1 min	note any movements

Note, breathing may or may not have been noted during some sections in this experiment according to the observer's ability to record each breath.

A.3 Protocol for Experiment 3 - Breathing

Participant Action	Logged Comments
Start lying on back	Note start with 's' or 'start'
Lie still for 3 minutes	record each breath with a 'b' and note any movements

continued on next page

Participant Action (con't)	Logged Comments
Breath quickly and shallowly for 30 seconds	record each breath with a 'b'
Breath normally for 30 seconds	record each breath with a 'b'
Breath deeply and slowly for 30 seconds	record each breath with a 'b'
Breath normally for 30 seconds	record each breath with a 'b'
Hold breath for up to 30 seconds	note when breath holding starts
Repeat procedure on side or front	note position (front/left/right)
Repeat procedure on position not yet assumed (side or front)	note position

A.4 Protocol for Experiment 4 - Ballistocardiogram / Heart Rate

Participant Action	Logged Comments
Perform light to moderate exercise	Note start with 's' or 'start'
Get into bed	'M'

continued on next page

Participant Action (con't)	Logged Comments
Lie still	heart rate recorded at as many points as possible
Hold breath	heart rate recorded at as many points as possible
Lie still	heart rate recorded at as many points as possible

Appendix B

Experiment Questionnaires

This appendix presents the research questionnaires posed to participants.

B.1 General Questionnaire

This questionnaire is answered by all participants.

B.2 Sleep Diary Questionnaire

The sleep diary questionnaire is answered by participants in nocturnal experiments. The first part is answered at night and the second in the morning after waking up. Two of each part is expected from participants since they are monitored over two nights.

Participant Number:_____ Date:_____

General Questionnaire

This questionnaire is to be filled out by all participants.

Weight: _____ lb/ kg Height: _____ feet and inches / cm

What type of mattress (top mattress) will you be using during the experiment?

☐ Coil / Spring ☐ Futon _____ in/cm thick ☐ Foam _____ in/cm thick

☐ Hospital type ☐ Other _____

How firm is this mattress?

☐ Soft ☐ Medium ☐ Firm ☐ Extra firm

What is below the top mattress?

☐ Box Spring Mattress ☐ Wood Slats ☐ Plywood Board ☐ Other _____

Is there a pillow-top or padding on the top mattresses?

☐ No ☐ Yes: _____ in / cm thick

Participant Number:_____ Date:_____

Sleep Diary

The sleep diary is filled out by participants doing Experiment Part B: Nocturnal Monitoring. Please keep this diary by your bedside so that you can fill it in right before going to bed and right after waking up in the morning. This questionnaire has been adapted from the Pittsburgh Sleep Diary questionnaire. It will be used to help interpret the data from the pressure sensor array.

Bedtime Questionnaire

Please answer the following questions just before going to bed.

Q1. Did you have any caffeinated drinks, alcoholic drinks or tobacco today? Circle: Yes / No (If no, go to Q 2)

Approximately how many **caffeinated** drinks

(a) before dinner? _____ (b) after dinner? _____

Approximately how many **alcoholic** drinks

(a) before dinner? _____ (b) after dinner? _____

Approximately how many/much **tobacco (e.g. Cigarettes, cigars, chewing tobacco)**

(a) before dinner? _____ (b) after dinner? _____

Q2 . Did you take any **drugs** or **medication** today that may affect your sleep tonight? Circle: Yes / No

Describe:

Q3. Did you do **exercise** any today? Circle: Yes / No

If yes, approximately how many minutes of

(a) low intensity (walking, slow cycling, etc) _____

(b) moderate or high intensity (running, cycling, swimming, etc) _____

Q4. Did you take any daytime **naps** today? Circle: Yes / No

If yes, approximately how many minutes in total? _____

Participant Number:_____ Date:_____

Waketime Questionnaire

Please fill out this part of the diary first thing in the morning.

Sleep Timing:(Please write in time and circle AM or PM)

Went to bed last night at _____AM / PM Turned out the lights at _____AM / PM

Finally woke up at: _____AM / PM Got out of bed at _____AM / PM

Minutes until fell asleep last night: _____ minutes.

Awakenings

Awakened by: (check one)

__ Alarm Clock/ radio

__ Someone whom I asked to wake me

__ Noises

__ Just woke

After falling asleep, woke up this many times during the night (circle)

0 1 2 3 4 5 or more

Total number of minutes awake: _____

Woke up to use the bathroom (circle # of times):

0 1 2 3 4 5 or more

Awakened by noises/child/partner (circle # of times)

0 1 2 3 4 5 or more

Awakened due to discomfort or physical complaint (circle # of times)

0 1 2 3 4 5 or more

Just woke (circle # of times) :

0 1 2 3 4 5 or more

Ratings (place a mark somewhere along the line)

SLEEP QUALITY:

very bad _____ very good

MOOD OF FINAL WAKENING:

very tense_____ very calm

ALERTNESS ON FINAL WAKENING:

very sleepy _____very alert